



HAL
open science

Development and characterization of 3D warp interlock fabrics as reinforcements for protective solutions against stabbing

Mengru Li

► **To cite this version:**

Mengru Li. Development and characterization of 3D warp interlock fabrics as reinforcements for protective solutions against stabbing. Mechanics of materials [physics.class-ph]. Université de Lille, 2021. English. NNT : 2021LILUI010 . tel-03625564

HAL Id: tel-03625564

<https://theses.hal.science/tel-03625564>

Submitted on 31 Mar 2022

HAL is a multi-disciplinary open access archive for the deposit and dissemination of scientific research documents, whether they are published or not. The documents may come from teaching and research institutions in France or abroad, or from public or private research centers.

L'archive ouverte pluridisciplinaire **HAL**, est destinée au dépôt et à la diffusion de documents scientifiques de niveau recherche, publiés ou non, émanant des établissements d'enseignement et de recherche français ou étrangers, des laboratoires publics ou privés.

Thèse

**Development and characterization of 3D warp interlock fabrics
as reinforcements for protective solutions against stabbing**

**Développement et caractérisation des tissus 3D interlocks chaines comme
renforts pour des solutions de protection contre les coups de couteau**

Présentée par:

Mengru LI

Discipline : Mécanique des solides, des matériaux, des structures et des surfaces

Soutenue le 11/01/2021 devant la commission d'examen

Jury members of comitee:

Xiaogang Chen, Docteur	University of Manchester	Rapporteur
Nadia Bahlouli, Professeur	Université de Strasbourg	Rapporteur
Pierre Ouagne, Professeur	ENIT	President/ Examineur
François Boussu, Professeur	ENSAIT	Directeur de thèse
Peng Wang, Professeur	Université Haute Alsace	Co-directeur de thèse
Damien Soulat, Professeur	ENSAIT	Examineur
Frederic Heim, Professeur	Université Haute Alsace	Invited

ACKNOWLEDGEMENTS

Throughout the three years of my PhD career, I have received a great deal of support and assistance and this research and work would not have been possible without the aid and support of many people in my life.

First and foremost, I would like to acknowledge the financial support of the China Scholarships Council for my PhD research.

I would like to express my sincere gratitude to my supervisors: Prof. Francois BOUSSU and Prof. Peng WANG and Prof. Damien SOULAT for their guidance, extremely thorough, timely supervision and the valuable discussions, and their patience throughout my PhD research.

I am thankful for all the staff members in GEMTEX who provided me with experimental and technical supports. In particular, my appreciations go to Mr Lucas Putigny, Mr Nicolas Dumont and Mr Valentin Laurent for their help on fabric weaving; Mr Frederick Veyet for repairing the machine; Mr Hubert Ostyn for changing the stab machine. I would like to thank the other technicians from GEMTEX lab for helping me in finishing my experimental work.

Special thanks to my academic colleagues and friends in GEMTEX: Hao Shen, Henri Lansiaux, Chan Hui, Zineb Samouh, Shenglei Xiao, Wenqian Zhai, Chen Chen, Liting Yao, and Anne-Clemence Corbin with whom I got helpful discussions during my entire study. I would also like thank to my friends for their help at all times: Xiang Yan, Yanni Xu, Petchprakai Sirilertsuwan, Balkiss Hamad and Shengchang Zhang.

Finally, I would like to express my deepest gratitude to my dearest parents and other family members for their unconditional support and encouragement during my PhD study. I would like to thank my boyfriend Zhenglei He for his love, patience and encouragement all the time.

ABSTRACT

An increasing demand for materials used for stab protection has been expressed to provide more protective, flexibility and lightweight. Researchers have mainly focused on studies about stab resistance of soft body armour based upon technical textile fibres and two-dimensional (2D) fabrics. However, the soft protective materials based on three-dimensional (3D) fabrics have been rarely studied. The overall aim of this current research has been oriented to explore different design of three-dimensional warp interlock fabrics (3DWIFs) that provide more efficient protective solution. Hence, this thesis has been concentrated on both the manufacturing process parameters and resulting product parameters of the 3DWIFs made with high molecular weight polyethylene (HMWPE) yarns. The production process parameters have been studied to optimize the manufacturing and the mechanical properties of 3DWIFs. The product parameters of 3DWIFs have been investigated to find the optimized combination for the best protective resistance against stabbing. The four main categories, namely, Angle/ Through-the thickness (A/T), Angle/ Layer-to-layer (A/L), Orthogonal/ Through-the-thickness (O/T), and Orthogonal/ Layer-to layer (O/L), of 3DWIF architectures were woven by twisted HMWPE yarns for reducing the hairiness during weaving process. The mechanical characteristics of different structures' 3DWIFs were systematically tested and compared. It showed that the tensile property in weft direction is larger than the counterpart of warp direction because the weft yarn density is almost four times larger than warp density. The wrapping angle related to the inter yarn friction of the 3DWIFs has an influence on the tensile properties of 3DWIFs. Besides, a dedicated experimental study has been performed on 3DWIFs subjected to low-speed impact, including single-stab and double-stab properties in terms of depth of penetration and trauma. The double-pass stabbing tests are complementary to single-pass stabbing tests. It was experimentally concluded that the Orthogonal/Through-the-thickness interlock (O/T) fabric, with lowest depth of penetration, shows a good stab resistance. Double-pass tests with same stab angle resulted in lower depth of penetration. Moreover, a new test, named pre-deformed stab-resistance test, has been proposed to simulate the knife attack of female breasts. It indicated that the in-plane shear angle effects the pre-deformed stab-resistance property of deformed fabric stacks.

Keywords: 3D warp interlock fabrics; HMWPE; Mechanical properties; Stab resistance; Protective material

RÉSUMÉ

Une demande croissante en matériaux utilisés pour la protection contre les coups de couteau a été formulée pour apporter plus de protection, flexibilité et légèreté. Les chercheurs se sont principalement concentrés sur les études relatives à la résistance aux coups de couteau des gilets pare-balles souples à base de fibres textiles et de tissus techniques 2D. Cependant, les matériaux de protection souples basés sur des tissus 3D ont rarement été étudiés dans les travaux de recherche récents, en particulier ceux qui révèlent que les architectures tissées en 3D peuvent jouer un rôle décisif lors d'un impact de couteau. Les tissus 3D interlock chaîne (3DWIFs) peuvent également être utilisés dans un gilet souple pour des applications anti-poignard. L'objectif général de ces travaux de recherche actuels est d'explorer les différentes conceptions de tissus 3D interlock chaîne (3DWIF) qui offrent la solution de protection la plus efficace. Par conséquent, cette thèse s'est concentrée sur les paramètres du processus de fabrication et les paramètres des produits résultants des tissus 3DWIF fabriqués avec des fils HMWPE. Les paramètres du processus de production ont été étudiés afin d'optimiser la fabrication et les propriétés mécaniques des tissus 3DWIF. Les paramètres produit des tissus 3D interlock chaîne ont été étudiés afin de trouver la combinaison optimisée pour la meilleure résistance de protection contre les coups de couteau. Les quatre principales catégories d'architectures de tissus 3D interlock chaîne, tels que : A/T, A/L, O/T et O/L, ont été tissées avec les mêmes fils retordus de polyéthylène à haut poids moléculaire (HMWPE). Les caractéristiques mécaniques des tissus 3D interlock chaîne (3DWIF) ont été systématiquement testées et comparées. En outre, une étude expérimentale spécifique a été réalisée sur des tissus 3D interlock chaîne soumis à un impact à faible vitesse, y compris les propriétés à simple et double passe en termes de profondeur de pénétration et de traumatisme. Les tests de double passage au couteau sont complémentaires des tests de simple passage au couteau. Il a été conclu expérimentalement que le tissu 3D interlock chaîne de type orthogonal à liage à travers l'épaisseur a une bonne résistance aux coups de couteau. Entre-temps, les liens entre la résistance aux coups de couteau, les propriétés physiques et les propriétés mécaniques des 3DWIF ont été analysés.

Mots-clés: Tissus 3D interlock chaîne; Fils polyéthylène haut module; Propriétés mécaniques; Résistance aux coups de couteau; Matériau de protection

Table of Contents

ACKNOWLEDGEMENTS	II
ABSTRACT	III
RÉSUMÉ	IV
Table of Contents	V
List of Figures	VII
List of Tables	XI
List of abbreviations	XII
General Introduction	1
Background	2
Problem statement	2
Aims and Objectives	3
Thesis Layout	4
Chapter 1 Literature review	6
1.1 Introduction to Literature Review	7
1.2 Introduction of 3D warp interlock fabrics	7
1.2.1 Materials for 3DWIFs weaving	7
1.2.2 Structures of 3DWIFs	9
1.2.3 Classification of 3D woven fabrics	10
1.3 Development and mechanical behaviour characterizations of 3DWIFs	14
1.3.1 Tensile properties	14
1.3.2 Impact properties	18
1.3.3 Shear properties	21
1.3.4 Stab resistance properties	26
1.3.5 Deformability	28
1.4 Summary of Chapter 1	29
Chapter 2 Manufacturing of 3D warp interlock fabrics	31
2.1 Introduction	32
2.1.1 Design of 3D warp interlock fabrics	32
2.1.2 Property of HMWPE yarn	34
2.1.3 Warping process	35
2.2 Manufacture of 3D Warp Interlock Fabrics	36
2.2.1 Warp yarn tension adjustment	37
2.2.2 Process and fabrics parameters	39
2.2.3 Yarn damage study	41
2.3 Summary of chapter 2	44
Chapter 3 Mechanical behaviour of 3D warp interlock fabrics	46
3.1 Introduction	47
3.2 Materials and experimental set-up	47
3.2.1 Tensile property characterisation	47
3.2.2 Yarn crimp in the 3DWIFs	48
3.3 Experimental results and discussions	49

3.3.1	Yarn crimp in the 3DWIFs	49
3.3.2	Tensile behaviour of 3DWIFs.....	51
3.3.3	Inter yarn frictions during the tensile test of 3DWIFs	54
3.3.4	Geometrical model and the wrapping angle	57
3.4	Summary of Chapter 3	61
Chapter 4	An exploration on the stab-resistance of 3DWIFs.....	62
4.1	Introduction	63
4.2	Research methodology	63
4.2.1	Single-pass stabbing.....	65
4.2.2	Double-pass stabbing.....	67
4.2.3	Measurement of the stabbing deformation	69
4.2.4	Image-analysis of fabrics' deformation after stabbing test.....	70
4.3	Experimental results and discussion	71
4.3.1	Single-pass results.....	71
4.3.2	Double-pass results	86
4.4	Summary of chapter 4	91
Chapter 5	Pre-deformed stab resistance of multi-ply 3DWIF	94
5.1	Introduction	95
5.2	Experimental set-up.....	96
5.2.1	Sample preparation	96
5.2.2	Stab test apparatus.....	98
5.2.3	Testing procedures and methods.....	98
5.3	Results and discussion.....	101
5.3.1	Deformation of fabric panel.....	102
5.3.2	Stab resistance properties after deformation.....	106
5.4	Summary of chapter 5	113
General conclusion.....		114
Conclusion		115
Perspectives.....		117
REFERENCES		118

List of Figures

Figure 1-1	The schematic representation in cross-section weft yarns views of 3DWIF [41].9	9
Figure 1-2	Representation model of 3DWIF architectures based on the binding step and depth and the number of layers, warp binding path ($X = 2$), and binding depth ($Y = 2$): (a) cross-sectional weft yarns view; (b) 3D view.....10	10
Figure 1-3	Photograph of inter-ply test apparatus [103].21	21
Figure 1-4	Shear deformation processes of 3D preform [103].....25	25
Figure 1-5	Three stages of 3D angle interlock fabric shear process [103].....26	26
Figure 2-1	The ultimate forces of different twists HMWPE yarns.35	35
Figure 2-2	The warping machine.....36	36
Figure 2-3	Different parts of dobby loom.....37	37
Figure 2-4	Improvement of tension adjustment (a) Installation method, (b) Comparison between the traditional dropper (left) and the ‘U’ shape dropper (right).....38	38
Figure 2-5	Schematic diagrams of the arrangement and position of yarn tension adjusters, (a) top view; (b) side view.....39	39
Figure 2-6	Effect of yarn twist on the mechanical properties of the yarn.42	42
Figure 2-7	Effect of warping and weaving process on the tensile properties of weft yarns.....43	43
Figure 2-8	Effect of warping and weaving process on warp yarns mechanical properties of 3D warp interlock fabrics (a) binding warp yarns, (b) stuffer warp yarns.44	44
Figure 3-1	Methods of avoiding testing slippage by adhesive bonding on both ends with an extension of 50mm: (a) the front photographic and schematic view; (b) schematic view of side plan; (c) actual operation.48	48
Figure 3-2	Micro-observation of a single binding warp yarn in (a) F2 and (b) F4 fabrics, cross-sectional view.....51	51
Figure 3-3	Tensile force / tensile extension curves of 3DWIFs in warp (a) and weft (b) directions.53	53
Figure 3-4	Example of the contact surface between stuffer and weft yarns (in the F1 fabric). 56	56
Figure 3-5	Average friction load-extension of the binding warp yarns during the tensile tests of five different 3DWIFs samples.....57	57

Figure 3-6	The definition of yarn wrapping angle (θ) in plain-woven fabric using Peirce's geometrical model.....	57
Figure 3-7	Schematic diagram (a) and geometrical model (b) of wrapping angles (θ) and linking points among the warp and weft yarns in the unit cell of the F2 fabric.....	59
Figure 4-1	Schematic of a stab test device (a) General view and (b) Details of the stab blade.....	64
Figure 4-2	Schematic of the coordinate system of the ply orientations panels for the stab test: (a) aligned panels $[0]_4$; (b) angled panels $[0/22.5/45/67.5]$	66
Figure 4-3	An illustration of the three stages of interaction between a knife and armour.	67
Figure 4-4	A schematic showing the coordinate system of fabric panel (a) 3D schematic diagram, (b) 2D schematic diagram.....	68
Figure 4-5	Double-pass stabbing tests (a) $0^\circ/0^\circ$; (b) $90^\circ/90^\circ$; (c) $90^\circ/45^\circ$; (d) $90^\circ/0^\circ$	69
Figure 4-6	The stabbing deformation: (a) Definition of the DOP and DOT, (b) Silicone print of trauma, (c) 3D scanning and (d) Surface damaged area of silicone print.....	70
Figure 4-7	Comparative example between real samples and model, (a) real sample before stab test, (b) real sample after double stab $90^\circ/0^\circ$, (c) sample model after double stab $90^\circ/0^\circ$	71
Figure 4-8	DOP of different aligned panels: 1 ply $[0]$, 3 plies $[0]_3$, 6 plies $[0]_6$	72
Figure 4-9	Observation of the stabbing deformation on the bottom surface in the single-pass stabbing test with 1 ply fabric panel.	72
Figure 4-10	DOP per unit thickness in stabbing tests with the stab angle of 0°	73
Figure 4-11	Comparison of DOP of 6 plies laminates from different fabrics in aligned panels $[0]_6$ and $[90]_6$ respectively submitted to stabbing tests.....	74
Figure 4-12	Damage morphologies of the stabbing deformation on the bottom surface of 6 plies fabric panels after single-pass stabbing tests in stab angle of 0° and 90°	75
Figure 4-13	Silicone prints of 6 plies aligned fabric panels after stab tests: (a) aligned panels $[0]_6$ and (b) aligned panels $[90]_6$	77
Figure 4-14	Surface damaged area after stab tests of 6 plies aligned fabric panels $[0]_6$ and $[90]_6$	77
Figure 4-15	Summary of different parameters from different fabrics.	78
Figure 4-16	(a) Illustration of the path, knife-edge travels at different penetrating angles; (b) cross-section weft yarns view of F4 fabric, and (c) 3D view of F4 fabric.	80

Figure 4-17	Comparison of DOP from 6 plies panels in different ply orientations.....	81
Figure 4-18	DOP of 8 plies panels in different ply orientations of F4 fabric.	82
Figure 4-19	Damaged area of 8 plies fabric panels of F4 fabric after stab tests of [0] ₈ , [90] ₈ , and [0/22.5/45/67.5] ₂	83
Figure 4-20	Silicone prints of 8 plies fabric panels of F4 fabric after stab tests: (a) [0] ₈ ; (b) [90] ₈ , and (c) [0/22.5/45/67.5] ₂	83
Figure 4-21	DOP of 16 plies panels in different ply orientations of F4 fabric.	84
Figure 4-22	DOP of different fabrics stabbed with the 0° angle configuration as related to the number of plies.	85
Figure 4-23	DOP of F4 fabrics stabbed in the angle of 0° as related to the number of plies. .	86
Figure 4-24	Stabbing deformation after double and multi-angles stabbing and comparison with the single-pass ones.....	88
Figure 4-25	Sixteen plies F4 fabric patterns from the top view after single-pass and double-pass stab with the different stab angles: (a) single 0°, (b) single 90°, (c) double 0°/0°, (d) double 90°/90°, (e) double 90°/0°, (f) double 90°/45°.	90
Figure 4-26	Observation of the damage morphology from bottom surface of sixteen plies fabric panel after different double-pass stabbing tests.	91
Figure 5-1	Schematic description of the different fabric ply types by two cutting methods.....	96
Figure 5-2	Ply orientation in the specimens (a) aligned fabric panel and (b) angled fabric panel.....	97
Figure 5-3	The steps of the experiment (a) Preparation of forming, (b) Forming (c) pre-deformed stab-resistance test.	100
Figure 5-4	Deformed 3DWIF after hemispherical forming test, (a) single [0°/90°] fabric ply and (b) single [-45°/45°] fabric ply.....	103
Figure 5-5	Material draw-in of single [0°/90°] fabric ply in warp and weft directions (distribution in ¼ zone A of the deformed ply).	103
Figure 5-6	Material draw-in of single [-45°/45°] fabric ply in warp and weft directions (distribution in ¼ zone B of the deformed ply).	104
Figure 5-7	Comparison of the shear angle distribution of single ply fabric after deformation: (a) [0°/90°] ply; (b) [-45°/45°] ply. (For interpretation of the references to color in this figure legend, the reader is referred to the web version of this article.)	106

Figure 5-8 Schematic of: (a) In the centre location, (b) In the middle area and (c) In the locking area (dimensions in mm).....107

Figure 5-9 Example pre-deformed stab-resistance tests (a) Preparation, (b) Preforming of fabric panel, (c) Deformed fabric panel, (d) Stabbing on the deformed fabric panel, (e) Bottom of fabric panel after pre-deformed stab-resistance tests.108

Figure 5-10 Depth of penetration of aligned and angled fabric panels at different locations.....109

Figure 5-11 Damage morphologies of $[0^\circ/90^\circ]_8$ aligned fabric panels after the experimental stab test: (a) Overview; (b) Partial enlarged view; (c) Side view.111

Figure 5-12 $[(0^\circ/90^\circ)/(-45^\circ/45^\circ)]_4$ angled fabric panels after the experimental stab test: (a) Overview; (b) Partial enlarged view; (c) Side view.....112

List of Tables

Table 1-1	The typical properties of commonly used filament material in the dry 3DWIFs studied by previous researchers.	8
Table 1-2	The classifications of major types of 3D woven fabrics.	11
Table 1-3	The classification types of 3DWIFs.	13
Table 1-4	Tensile properties of 3DIWFs.	15
Table 1-5	Impact properties of 3DIWFs.	22
Table 1-6	Shearing properties of 3DWIFs.	24
Table 1-7	Knife penetration properties of 3DWIFs.	28
Table 2-1	The structural parameters of five 3DWIFs tested.	34
Table 2-2	Main physical properties of HMWPE yarn.	34
Table 2-3	Structural properties of 3DWIFs.	40
Table 3-1	Average crimp values of all warp and weft yarns for all the 3DWIFs.	50
Table 3-2	Breaking force (St) and failure value (ϵ) of tensile tests in the warp and weft directions.	54
Table 3-3	The wrapping angles between binding warp and weft yarns and the yarn interlacing shapes in different fabrics.	60
Table 4-1	The conditions for drop tower testing.	65

List of abbreviations

PPE	Personal protective equipment
3DWIFs	Three-dimensional warp interlock fabrics
2D	Two-dimensional
3D	Three-dimensional
LVI	Low-velocity Impact
HVI	High-velocity Impact
HMWPE	High molecular weight polyethylene
A/T	Angle interlock/through-the-thickness
A/L	Angle interlock/layer-to-layer
O/T	Orthogonal interlock/through-the-thickness
O/L	Orthogonal interlock/layer- to-layer
SHTB	Self-designed split Hopkinson tension bar
LCM	Liquid Composites Moulding
tpm	Twist per meter
W_f	Fibre weight fractions
DOP	Depth of penetration
DOT	Depth of trauma

General Introduction

Background

Throughout human history, various types of weapons were invented and used which led to the development and application of personal protective equipment (PPE). At present, frequent attacks on police officers and civilians are not a new issue [1], such as gun and knife attack. While since increasingly stringent gun control legislation, stabbings attacks with knives and other sharp objects are still a persistent and worrying concern and happens frequently, because of their widespread availability, especially in Europe and Asia [2,3]. Thus, there is an increase demand for materials used for stab protection [3] as it is a practical problem needing to be addressed in social development.

The evolution of body armour with time has been briefly reviewed by Yadav et al. [4] covering the evolution of body armour systems and introducing some futuristic material options. It's well-known that the drawbacks of hard body armour have resulted in the development of soft body armour with flexibility (wearability and mobility of the wearer), lightweight, and damage resistance [5]. Besides, a growing trend of females joined the law enforcement police and military services across the world for the last few decades. Compared with male body armour, the problems of manufacturing the female body armour are the curvaceous shape of the female body [6]. If the female officers wear the body armour designed for males, it is perhaps not suitable. By contrast, the development of female body armour is more complicated and both the flat and curvaceous body parts should be considered.

Problem statement

Since soft body armour is composed of flexible fibrous material [7], different fabric structures, such as unidirectional, two-dimensional (2D) woven and three-dimensional (3D) woven, were used as soft body armour materials. In terms of unidirectional fabric, resins or thermoplastic sheets are used to make collimated filaments be intact [8]. Woven fabrics are still very popular for soft vests which can provide high yarn packing density [9]. As for 2D woven fabric, for example, stitching method is applied for bonding more layers of 2D fabric together to improve the protection effect [10]. However, both the unidirectional sheets and stitching fabric have their own disadvantages, such as inferior inter-laminar fracture toughness. Therefore, the 3D woven fabric has been considered to fill in the gap.

Although, from the macro shape point of view, there are solid, hollow, shell and nodal 3D woven structures [11], three-dimensional warp interlock fabric (3DWIF) as one of them, has been widely

investigated in the past few years. They have good mechanical properties in through-the-thickness direction, better structural integrity, good layer to layer stress transfer [12]. Because of these excellent performance, they have been studied as the ballistic body armour [13]. Different variants of 3D woven structures have been reported by different researchers for ballistic applications [13,14], more details can be seen in the review [15]. However, the application for stab resistance protective materials of 3DWIFs have been rare developed [12,16]. In addition, there are few comparative studies on the properties of different types of 3DWIFs.

Moreover, presently, the constant need for reducing weight and enhancing performance of soft body armour [17], as well as improvement in comfort and fit, has never been changed. The demands for developing the protective materials with lightweight and wear comfort at a reasonable cost become the driving force for the present research. Polymeric materials, such as high molecular weight polyethylene (HMWPE), are some of the most widely and increasingly used materials in the literature about the development of protection materials due to their low weight, toughness, and excellent resistance to penetration [18–20]. The present study represents efforts to thoroughly explore this problem, targeting on the development of structural and protective materials with 3DWIFs and hence the possibility of structural improvement and weight reduction.

Aims and Objectives

The overall aim of current research is to investigate the stabbing resistance properties involving both flat part and curvaceous part of 3DWIFs for the female body armour application. To fulfil the aim, more profound and comprehensive understanding needs to be established of the mechanical properties and stab resistance of different architectures of 3DWIFs fabric panel. The research is planned to be carried out at the GEMTEX laboratory (EA n°2461 ENSAIT) within the framework of China Scholar Council (CSC) funding. The research is subdivided into third parts.

The first part of the current research is to manufacture 3DWIFs integrally with the same process parameters during the production, which includes designing, selecting yarn, winding, warping, drawing-in until weaving fabrics.

a) To select the yarn with reasonable twist per meter (tpm) that would be used for manufacturing the 3DWIFs, the tensile strength of the HMWPE yarns with different twists is to be experimentally investigated and compared;

b) To design five 3DWIFs architectures with different binding steps and binding depth following the four main categories: Angle interlock/Through-the-thickness binding (A/T), Angle interlock/Layer-to-layer binding (A/L), Orthogonal interlock/Through-the-thickness binding (O/T), Orthogonal interlock/Layer-to-layer binding (O/L);

c) To manufacture and produce 3DWIFs integrally with designed weave specifications, two beams of binding warp yarn and stuffer warp yarn systems were applied on an improved Dornier loom for producing the five different 3DWIFs architectures with the same warp and weft densities.

The second part focuses on the mechanical properties of 3DWIFs woven by HMWPE yarns to engineer and optimise 3DWIFs for structural and protective materials. The objectives in this part of the work are:

- a) To characterise the geometric and structural parameters of these structural fabrics;
- b) To discuss and compare the tensile properties of the different fabric structures with good mechanical property;

The third part focuses on the stab resistance property of 3DWIFs placed flat.

- a) To optimise 3DWIFs with good structure for single-pass stab test;
- b) To explore the double-pass stab resistance property which simulates the limiting case that the body armour does not penetrate by the knife attack;

The fourth part focuses on the pre-deformed stab resistance property of 3DWIFs. The objectives in this part of the work are:

- a) To study the in-plane shear property of 3DWIFs.
- b) To investigate the pre-deformed stab resistance property of 3DWIFs, in the hope to simulate the knife attack of female breast.

Thesis Layout

After the introductory chapter, the rest of this thesis is organised as follows:

Chapter 1 presents a review of literature in areas regarding: introduction of 3DWIFs (materials used, structures, classifications), development and mechanical behaviour characterization of 3DWIFs, and the applications of dry 3DWIFs.

Chapter 2 presents the manufacturing of 3DWIFs architectures following the four main categories with A/T, A/L, O/T, and O/L structures woven by twisted HMWPE yarns.

Chapter 3 presents the experimental study on tensile property of 3DWIFs woven by HMWPE yarns.

Chapter 4 presents the experimental study on stab resistance property, including single-stab and double-stab properties in terms of depth of penetration and depth of trauma.

Chapter 5 presents and analyses pre-deformed stab resistance property of 3DWIFs.

And at the end of the thesis, conclusions and suggestions for future work were done.

Chapter 1 Literature review

1.1 Introduction to Literature Review

The aim of the present research is to develop 3DWIFs for structural and protective materials. The topic covers a wide range of knowledge and literature from the structures, mechanical properties, to the applications of 3DWIFs. Thus, it is necessary to have a thorough comprehension of the development and mechanical performances of 3DWIFs, as well as the application. This chapter reviews studies on 3DWIFs from the following aspects, 1) the fibre tows/ filaments/ yarns for weaving 3DWIFs and the structures and categories of 3DWIFs; 2) the study of crucial mechanical properties of 3DWIFs, including tensile, impact, stab resistance property and so on; Besides, the weaving process to manufacture 3DWIFs will be described in the following chapter.

1.2 Introduction of 3D warp interlock fabrics

Fabric architecture plays a significant role in the mechanical performance of fabric and composite laminate [21]. Besides, structure-property correlation is a critical textile research area explored by various researchers and many factors have been proposed over the years for predicting/comparing/designing woven fabrics [22]. 3DWIFs contain not only the woven structure but also the process parameters, such as the warp and weft densities, types of warp yarns inside the structure (surface, stuffer and binding warp yarns) and the number of layers. Thus, a better understanding of the 3DWIFs, including the classification, materials, and structures, could be a prerequisite to understand their mechanical properties [23] and design new types of 3DWIF structures for different applications [24].

1.2.1 Materials for 3DWIFs weaving

Generally, 3DWIFs compose continuous high-strength multi-filaments yarns or tows, which mainly contribute to their performances. For instance, tensile properties are affected by the waviness of the load-bearing fibres, and the structural integrity of fibrous preforms is mainly derived from inter-fibre friction [25]. Therefore, it is necessary to gain deep knowledge and understanding of the fibres materials for purposes of designing efficient structures.

According to the related literature, the 3DWIFs can be woven in the monolithic or hybrid form using almost any type of fibre tows/filaments/yarns. Although, in the earliest reports of the related study, cotton [26] and polyester [27,28] were used for 3DWIFs, the frequently used fibre materials for technical applications are mainly glass fibres, aramid fibres, carbon fibres, and HMWPE fibres. In addition, other

fibre materials, such as quartz yarn, basalt, are rarely used for the manufacture of 3DWIFs. For example, to maintain the quartz fibre integrity during weaving process, it is necessary to use the infiltrating agent which were organic compounds in the production of quartz fibre. Wei et al. [29] showed that heat treatment in the high temperature was a useful means to eliminate the agent on the surface of silica fibre, but there was great thermal damage for silica fibres, and the tensile strength decreased significantly. Recently, it was reported that cellulose-based natural fibres as flax yarns [30] were also used as preforms in 3DWICs owing to their environmentally friendly character, their recycling properties, and their relative low-cost prices. The typical properties of commonly used materials reported in literature are listed in the Table 1-1. It can be seen that HMWPE filaments have the lowest density and good tensile strength compared with other high-performance filaments. Thus, 3DWIFs can be made by with lightweight HMWPE yarns. However, using all these high-performance yarns into 3DWIFs has led to some difficulties during the weaving process, especially in the management of warp tensions, compared to classical yarns such as cotton or polyester [31].

Table 1-1 The typical properties of commonly used filament material in the dry 3DWIFs studied by previous researchers.

Trademark name	Filament material	Density (g/cm ³)	Young's modulus (GPa)	Tensile strength (GPa)	Strain to failure (%)	Refs.
-	Flax	1.4-1.5	27.6-103	0.3-2.0	1.2-3.3	[32]
E-glass [®]	Glass	2.5-2.6	70-76	2.00-3.50	1.8-4.8	[32]
S2 glass [®]	Glass	2.47	88	4.70	5.7	[33,34]
Kevlar [®]	Para-aramid	1.44	64	2.86-3.75	2.4	[34,35]
Twaron [®]	Para-aramid	1.44-1.45	60-120	2.4-3.6	2.2-4.4	[36]
Spectra [®] 1000	HMWPE	0.97	113	3.25	2.9-3.2	[33,37]
HexTow [®] IM7	Carbon	1.78	276	5.52-5.65	1.9	[38]
Torayca [®] T700S	Carbon	1.80	230	4.90	2.1	[39]

1.2.2 Structures of 3DWIFs

Ansar et al. [40] have described 3DWIF as multi-layered fabrics produced by interlacing three sets of fibre tows (strands or yarns) in the weaving machine, including warp yarns that runs in the machine direction (weaving direction), fill or weft yarns that runs transverse to the machine direction and binder tows (warp weavers) system interlocked/interlaced the warp and the fill layers. While the other researchers [41,42] stated that 3DWIF structure includes four systems: (1) warp yarn (tow/strand) located at the top/bottom surface, (2) weft (filler) yarn perpendicular to the warp yarns, (3) inserted (stuffer warp/longitudinal) yarn located between two layers of weft yarns and perpendicular to the weft yarns, and (4) binding warp (weaver or web) yarn to link the various layers of the fabric. The schematic representation is shown in Figure 1-1. The main differences between the above different statement of 3DWIF structure are the yarns at the top/bottom surface (as called surface weaver) are integrated into the woven structure [42].

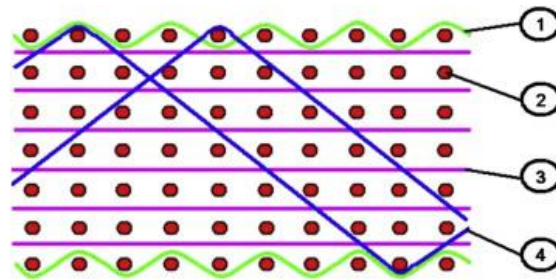


Figure 1-1 The schematic representation in cross-section weft yarns views of 3DWIF [42].

Actually, binding warp yarns play a vital role in 3DWIFs. The presence of them determines the mechanical properties of fabrics, improves the structural integrity and achieves high out-of-plane mechanical properties [43,44]. But, as shown in recent studies [45,46], the weaving of the binding warp yarns has opposite effects depending on its woven orientation with respect to the loading direction. It weakens the material by crimping weft tows, and strengthens the warp direction by becoming an additional load-bearing component without crimping them, resulting in the warp direction being stronger. It is also significant that both warp binder path and binding depth have a certain impact on the mechanical properties of 3DIWFs [47]. Figure 1-2 showed a weft cross-section and 3D views of the geometrical representation of a 3DWIF example. The binding step (denoted X) and the binding depth (denoted Y) are equal to 2 and the number of layers is equal to 3.

In 3DWIFs, the binding step (X) represents the weft yarns' number between two interlacing points (located in the same layer) of a binding warp yarn; and the binding depth (Y) represents the depth position of weft yarns' layers linked with a binding warp yarn. The weft yarns determine the number of layers of the 3DWIF. In other words, the number of fabric layers is the same as the number of weft yarn layers. Specifically, the warp binder path (X) influences the properties both in the warp and weft directions and the binding depth (Y) of interlocking warp plays an important role in determining the efficiency of the fabric in the loading direction [47]. There is no doubt that binders are helpful to improve the mechanical behaviour of the 3D composite [48], for instance, the delamination toughness [21,49–52], impact damage resistance, and post-impact mechanical properties and tensile strain-to-failure values [50]. For the purpose of the good properties mentioned above, these can be achieved by controlling the number of Z yarns, with a low volume content of z -binders [53] and usually less than 5% [50].

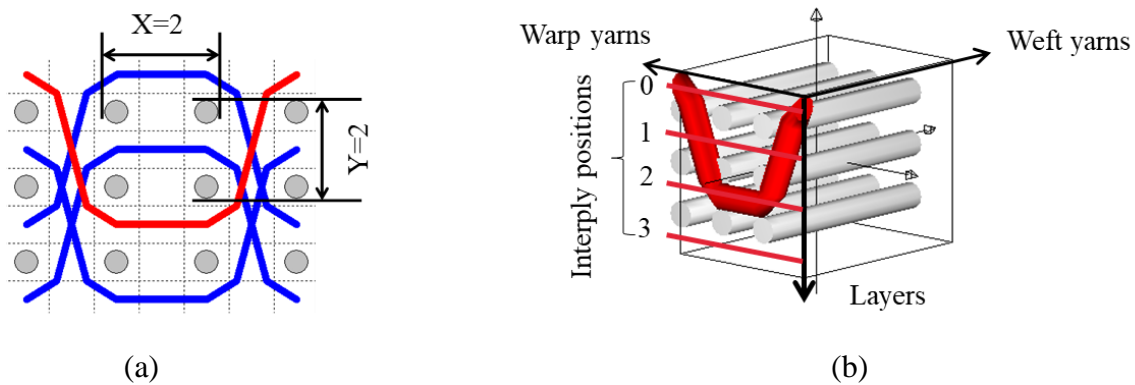


Figure 1-2 Representation model of 3DWIF architectures based on the binding step and depth and the number of layers, warp binding path ($X = 2$), and binding depth ($Y = 2$): (a) cross-sectional weft yarns view; (b) 3D view.

1.2.3 Classification of 3D woven fabrics

3D textiles, including woven, knitted, braided, stitched and non-woven fibrous assemblies, are those materials that have a system or systems in all three axes of plane [54]. 3DWIFs belongs to the branch of 3D woven fabrics class [40]. A good understanding of 3DWIFs classification can contribute to the study of its structure and performance. In general, 3D woven fabrics have been divided into several types according to different classification methods, as shown in Table 1-2. The main classification method is based on the weaving process, yarn interlocking mechanism, and manufacturing methods. However, there is no unification in classification. A 3D woven fabric can be completely specified by different

parameters including the nature of fibre used, number of layers of weft and warp yarns, binding type, number of filaments in a warp and weft yarns, warp and weft yarn densities, fabric areal density, and fabric thickness [55], etc. 3D woven preforms are classified, which is an arduous task because of the different criteria [56], based on various parameters such as fibre type and formation, fibre orientation and interlacements and micro- and macro- unit cells [57].

Table 1-2 The classifications of major types of 3D woven fabrics.

Classification method basis	Number of types	Classification	Ref.
Methods of manufacture	2	Linear element (3D braid, Multi-ply weave, Triaxial 3D weave, Multi-axial 3D weave), Plane element (Laminate type, H or I beam, Honeycomb type)	[58]
Weaving process	3	Non-interlaced fabric with conventional 2D weaving process, Fully interlaced 3D fabric with 3D weaving process, A non-woven, non-interlaced 3D fabric forming process.	[59]
Weaving process	4	Non-interlaced fabric with conventional 2D weaving process, Fully interlaced 3D fabric with 3D weaving process, Interlaced fabric with 2D weaving process, A non-woven, non-interlaced 3D fabric forming process.	[60]
Shedding	3	Orthogonal with through-the-thickness (multilayer) structure, Non-woven structure, Orthogonal structure.	[61]
Yarn interlacement and process type	2	Orthogonal and multi-axis fabrics (traditional or new weaving, and specially designed looms weaving process)	[62]
Configurations and geometries features	4	The 3D solid, hollow, shell, and nodal woven fabrics.	[63]
Manufacturing process	2	3D woven 3D fabric, 2D woven 3D fabric	[64]
Interlocking mechanism	2	Multi-axial woven fabrics, 3D interlock woven fabrics	[40]
Interlacement and fibre axis	4	Fully interlaced 3D woven, 3D orthogonal woven, Multi-axis fully interlaced 3D woven and Multi-axis 3D woven	[65]

3DWIFs have been widely investigated in the past few years with the results of a variety of structures. Umair et al. [66] divided the 3D interlock woven fabrics into two types: warp and weft interlocks, based on the fact that the dedicated binding yarn can link the layers (either warp or weft). It is not easy, indeed, to understand the variety of 3DWIFs due to the wide variety of fibre architectures [67] which can be produced with controlled amounts of binder yarns for the through-the-thickness reinforcement [50] and the classification criteria which can be different [41,55], as shown in Table 1-3. Ding et al. [68] and Chu et al. [55] use the same classification, and Gu et al. [43] and Chen et al. [63] have added the geometric features. In fact, the former classification gives more detailed compared with the latter classification. On the basis of the interlocking mechanism which considered the weave pattern of interlock with binding yarns in fabric thickness, the 3DWIFs are commonly categorized into two main types [50,69]: 3D angle interlock woven fabrics and 3D orthogonal interlock woven fabrics, and each type involves the through-the-thickness and layer-to-layer binding. If the penetration depth of binders is concerned, each type can be divided into two kinds: layer-to-layer fabrics and through-the-thickness fabrics [40,55]. Due to the complex structure of 3DWIFs, it creates some confusion among various researchers, scientists, and weaving technologists. Considering such problems, some researchers have studied on detailed descriptions, components and general design specification of 3DWIFs for better clarification and understanding [42]. From a global point of view, it can be distinguished four main categories of 3DWIFs [42]: Angle interlock/Through-the-thickness binding (A/T), Angle interlock/Layer-to-layer binding (A/L), Orthogonal interlock/Through-the-thickness binding (O/T), Orthogonal interlock/Layer-to-layer binding (O/L).

Another research study has highlighted the achievement of 3D weft interlock fabric, produced on a specific shuttle weaving loom equipped with Jacquard warp selection, which also revealed the higher crimp of weft yarns compared to strictly high straight warp yarns, mainly due to a very applied tensile load on warp yarns and poor tensile load on weft yarns [11].

There are also differences in the performance of two types of 3DWIFs. By the way of comparison, 3D warp orthogonal-interlock fabric can provide better fibre volume fraction especially in the thickness direction [40] and larger surface damaged area [70], while the 3D warp angle-interlock fabric can greatly increase folding ability, distortion capability [40], the structural stability, and resistance to delamination [71]. It also provides a relatively good through-the-thickness mechanical properties [72], which is mainly owing to the weft yarns that are interlaced through the different layers of the warp yarns in the fabric architecture [71]. By contrast, 3D warp angle-interlock fabric have low shear rigidity compared to woven

fabrics with other structures [28]. In particular, non-crimp 3D orthogonal woven preforms composites, having practically straight in-plane fibres, show significantly better in-plane stiffness and strength properties than respective properties of conventional type 3D warp interlock composites [45]. When compared to the layer-to-layer binding with the through-the-thickness binding, the latter provides a greater volume of fibres in the fabric, however, O/T fabric is less flexible than A/L fabric [54,73].

Table 1-3 The classification types of 3DWIFs.

Classification method basis	Number of clusters	Architecture description	Ref.
-	3	Multi-layer, Angle-interlock, Orthogonal structures fabrics	[74]
The weave pattern of binder yarn	2	Orthogonal and layer interlock	[50]
The orientation of binders and penetration depth	4	Angle interlock/through-the-thickness binding (A/T) Angle interlock/layer-to-layer binding (A/L) Orthogonal interlock/through-the-thickness binding (O/T) Orthogonal interlock/layer- to-layer binding (O/L)	[68]
Crossing pattern of yarns	2	Orthogonal interlock and angle interlock	[43]
Configurations and geometries features	2	Orthogonal interlock and angle interlock	[63]
Geometric features	4	Angle interlock/ Through-the-thickness binding (A/T) Angle interlock/Layer-to-layer binding (A/L) Orthogonal interlock/Through-the-thickness binding (O/T) Orthogonal interlock/Layer-to-layer binding (O/L)	[55]
The angle of binder yarns, angle and orthogonal weaves	2	3D angle-interlock woven fabrics, 3D orthogonal woven fabrics	[41]

In conclusion, the definition of a systematic classification method of 3DWIFs is beneficial for the comparison of performances of different structures fabric and is also conducive to the design of new structures. Moreover, the pros and cons of these materials' performance can also be considered to select the adapted structures for different application fields.

1.3 Development and mechanical behaviour characterizations of 3DWIFs

In order to characterize and obtain relevant data to optimize the applications of 3DWIFs and their reinforced composites, the experimental approaches are commonly used methods to investigate the mechanical performance of 3DWIFs. Great efforts have been made to characterize the mechanical properties of 3DWIFs. In this chapter, only the results of mechanical characterizations of 3DWIFs have been considered. The mechanical performance of 3DWIFs may be influenced by several factors [75]:

- The fibres (para-aramid, carbon, E-glass, etc.),
- The type of yarns (single yarn, plied yarn, filaments, etc.),
- The architectures (angle-interlock, orthogonal-interlock, etc.),

1.3.1 Tensile properties

Despite the fact that tensile behaviour is the basic property for designing the 3DWIF products, there is less research with regard to the tensile fracture mechanism in literature. Table 1-4 shows the tensile properties of 3DWIFs. Uniaxial tensile tests or unidirectional tensile tests have been done to evaluate the tensile behaviour of 3DWIFs, while these tests rarely highlight biaxial tensile tests, and all of them are the quasi-static uniaxial tensile tests. All these tests have been performed considering the following standards as: ASTM D5035 [76], NF ISO 4606 [47], ASTM D3039 [51] and EN ISO 13934-1 [77]. With respect to the existing experimental apparatus, different types of tensile machines were frequently used. However, Hou et al. [78] tested by using a self-designed split Hopkinson tension bar (SHTB) apparatus which has become a standard machine to perform tensile tests at low to medium and high strain-rates currently. While there is no clear standard procedure for the high strain rate tensile tests by SHTB.

Table 1-4 Tensile properties of 3DIWFs.

Architectures	Material	The emphasis of the test	Results	Ref.
3D woven orthogonal structures	Double-strand cotton yarn of (49. 1 Tex)	Influence of the binding weave and number of layers	The breaking elongation of the orthogonal structures primarily depends on the yarns used, which is independent of both the binding weaves and the number of layers; The binding weave does not contribute significantly to the tensile stiffness, to the strength, or to the elongation.	[26]
A/L	Torayca [®] carbon fibre tows (198 Tex)	High strain rate (1180 s ⁻¹ -2040 s ⁻¹) tensile behaviours	Tensile behaviours are sensitive to the strain rate.	[78]
3D-A fabric	Polyester plied yarn (100 Tex)	Effect of different weft densities	The increased values of weft densities resulted in better tensile load-strain performance with more than 10% elongation improvement.	[79]
2D Plain & 3D-A fabric	Aramid (Kevlar 29) yarns (1000 Denier) and basalt yarns (2700 Denier)	Influence of hybridization	The hybrid 3DWAIF had 42% to 59% higher tensile module than the other two pure ones in the warp direction.	[76]
Orthogonal and interlock structures	E-Glass tows (1200, 600 and 300 Tex)	Structural influence	The tensile properties are completely dominated by the linear density as well as crimp of warp tows.	[79]
A/L 4 3-2 twill 4, O/L 3 4-2 twill 5,	Twaron 2000 filaments/yarn (336 Tex)	Influence of weaving parameters	The binding can affect the crimp loss value correlated with the elongation value, both in the	[77]

O/T 4 3-4 basket 3-3, A/T 4 5-4 twill 6 shaped weave.			warp and weft directions. A high pick density value can also affect the geometry of the fabrics and lead to an equilibrium of floats.	
O/L	P-aramid Kevlar yarn (168 Tex)	Influence of fabric densities	Tensile strength of 3DWIF were influenced by the yarn densities of the preform in the respective directions.	[80]
O/T 4 3-4 Basket 3-3 A/T 4 5-4 Twill 6	E-glass (900 Tex), para-aramid (336 Tex) and flax yarns (500 Tex)	Influence of the raw material of yarns and fabric structures	The warp shrinkage of warp yarns inside the woven structure has a major influence on the whole fabric behaviour.	[30]
Structures with and without stuffer warp yarns	Flax rovings (547.9±64.4 Tex)	Influence of the manufacturing parameters	When the tensile load in warp direction increases, the maximal load in the weft direction decreases and inversely.	[81]
O/T 5 3-5 Twill 4 O/L 5 3-4 Twill 4 O/L 5 3-3 Twill 4	Flax yarn	Structural influence	The recorded maximum load seemed higher for structures bound using through the thickness pattern.	[82]
Orthogonal and interlock structures	E-Glass tows (1200, 600, and 300 Tex)	Stuffer layers and fibre volume fraction	The tensile properties are governed by warp tow crimp%, the number of warp tows per unit width as well as fabric assistance.	[83]
A-L 3-2 4 Twill 4 O-L 3-2 4 Twill 4 A-L 5-3 4 Twill 6 O-T 5-4 4 Twill 6 A-T 5-4 4 Twill 6	High-Molecular-Weight Polyethylene yarn (135 Tex)	Structural influence	The binding depth and the crimp angles/total crimp angles of interlocking warp plays an important role in determining the efficiency of the reinforcement in the loading direction.	[84]

Table 1-5 gives a conclusion about the results of tensile tests relative to 3DWIFs. In the previous study, the researchers paid more attention to the effect of the weaving parameters [26][77][80][85] of the 3DWIFs tensile properties. Chen and Zanini [26] studied the influence of the binding weave and the number of layers on the tensile properties of different binding weaves of 3D orthogonal interlock fabrics. It is understandable that the binding weave does not contribute significantly to the tensile stiffness, to the strength, or the elongation. This may be explained by the configuration of the orthogonal structures. Boussu et al. [77] compared the tensile properties of four different types 3DWIFs (A/L, O/L, O/T, A/T) in warp and weft directions respectively. It was pointed out that 3D A/T interlock fabrics had the two peaks in the force-elongation curve of warp direction, which was similar as presented by Bandaru et al. [76]. In the study of Lansiaux et al. [82], two peaks were observed on the obtained curve, indicating distinctive rupture of the two types of stuffer and binding warp yarns. The yarn crimp, namely undulations or waviness resulted by interacting with other yarns, from two systems was attributed to the difference in fabric. While for the test in the weft direction, the influence of the binding warp yarns appears less sensible than in the warp direction, but most of the mechanical properties depend on the resulted geometry given by the 3DWIF architecture. It was also demonstrated by Bandaru et al. [76] that the strength and failure strain in the weft direction was greater than in the warp direction, also taking three different materials into account, which means that, in the warp direction, stuffer warp yarns were straight and binder warp yarns were orientated at an angle, while all the yarns were parallel and straight in the weft direction. However, as a matter of fact, no matter the yarns in the warp or weft directions, all the yarns were not straight inside the fabrics.

Furthermore, the effects of the type of yarns on tensile properties were studied by Bandaru et al. [76] and Corbin et al. [30]. In the case of 3D-A fabrics, the failure strain was different in both the warp and weft directions. Though the strength of Kevlar 3D fabrics was superior to the basalt 3D fabrics, the hybrid combination of basalt and Kevlar yarns (H3D) improved the failure strain by 6.53-36.71% and 4.46-23.31% in both the warp and weft directions, respectively. Although the areal density of basalt 3D fabrics was higher, these fabrics exhibited lower failure strain due to the brittle failure of basalt yarns in the loading direction. An alternative way (i.e., intra-layer hybridization at the fabric level) was suggested to improve the mechanical performance of the fabrics under static and dynamic loadings with reduced areal density. It was presented [30] a similar behaviour in the weft direction of the two architectures and mainly for the para-aramid and E-glass yarns, which reveals a lack of influence of the 3D woven structure onto the weft yarns.

The influence of fabric architecture on tensile properties was also explored by Dash and Behera [79] and Bandaru et al. [76]. The former resulted that higher strength, in comparison to other structures, is obvious due to the role of coarser binder tows that were used during weaving for these structures. The better tensile response of 3D-A fabrics was due to the presence of binder yarn and more number of yarns/inch in the warp and weft directions than the 2D-P fabrics. The increase in strength and failure strain of 3D-A fabrics was due to the addition of binder yarns in the thickness direction, which improved the strength and in-plane stiffness of the fabrics [86,87]. Therefore, the binder yarns are beneficial to the tensile properties of 3DWIFs because they can hold the warp and weft yarns together in the thickness direction and then, the in-plane stiffness and strength of the fabrics are improved [88]. Previous researchers proposed that the percentage of yarn crimp presence will directly affect the tensile performance. Behera et al. [89] worked on the tensile strength analysis between 3D angle interlock and orthogonal. Results have shown that angle interlock tensile strength outperform the orthogonal in the warp direction. However, orthogonal tensile exceeded the tensile performance than angle interlock in the weft direction. This happens as the weft direction contribute to a greater yarn interlacement compared with warp direction. Nasrun et al. [85] indicated that fabric samples that resulted in lower crimp percentage tend to be less stiffness on fabric and will produce better tensile strength performance.

As initially investigated, Hou et al. [78] have achieved experimental testing and theoretical modelling regarding the tensile behaviour of the 3D angle-interlock woven fabric under high strain rates. Before this study, high strain rate tensile tests about woven fabrics were only confined to 2D woven fabric structures, especially on plain-woven fabric [90–92]. When the specimen was stretched under quasi-static loading, the whole fabric has sufficient time to be in a uniform stress state. But when the 3D-A fabric was subjected to a high strain rate load, there was no time for the stress wave to spread into the entire structure before some fibre tows are fractured. The principal reason for such a difference could be attributed to the stress wave propagation in this unique architecture. One possible reason for the strain rate sensitivity comes from the non-simultaneous fracture of the fibre tows in the different layers and the stress wave reflection at the cross-points of the warp and weft fibre tows. In a word, tensile behaviours of other types of 3DWIFs, like O/T or O/L, have not been explored under high strain rates which might extend the application of 3DWIFs in special conditions.

1.3.2 Impact properties

An impact with the same energy may happen with two distinct situations: low-velocity impact (LVI) and high-velocity impact (HVI). The former is generally simulated using a falling weight or a swinging

pendulum with low velocity and the latter using a gas gun or some other ballistic launcher with high velocity up to several hundred meters per second [93–95]. The energy loss of the projectile is an effective way to measure the fabric's capability of absorbing energy which is difficult to measure directly [93]. The impact on a woven textile panel is different from the equivalent impact on a single fibre due to the complex interaction at fibre crossover points [96]. Table 1-6 gives a consequence about the 3DWIFs with different architecture, materials and energy level used relating to the impact properties. In comparison, many researchers attach more importance to the HVI properties rather than LVI properties. The reason is that many military and law enforcement agencies have made it mandatory for their officers to wear ballistic vests while on duty [13].

1.3.2.1 Low-velocity Impact (LVI)

Taking into consideration the final application of the composites, fabrics were tested to know their impact properties. CEAST9350 impact tester was used for the LVI impact property according to ASTM D3763 standard, as shown in Table 1-6. It is established that 3D fabrics exhibit better impact resistance properties in terms of total energy, peak absorbed energy, and peak resistance when compared with an equivalent areal density of 2D fabrics [76,97]. This is due to the increased structural integrity of fabrics that improve the in-plane stiffness, damage tolerance, and energy absorption and fracture toughness. That is to say, the yarns in the thickness direction of 3D fabrics play a vital role in holding all the weft and warp yarns together.

The influence of hybridization and fabric architecture on the LVI response was studied by Bandaru et al. [76]. Pure Kevlar 2D plain woven fabric and Kevlar 3D angle-interlock with the lower areal density exhibited poor LVI performance. However, due to the hybridization, the LVI of fabric performance of these fabrics was enhanced by 41.28-42.73% and 36.89-37.71% for 2D plain woven fabrics in terms of peak force and energy absorption, respectively. Similarly, 14.70-41.44% and 13.45-20.14% improvement in the peak force and energy absorption of 3D angle-interlock fabrics were observed, respectively, due to hybridization.

1.3.2.2 High-velocity Impact (HVI)

Woven fabric has been used for constructing of soft body armour in the last few decades [98,99]. In general, the ballistic impact is the most common test in HVI characterization. Ballistic protection can be classified into two types: the soft protection, which is mainly dedicated to the body armour to protect humans (civilians and soldiers), and hard protection, which is used for protection of mobile platforms

[100]. Enhancing soft body armour performance constructed from 3DWIFs requires a full understanding of the ballistic impact response and wave propagation during the ballistic impact process.

Several papers [6,93] have described the impact behaviour of 3DWIFs and have been compared to existing 2D laminates, as summarized in Table 1-6. 3D fabrics woven are more resistant to impact when compared to the 2D fabrics due to the availability of unique energy dissipating mechanisms introduced by the presence of reinforcement along the Z direction (Z yarns) [6]. It also shows high performance in ballistic protection with high flexibility and lightweight [6] over 2D woven structures [100]. Yang et al. [93] showed that 3D-A fabric demonstrates relatively low capabilities of absorbing the impact energy, compared to fabrics of other structures. This is mainly determined by angle-interlock woven fabric structure, which consists of layers of weft yarns laid straight and bound by a single layer of warp yarns to lock the layers of weft yarns together. This unique structure leads to less interlacement which, however, limits the stress wave propagation in the fabric during the high-velocity impact.

From the above review of previous studies, it is clear that few works have been focused on the role of impact localization on the ballistic performance of dry 3DWIFs [55]. Moreover, Ha-Minh et al. [67] carried out ballistic tests on the impact behaviour of a 3DWIFs of 4 layers in two cases: perforation (400 ms^{-1}) and non-perforation (306 ms^{-1}). This paper has also indicated that the complex geometry of 3D woven fabrics due to the weaving process is extremely difficult to take into account. Besides, there is no clear trend between the thickness of the structure and the trauma depth, and more information data from further investigation are requiring to establish a conclusive relationship [6]. Increasing thickness of the angle-interlock fabrics seems to influence trauma depth, with the same warp and weft densities under the same standard, and higher areal density does not indicate better ballistic performance [6].

The failure mechanism of 3DWIFs and effects of boundary conditions and friction has been investigated by Chu et al. [55] using numerical modelling which is validated by experimental tests. The result shows that the global localization affects the deformation of the whole fabric through the primary weft yarn pulled-out mainly on the side near the free edge of the fabric, while the impact location decides the failure mechanism of primary weft and warp yarns around impact location. In addition, Ha-Minh et al. [101] analysed damage mechanisms of 3DWIF subjected to ballistic impact using a numerical model in two corresponding impact cases: no-perforation and perforation. Indeed, when the projectile does not penetrate through the target, the propagation and reflections of strain waves exist during the whole impact event. When the projectile penetrates through the target, strain waves propagate until fabric edges. It is noted that strain waves go following in the weft direction more rapidly than in the warp direction. This

is due to the lower yarn undulation in the weft direction than in the warp direction. Besides, the effect of boundary conditions on fabric damage zones also indicates that they significantly influence damage mechanisms and ballistic performance of the 3D fabric.

In general, these results are not enough to characterize the ballistic behaviour of 3D woven fabrics, because failure mechanisms during impact are not studied enough. More tests should be done to extend the results with other bullets impacts.

1.3.3 Shear properties

3DWIFs as a preform in the textile composites manufacturing involves shearing phenomena under the high and complex load of such composites in real applications [75]. As two important and valuable factors to study in the case of performance and appearances, the in-plane and inter-laminar shear properties of 3DWIFs have rarely been demonstrated. For example, in the stamping process, the in-plane shear deformation of 3D preform still predominates the deformation mode as well as 2D fabrics.

Both SHIMADZU 1kNE universal testing machine [102], picture frame [103–105], a KES-FB-M1 shear tester [28] and bias-extension test [103,106,107] were used to carry on the in plane-shear tests. Besides, a new test apparatus was designed to characterize 3D warp angle interlock fabric out-of-plane shear property according to the ASTM: C273 standard [102], as displayed in Figure 1-7 which showed that the left side and right side of the sample are connected respectively by the top part and bottom part. The test apparatus was equipped with two sensors (a displacement sensor and a force sensor) which can acquire force and displacement data by computer. The in-plane shear deformation is limited by local wrinkling until yarns reach the so-called “locking angle”.

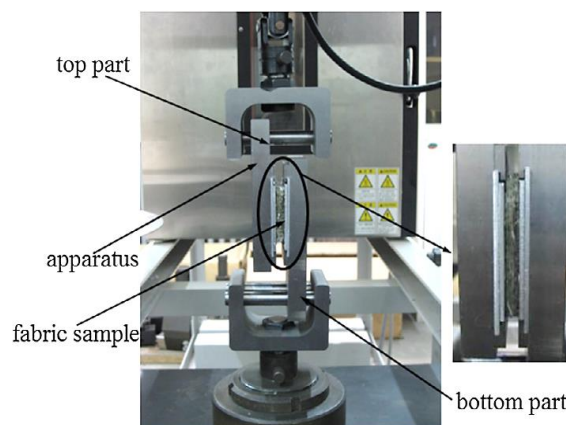


Figure 1-3 Photograph of inter-ply test apparatus [102].

Table 1-5 Impact properties of 3DIWFs.

Architectures	Material	Test device/ Standard	Energy level/ striking velocity	Results	Ref.
LVI Properties					
Orthogonal and interlock structures	E-Glass tows (1200, 600 and 300 Tex)	CEAST9350 impact tester/ ASTM D3763	4.5 m/s	The number of crossover points in the weave structures offered excellent association with the impact energy absorption.	[79]
2D plain & 3D orthogonal structure	Kevlar (333 tex) and Zylon (325 tex) tow	CEAST9350 Impact Tester/ ASTM D3763	5 m/s	Peak energy and peak force were observed to be 55% and 43% higher for Kevlar and 60% and 20% higher for Zylon 3D structure.	[97]
2D Plain & 3D-A fabric	Kevlar 29 yarns (1000 Denier), basalt yarns (2700 Denier)	CEAST9350 Impact Tester/ ASTM D3763	240 J	It can be concluded that hybridization enhanced the energy absorption of 2D-P fabrics by 8.58-37.71% and 3D-A fabrics by 13.45-20.14% respectively.	[76]
HVI Properties					
Orthogonal interlock fabric	Aramid Twaron [®] 930 dtex, polyethylene Spectra [®] 1760 dtex	25-mm calibre powder gun	910 m/s, 360 J	It is better to use aramid fibre instead of PE fibre for the same soft ballistic protection, even though PE fibres have better mechanical properties than aramid.	[100]
3DWIFs	Twaron 1100 dtex	5 mm diameter steel ball	660 and 697 m/s	Similar warp and weft densities have better energy absorption behaviour.	[100]

3D interlock woven fabric	Twaron 3360 dtex	Designed experimental apparatus	No perforation & perforation	The complex geometry of 3D woven fabrics due to the weaving process is extremely difficult to take into account.	[67]
3D interlock A–T 7-4-4	3360 dtex para-aramid yarn	a 1.11 g, 5.45mm diameter rigid FSP projectile	306 m/s	The impact location decides the failure mechanism of primary weft and warp yarns and the ballistic performance of the fabric in the fabric’s quart centre impact is less significant than that in the fabric centre impact.	[55]
3D four-and five-layers-angle-interlock fabrics 2D-P	Kevlar® 49 1500 denier	NIJ standard	339.19±11.01 m/s, 795.99 m/s	3D angle-interlock fabrics had shown a better ballistic impact resistance property than the conventional 2D plain-woven fabric pattern ballistic armors. There is no obvious trend between the areal density and the trauma depth.	[6]
3D Hybrid layer-to-layer and 2D-P	S-glass	Instron CEAST Model 9350 drop weight impacting system	3, 6, 9 and 12 Joules	3D fabrics are more resistant to impact when compared to the 2D fabric due to the availability of unique energy dissipating mechanisms introduced by the presence of reinforcement along the Z direction.	[108]
2D woven fabrics & 3D angle-interlock woven fabrics	Kevlar® 49 158 Tex	7.6-mm rifle barrel/-	480 m/s	3D angle-interlock woven fabric demonstrates relatively low capabilities absorbing the impact energy, compared with fabrics of other structures.	[93]

Table 1-6 lists the results study about the influence of the bending weave and the number of layers, the warp and weft densities, and intra/inter-ply shear deformation [102]. The researchers paid more attention to the shear properties on 3D angle-interlock fabrics rather than 3D orthogonal-interlock fabrics. The fabric density does have a great influence on the shear properties of 3DWIFs [26,28], which resulted that the shear rigidity increased with an increase of warp or weft density.

Table 1-6 Shearing properties of 3DWIFs.

Architectures	Material	Results	Ref.
3D orthogonal woven	Double-strand cotton yarn (49.1 Tex)	Tighter binding weave will produce a higher shearing rigidity and hysteresis. Moreover, shear rigidity and shearing hysteresis increase with the number of layers increases.	[26]
Angle-interlock woven	Textured polyester yarn (65.4 Tex)	The shear rigidity increased with an increase of warp or weft density. While both the shear rigidity and hysteresis decreased with the increase of weft layers, which is under a given warp and weft density per layer.	[28]
3D angle interlock fabric	Glass fibre filament warp and weft (1200 Tex) the binder warp (240 Tex)	The overall shear stiffness increases with the fabric density increasing. The shear strength along the warp is larger than that of the weft. The inter-ply shear behaviour of 3D fabric, is also restricted by the binder yarns.	[102]
A/L	48,000 carbon fibre	Two in-plane shear behaviours are identified that the behaviour is nearly quadratic for small shear angles and becomes exponential for larger angles.	[109]
with and without stuffer warp yarns	Flax rovings (547.9±64.4 Tex)	Compared to 2D fabrics, locking angles of these 3DWIFs can reach significant values (near to 40°).	[81]
3-D A/L interlock woven fabric	T300 carbon fibre	The yarn fineness and number of yarn layers play a key role in the in-plane shear properties of 3-D layer-to-layer angle-interlock woven fabric.	[110]

Chen and Zanini [26] discussed the influences of the binding weave and the number of layers. It has been demonstrated that tighter structure provides more friction between the warp and weft threads and thus more resistance to the shearing deformation. More binding to a given size of the orthogonal structure will provide more resistance to the shearing deformation and thus higher shearing rigidity. Moreover, the friction between yarns is the main cause of shearing rigidity and hysteresis. A higher binding force generates a higher normal pressure and higher friction, and thus higher shearing rigidities and hysteresis. Chen et al. [28] mentioned that 3D angle-interlock fabrics have lower shear rigidities than multilayer fabrics, which is mainly because an angle-interlock fabric has substantially fewer crossover points per unit area than multilayer fabrics. Charmetant et al. [109] tested the in-plane shear and transverse shear properties respectively in the warp and weft directions of 3D A/L interlock reinforcement.

In addition, Zhang et al. [102] presented the in-plane shear and inter-laminar shear behaviour of the 3D angle interlock preforms with different fabric densities. Some improvement has been made based on the existing questions for picture frame test. Figure 1-5 shows the shear deformation of the 3D fabric sample at different stages. In the beginning, the warp and the weft are orthogonal (Figure 1-4 (a)), there is no shearing. Then, the warp and weft rotate around the weaving point, the shear deformation resistance is mainly from the friction between the warp and weft yarns before the locking angle (Figure 1-4 (b)). During the shear process, the gap between the yarns vanishes gradually and the adjacent yarns contact each other, but the width of yarn almost does not decrease (Figure 1-4 (c)). The width of yarn starts to decrease under lateral compression after the locking angle during the large shear deformation, which can offer more space for the fabric to be sheared before wrinkling. The shear load increases rapidly (Figure 1-4 (d)).

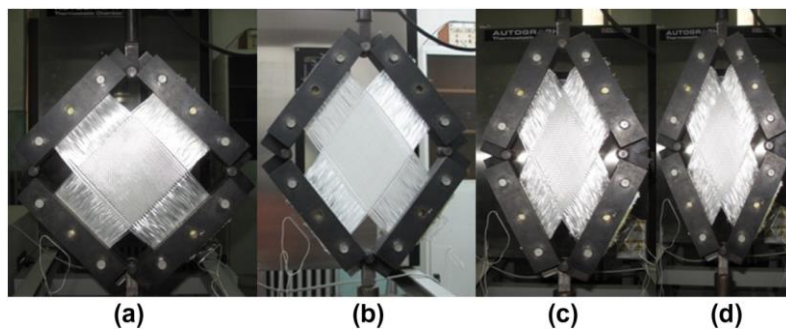


Figure 1-4 Shear deformation processes of 3D preform [102].

The inter-ply shear mechanism of 3D preforms is different from the 2D fabrics. The shear behaviour of 2D fabric is largely driven by the friction between the fabric layers, while the shear properties of 3D fabrics rely on the binder yarns interlacing with weft [111]. Three typical stages [102] can be divided during the large shear deformation of the 3D angle interlock fabric, as shown in Figure 1-4. In the first stage, the width of yarns may keep no variation and the friction is the main resistance to the shear deformation. In the second stage, the yarn width decreases rapidly and the binder yarns are compressed to flat. In the third stage, local wrinkling occurs on the fabric while the width of yarn is keeping constant because the fabric is up to the maximum fibre volume fraction.

In general, a tighter binding weave and an increase of warp or weft densities can be helpful to the shear rigidity of 3DWIFs. Similar to tensile behaviour, shear behaviour also depends on the loading direction of the testing specimen. The shear stiffness depends on yarns cross-linking in the weave diagram. More cross-linking yarns increase fabric stiffness [75]. In general practice, a fabric experiences deformation in all directions during mechanical handling or use, so the study of the shear properties has its practical significance.

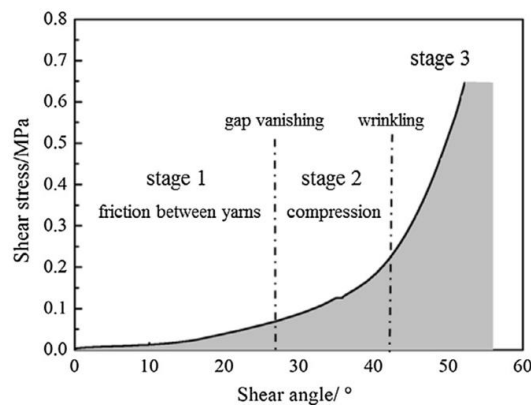


Figure 1-5 Three stages of 3D angle interlock fabric shear process [102].

1.3.4 Stab resistance properties

Flexible, comfortable systems are required to protect law enforcement and security personnel against stab attacks which are not a new issue. Recent trends have led to an increase in the number of applications for body armour with stab protection. Stab threats can be classified into two categories: puncture and cut [2,112]. Puncture refers to penetration by instruments with sharp tips but no cutting edge, such as ice picks or awls. These threats are of primary concern

to correctional officers since sharply-pointed objects are relatively easy to improvise. Knife threats are generally more difficult to stop than a puncture since the long cutting edge presents a continuous source of damage initiation during the stabbing event.

Generally, conventional body armour is designed for ballistic protection, which is not necessarily resistant to penetration of blades and offers little resistance to the puncture and stab. Armour specifically designed to withstand blade penetration can offer excellent stab protection but is prohibitively bulky, heavy [113] and inflexible, making them uncomfortable to wear [114] and difficult to conceal [2]. Therefore, increasing demand for materials used for stab protection should be more protective, flexible and lightweight. So far, the materials used for stab protection take on many forms. Many researchers have focused on studies about stab and puncture resistance of soft body armour based upon technical textile fibres and polymer fabrics, ranging from fabric manufacturing [115], experimental investigation of stab resistance property [116–118], analytical model and FEM [119,120] and the shear-thickening fluids (STF) treatment [2,121,122], and metallic elements [123].

As a special characteristic, the knife penetration properties have been investigated by the researchers. These properties are different from the impact properties presented in section 3.2. As shown in Table 1-10, knife penetration requires further understanding. Behera et Dash [97] showed that the results of the knife penetration tests are dominant when the linear density of binder tow is coarser, while the impact properties are affected by the number of interlacements in the in-plane region of fabric. They also observed that 3D orthogonal fabrics were more superior to 2D plain fabric layers of equivalent weight in terms of knife penetration resistance. Furthermore, there was a considerable improvement in energy at the break of 3D woven fabrics due to the presence of yarns in the Z direction. The Z yarns lead to a more integral structure and contribute to absorb the energy.

Table 1-7 Knife penetration properties of 3DWIFs.

Architecture s	Material	The emphasis of the test	Results	Ref.
Orthogonal interlock	E-Glass tows (1200, 600 and 300 Tex)	The linear density of binder tow	The knife penetration results are dominant when the linear density of binder tow is coarser rather than several interlacements in the in-plane region of fabric, which is unlike to impact properties explained earlier.	[79]
2D plain & 3D orthogonal structure	Kevlar (333 tex) and Zylon (325 tex) tow	Compared with 2D plain woven fabrics	The breaking load of 3D fabrics was 12% and 13% higher than single and two layers of 3D fabrics compared with three and six layers of 2D plain woven Kevlar fabrics at equivalent weight, respectively.	[97]
Orthogonal and interlock structures	E-Glass (1200, 600, and 300 Tex)	Stuffer layers and fibre volume fraction	The resistance to impact was better shown by orthogonal than interlock fabrics of the same stuffer layer as well as the same fibre volume fraction.	[83]

The present study noted in Table 1-10 highlights that the higher linear densities of the binder tows used for these weave designs attributed to the normalized peak energy. Both the results of the determination of peak energy and impact energy absorption relate directly to the number of crossover points. It is interesting to observe that the knife penetration results are dominant when the linear density of binder tow is coarser rather than several interlacements in the in-plane region of fabric which is unlike to impact properties explained earlier. The linear densities of in-plane tows play a major role in deciding the result. This is unlike impact property which is mainly dominated by the number of interlacements in a particular area.

1.3.5 Deformability

Forming fibrous 3DWIF appears to be one of the ways to make complex shape. Analysis of the deformability of the fabric during the forming step has been widely studied but the analysis of 3D warp interlock structures forming behaviour appears as less studied. Pazmino et al. [124] investigated the formability of non-crimp 3D orthogonal woven reinforcement with a single layer. Dufour et al. [125] pointed out that the layer to layer warp interlock preform has a better stamping behaviour, in particular no forming defects and good homogeneity in thickness. Dufour et al. also [126] measured the local strain of yarns inside of 3DWIF during forming process. Abteu et al. [80] indicated that the fabric and yarn density has a great impact on various mouldability characteristics of 3D warp interlock preforms during deformation. These experimental results can be an important dataset and be helpful for numerical simulations of any complex shape with the considered 3D fabric composite reinforcement.

1.4 Summary of Chapter 1

In this chapter, studies related to the theme of this thesis have been reviewed to get a profound understanding of the research background and propose reliable and feasible methodologies for this research. The mechanical properties of 3DWIFs have been clearly recognized and systematically classified based on different mechanical performance, i.e., tensile, impact, shear and other properties. 3DWIFs have good mechanical properties in through-the-thickness direction, better structural integrity, and good layer to layer stress transfer. There are only several papers discussed about the mechanical properties among different types of 3DWIFs. From the perspective of structure-property relationships, this review covers the recent and rapidly advancing subject of 3DWIFs according to the different process and product parameters chosen in the different research studies.

3DWIFs with good mechanical properties is widely used in the research of HVI, such as ballistic impact. Most of researches focused on the stab resistance property of flat 3DWIFs. Little research is considered the curvaceous fabric to simulate the female body armour. The stab resistance of both flat and curvaceous parts should be discussed. Besides, the stab resistance with different stab locations has been rarely studied which might be promising useful and advantageous by enhancing the properties and can extend their application.

The whole thesis systematically unfolds by gradually explore the stab resistance of 3DWIFs. This includes the manufacturing of 3DWIFs architectures following the four main categories with A/T, A/L, O/T, and O/L structures woven with twisted HMWPE yarns, the experimental study on tensile property of 3DWIFs, the experimental study on stab resistance property, including single-stab and double-stab properties in terms of depth of penetration and depth of trauma and analyses the links among stab resistance, physical properties and mechanical properties of 3DWIFs. All these aspects will be covered in the present research work and presented in the following chapters.

Chapter 2 Manufacturing of 3D warp interlock fabrics

2.1 Introduction

As mentioned in Chapter 1, various studies have revealed that 3DWIFs as fibrous structures possess outstanding mechanical properties and other advantages over the 2D laminates. It can be summarized three main advantages of 3D textile structures in comparison with the 2D counterparts: (1) higher resistance to multi-impacts (less damage for an impact) [67,76]; (2) easier and cheaper achievement of structures with complex shapes [67]; (3) better performance in the through-the-thickness direction [24,88] with lower labour time [127].

In this chapter, 3DWIFs structures, following the four main categories of A/T, A/L, O/T, and O/L structures, are used to be designed and manufactured by HMWPE yarns. Wisetex[®] and DB-WEAVE software play key roles in designing 3DWIFs. The former software can help you design dobby loom patterns. It supports weaving such patterns on a variety of supported loom types (e.g. ARM Patronic). There are virtually no limits on size and complexity of the patterns. DB-WEAVE is powerful yet intuitively usable. Five different types of 3DWIFs were manufactured based on the geometrical design of the architecture generated on Wisetex[®] software and the fabric peg plan was designed and transferred to the weaving machine using DB-WEAVE program. A new method is proposed to adjust the warp yarns' tension during the weaving process. Besides, the abrasion of yarn from different systems are also discussed.

2.1.1 Design of 3D warp interlock fabrics

This work aims to investigate the influence of different structures on mechanical properties of 3DWIFs. The weave parameters are taken into account as they are fundamental elements for the fabric construction. Different types of 3DWIFs were manufactured based on the geometrical design of the architecture generated on Wisetex[®] software and the fabric peg plan was designed and transferred to the weaving machine using DB-WEAVE program. Five different types of 3DWIFs were woven with two different weave designs. According to the general definition of 3DWIF given in the study [42], the abbreviated name of fabric structure were given in the second column of Table 2-1.

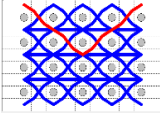
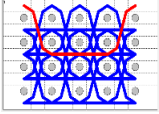
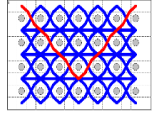
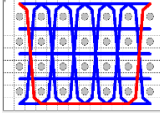
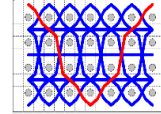
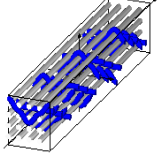
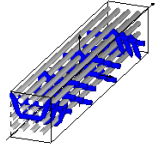
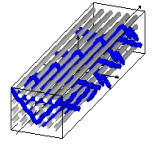
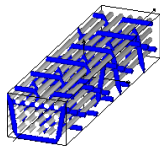
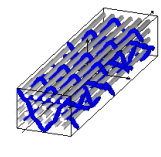
Table 2-1 General definitions of three different types of 3DWIF used in research work.

Fabrics	General definition of 3D warp interlock fabric:
F1	A-L 3-2 4 Binding {Twill 4 pattern weft effect left shift} {1 7 13 19 – 3 9 15 21 – 5 11 17 23 – # – #} – Stuffer {# – 2 8 14 20 – 4 10 16 22 – 6 12 18 24 – #}
F2	O-L 3-2 4 Binding {Twill 4 pattern weft effect left shift} {1 7 13 19 – 3 9 15 21 – 5 11 17 23 – # – #} – Stuffer {# – 2 8 14 20 – 4 10 16 22 – 6 12 18 24 – #}
F3	A-L 5-3 4 Binding {Twill 6 pattern weft effect left shift} {1 5 9 13 17 21 – 3 7 11 15 19 23 – # – # – #} – Stuffer {# – 2 8 14 20 – 4 10 16 22 – 6 12 18 24 – #}
F4	O-T 5-4 4 Binding {Twill 6 pattern 1U5D-3U1D2U effect left shift} {1 3 5 7 9 11 13 15 17 19 21 23 – # – # – # – #} – Stuffer {# – 2 8 14 20 – 4 10 16 22 – 6 12 18 24 – #}
F5	A-T 5-4 4 Binding {Twill 6 pattern 1U5D-3D1U2D effect left shift} {1 3 5 7 9 11 13 15 17 19 21 23 – # – # – # – #} – Stuffer {# – 2 8 14 20 – 4 10 16 22 – 6 12 18 24 – #}

Note: In 1U5D-3U1D2U and 1U5D-3D1U2D, ‘U’ is up and ‘D’ is down.

Table 2-2 shows the structural parameters of five 3DWIFs tested. It can be seen that all the 3DWIFs samples have the same number of layers, warp and weft linear densities of tows, and the same ratio of binding and stuffer warp yarns inside the structure. Therefore, all the basic structural parameters were kept the same for all the fabrics except for the binding step (X) and binding depth (Y). As for the F1 and F2 fabrics, the minimum binding depth was chosen (Y = 2) to design A/L and O/L 3D warp interlock structure, and for F3 fabric, the binding depth was increased (Y = 3). The A/T and O/T interlock weave, which are the structures of F4 and F5 fabrics, have the maximum binding depth of binding warp yarns (Y = 4). Regarding the binding step, F1 and F2 fabrics have the same binding step (X = 3), and F3, F4 and F5 fabrics have the same binding step (X = 5).

Table 2-2 The structural parameters of five 3DWIFs tested.

Fabrics	F1	F2	F3	F4	F5
Cross-section weft yarns view					
3D view					
Binding step (X)	3	3	5	5	5
Binding depth (Y)	2	2	3	4	4

2.1.2 Property of HMWPE yarn

HMWPE yarns (Spectra[®], Honeywell Company, USA) of 1350dTex were used as warp and weft yarns to fabricate the 3DWIFs. Because HMWPE yarn has high strength and good cut resistance properties which is suitable for body armour. All the produced 3DWIFs were manufactured with the same warp (10 ends/cm) and weft densities (40 picks/cm). The linear density is characterized according to ASTM D 1907/D 1907M [128]. Besides, the fibre density is obtained from the manufacturer. The main physical properties of HMWPE yarn are noted in Table 2-3.

Table 2-3 Main physical properties of HMWPE yarn.

Product Family	Linear Density (Tex)	Density (g/cm ³)	Elongation (%)	Breaking Strength (N)
Spectra [®] 900	135	0.97	4.12 ± 0.01	350.69 ± 6.13

Figure 2-1 shows the breaking tensile load for different twist values of HMWPE yarns. To reduce the hairiness during the weaving process, the yarns were twisted with different twist level. The tensile properties of these different twist per meter (tpm) of HMWPE yarns were tested by MTS Criterion Testing Systems according to the ISO 2062 (1993) standard [129]. It can be observed that at the weak twist level (0–50 tpm), the breaking tensile load increases with the increasing of yarn twist value. This phenomenon agrees well with the work reported in [28], which illustrated that the strength of high-performance fibre yarns can be improved by

a slight twist. The increase in strength is mainly due to an interlocking mechanism where the filaments are held together by radial forces and frictions, which, in effect, enables a single fibre to fail more than once. However, the greater the twist value is, the less the maximum tensile load is. This means there is a decrease in the breaking strength of the HMWPE yarns after exceeding a certain value of twist (the critical twist, 50 tpm in the present case). As the yarn twist value increases, the inclination of the fibre to the axis of the yarn increases, while the strength of the fibre can withstand the axial force of the yarn. Moreover, if the twist of yarn is too large, the fibre stress distribution inside and outside the yarn will be uneven, which will aggravate the different times of fibre breakage. Therefore, the parameters of 50 tpm and “Z” twist were applied on the HMWPE yarns for the manufacturing of the 3DWIFs.

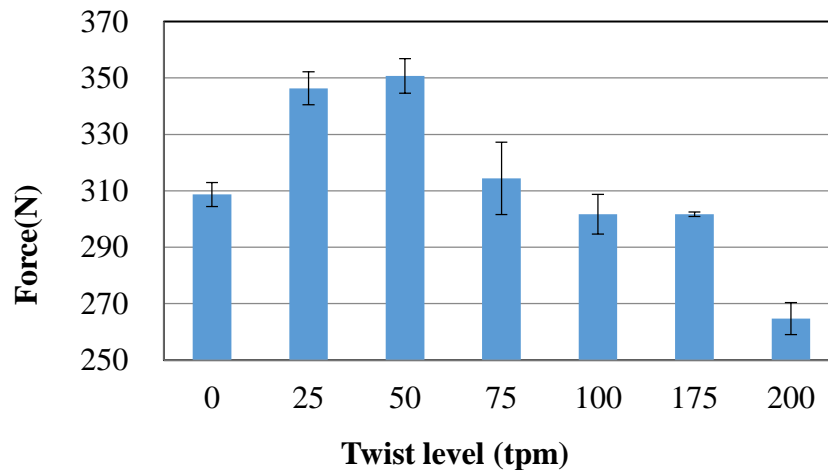


Figure 2-1 The ultimate forces of different twists HMWPE yarns.

2.1.3 Warping process

A binding warp yarn in Z direction, interconnected the weft yarns and stuffer warp yarns, is compulsory for producing 3DWIF following by the conventional 2D weaving process. Two beams have to be used for the binding warp yarn and the stuffer warp yarn, respectively, on the Suzuki warping machine (see Figure 2-2). According to the width of fabric and the weft yarn density, the number of yarns were calculated. The length of yarns were obtained by the estimated total length of fabric. Warp yarns were wound on the warping drum after the yarn is drawn from the bobbin. Then, all the warp yarns on the drum are withdrawn counterclockwise with the rotation of the spinning shaft to re-wind to the spinning shaft. At the end of winding, the yarns were transferred on a weaving warp beam in parallel and uniformly for binding warp yarn and stuffer warp yarn separately. These two beams has same length of yarns and yarn number.



Figure 2-2 The warping machine.

2.2 Manufacture of 3D Warp Interlock Fabrics

It is agreed that 3D woven fabrics can be manufactured on conventional weaving machines due to two reasons [56]. The one is that some of the needed 3D fabrics are not always beyond the capability of conventional weaving machines. The other one maybe because of the broad base of conventional weaving machines that is readily available for 3D fabric production. Better understanding of the weaving conditions to obtain these new types of fabrics are reviewed by Boussu et al. [130]. All the 3DWIFs were manufactured on the same automatic rapier weaving machine (Lindauer DORNIER GmbH, Rickenbach, Lindau, Germany) at the speed of 75 picks/min (see Figure 2-3). At present, the 3D weaving process in most looms can be divided into five loom motions, classified from start to finish as: warp beam letting-off, warp yarns tensioning, warp yarns shedding, reed beating-up, and fabric taking-up [131]. After the warp yarn shedding is open, the weft yarn is inserted by weft insertion of gripper. The yarns let-off in the two systems beams is different during the weaving process in that binding warp yarns beam controls a larger yarn let-off and stuffer warp yarns beam was on automatic let-off depending on the weft yarn density. The above weaving procedure was repeated continuously to make the 3DWIFs. The dobby loom provides ways to vary weaving patterns through the automatic control of individual heddles for manufacturing different 3DWIFs structures.

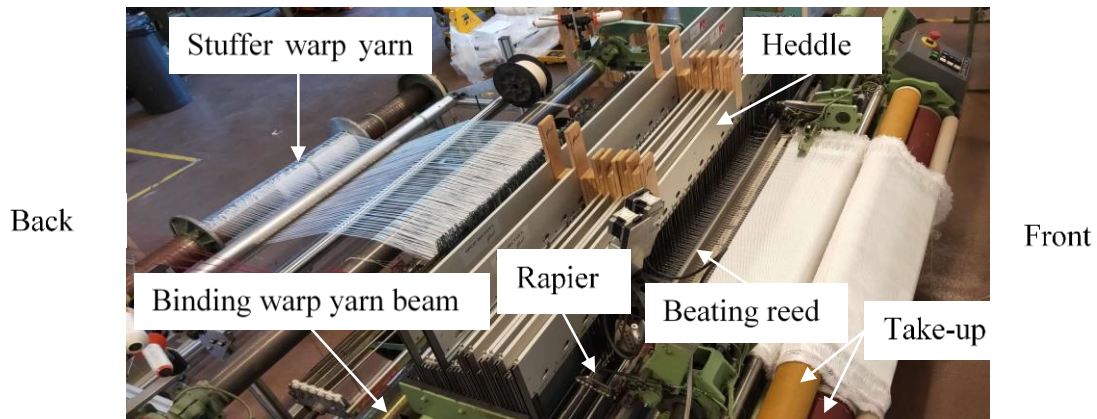


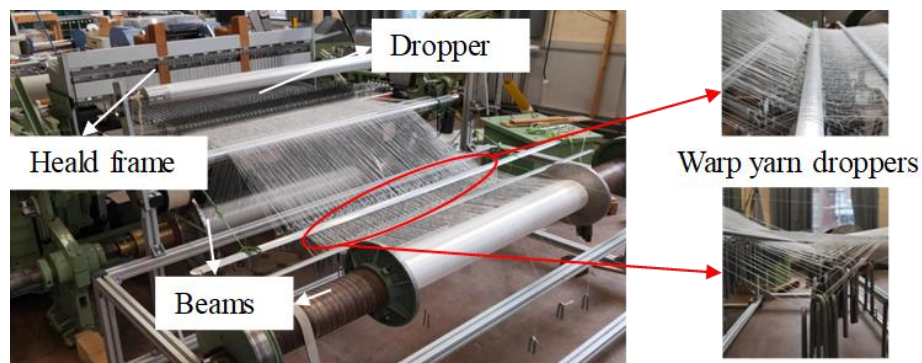
Figure 2-3 Different parts of dobbie loom.

2.2.1 Warp yarn tension adjustment

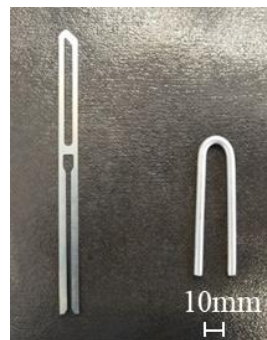
In the process of weaving, the tension of the yarn is essential to manufacture fabrics including the 3DWIFs. The tension of each warp yarn varies from stuffer warp yarn beam to binding warp yarn beam. Warp yarns with low tension or high tension lead to defects during manufacturing process. For example, there are loops on the surface of fabric with low warp yarn tension. While warp yarn with high tension has also influenced the final fabric which can cause fabric deformation, fabric hole and over extension gives a permanent change in the internal structure of fibres [132]. Besides, it may even cause the yarn breakage resulting in a loss in machine productivity and deterioration in the product quality and performance. Therefore, it is essential to pay intensive attention to the warp yarn tension during the weaving process for producing a high-quality fabric with good efficiency.

Yarn tension is the most important factor that affects weaving performance and fabric property [133]. Generally, warp yarn tension requirements will vary depending on fabric structure. Proper tension of the warp yarn is vital for forming clear shed for the insertion of weft yarn. Besides, the warp yarn tension is not same throughout the weaving cycle, but will be affected by the different motions of weaving machine. The warp yarn tension is also necessary for holding the fell of the fabric in the correct pre-set position for obtaining the predetermined pick spacing of the fabric [134]. The warp yarn break as one of factors affect the performance and the efficiency of a weaving machine. The warp yarn breakage rate increases with the repeated fluctuation of the warp yarn tension during the weaving process [135].

Warp yarn droppers, serving as individual tension adjusters with ‘U’ shape per yarn, with a certain weight and smooth surface, are used for each warp yarns, as shown in Figure 2-4. The ‘U’ shape warp yarn dropper has larger quality ($25.03 \pm 0.07\text{g}$) compared with the traditional one ($2.7 \pm 0.02\text{g}$) (as shown in Figure 2-4 (b)). The specific installation method and position can refer to the schematic diagram (Figure 2-5). Warp yarn droppers are lifted by individual warp yarns thanks to its tension, as shown in Figure 2-5 (a), but the two adjusters next to each other will be staggered (Figure 2-5 (b)). It is relatively difficult for warp yarns droppers to slide back and forth and interfere with each other due to the two support bars. At the same time, when the warp yarn density is very high, friction between warp yarns and warp yarn droppers increases. No matter how large the yarn crimp is, the yarn tension can be controlled independently through individual yarn during the automatic weaving process, which is convenient for installation with time-saving and low-cost. Therefore, it is recommended to put on the dropper with more weight for each yarn and increase the space for it to move up and down. Thus, even though the fabric structure has been changed, the warp yarn tension can be adjusted automatically.

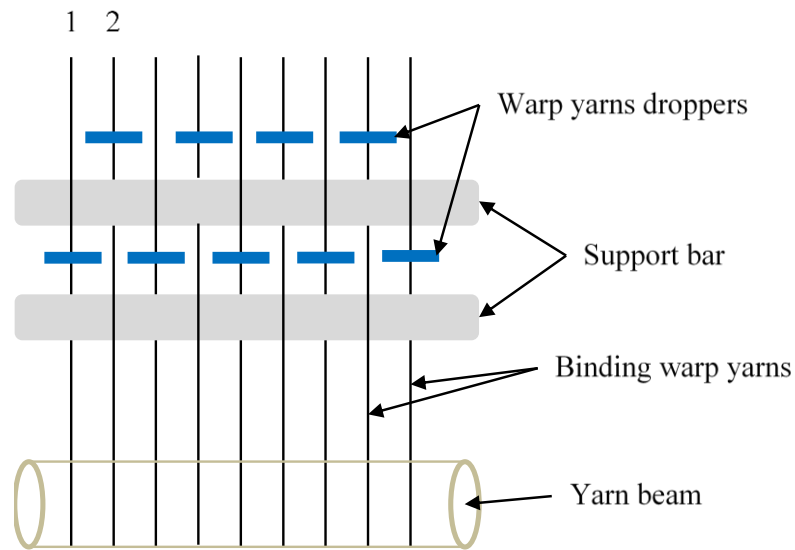


(a)

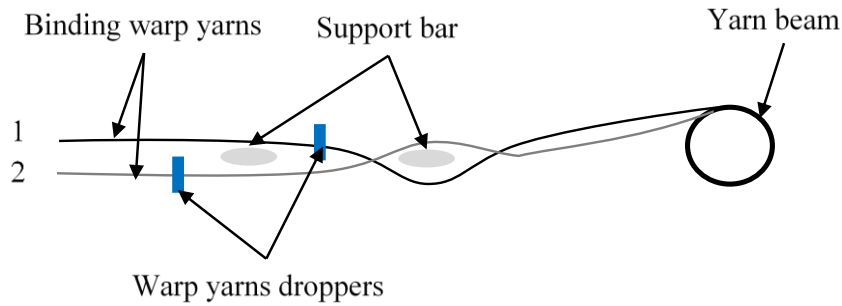


(b)

Figure 2-4 Improvement of tension adjustment (a) Installation method, (b) Comparison between the traditional dropper (left) and the ‘U’ shape dropper (right).



(a)



(b)

Figure 2-5 Schematic diagrams of the arrangement and position of yarn tension adjusters, (a) top view; (b) side view.

2.2.2 Process and fabrics parameters

For all the fabrics, the average thickness of the specimens was precisely determined using an electromagnetic sensor thickness measuring apparatus based on the standard NF EN ISO 5084. The area of presser foot is $2000 \pm 20 \text{ mm}^2$ and the level of compression force is $1 \pm 0.01 \text{ Kpa}$ for thickness test. The areal density values were measured according to NF EN 12127. Thickness of all the fabrics decrease from F1 to F5 fabrics. This implies that the F1 fabric has the least compact structure and F5 fabric the most compact one.

In the system of the 3DWIFs, stuffer warp yarns are selected by the heddles of the weaving loom and contribute to the longitudinal mechanical properties of fabric, and the binding warp yarns allow linking the various weft yarn layers in the thickness direction. The location of

binding warp yarn plays a role in determining the thickness of the fabric. It helps to maintain cohesion throughout the woven structure according to their density inside the structure and thus contributes to increase significantly the delamination resistance [22]. There is no doubt that tow waviness also influences the thickness of the dry fabric, through undulation frequency and amplitude, as described in [23]. Moreover, fabric in the thickness directly influences the fibre weight fraction of 3DWIFs, as all the fabrics have equal warp density (ends/cm) and weft density (picks/cm) values. Therefore, the fibre weight fractions (W_f) increase from the F1 fabric to F5 fabric, mainly due to the 3D woven structure, which allows better compaction for F5 fabric compared to other fabrics. In addition, there is only a slight difference between the five of them regarding the areal density values due to their different crimp values. The F5 fabric has the least thickness and the greatest fibre weight fraction, whereas the F1 fabric has the greatest thickness and the least value of fibre weight fraction. Because F5 fabric has larger binding step and the binding depth compared with F1 fabric under the same weaving condition. W_f is calculated by using the equation given below [47]:

$$W_f = \frac{W_{fabric}}{1000 \times \rho \times T} \times 100(\%) \quad (2-1)$$

where W_{fabric} is the areal weight of the fabric (g/m^2), ρ is the HMWPE fibre density (0.97 g/cm^3) and T is the thickness of the fabric (mm).

Table 2-4 shows the geometrical structure parameters and specifications of the five fabrics, including areal density and linear density of the yarns. All the fabrics have the same warp and weft densities and the thickness among each structure has a slight difference.

Table 2-4 Structural properties of 3DWIFs.

Fabrics	F1	F2	F3	F4	F5
Warp density (ends/cm)			10		
Weft density (picks/cm)			42		
Thickness (mm)	2.5 ± 0.3	2.1 ± 0.1	1.9 ± 0.1	1.7 ± 0.1	1.6 ± 0.1
Areal weight (g/m^2)	735.8 ± 36.5	720.0 ± 12.3	688.7 ± 13.2	710.6 ± 12.2	714.1 ± 9.6
W_f (%)	30.3 ± 1.5	35.3 ± 0.6	37.4 ± 0.7	40.7 ± 0.7	46.0 ± 0.6

2.2.3 Yarn damage study

Damages to yarns during the weaving process can lead to a severe loss of mechanical properties in the final woven fabrics, which are caused by abrasion between fibres, and abrasion between yarns and the weaving loom components. An analysis, from yarn twisting to the warping and weaving was carried out to measure the loss of properties of warp and weft yarns. According to [29], the yarn from different system, including stuffer warp yarn, binding warp yarn and weft yarn could delineate the properties of the fabric. It is very important to understand the effects of different yarn composition inside the fabric and the production process while producing 3DWIF on the yarn damage [136], which could give a better insight for producing the intended fabric with less fibre damage and better mechanical properties for the final material solutions. Thus, the current section aims to investigate the effects of yarn preparation and weaving on the yarn damage and its mechanical performances.

2.2.3.1 Tensile tests of the yarns

The yarn at the different stages of the twisting, warping and weaving preparations till to the fabric stage has been carefully drawn and tested. The warp yarns were obtained by moving the weft yarn from the fabric in the length of 300 mm in warp direction using the needle. The binding warp yarn and stuffer warp yarn were distinguished by the fabric structure at the same time. Besides, the same method was used to get the weft yarns. Tensile test of the individual yarn specimens was performed by MTS Criterion Testing Systems based on the NF EN ISO 2062 standard with a tensile speed of 50 mm/min [136]. Each test has been done ten times for better results repeatability. The nominal distance between the two adapted clamps of the tensile testing machine to maintain the yarn was 200mm. Besides, resin was used on both sides of the yarn for better clamping of the yarns to limit their slippages. The testing process for each specimen was carried out until yarn fracture takes place.

2.2.3.2 Results and discussions

Figure 2-6 shows average force and force-extension curve between the yarn curve at the untwisted yarn and its comparison for the twisted yarns. As discussed in section 3.2.2, the twisting level of the yarn contributes to increase the tensile properties due to the involvement of fibre orientation and consolidation which leads to additional breaking resistance. The twisted yarn average extension at break was recorded with a slightly increase (around 0.21%) larger values as compared to the untwist yarn, which is due to the increased binding force among the

inside fibres after twist that can resist the slippage among each other inside the yarn structure. Besides, compared to the yarn at the bobbin and after the twisting process, an increase of maximum breaking load (42 N) has been observed.

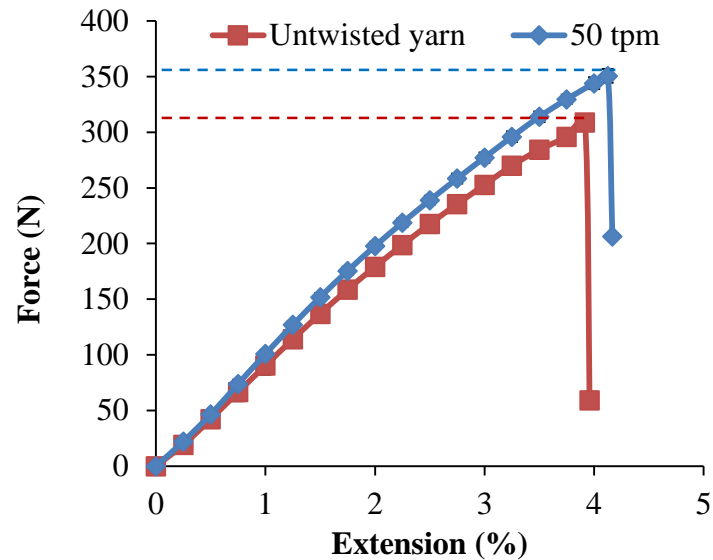


Figure 2-6 Effect of yarn twist on the mechanical properties of the yarn.

Figure 2-7 shows the effect of warping and weaving process on the mechanical properties of weft yarns of all the 3DWIFs, which has considered the average force of weft yarns from each layer of 3DWIF. As seen from the error bar in the Figure 2-7, there is no big different of tensile property from between different layers. In the initial stage of yarn extension, the slope of the curves at the beginning are very small because the crimped weft yarn was straightened at this stage. In terms of the weft yarn abrasion, the main cause of damage happened when the shed is opened during the weft yarns insertion. In general, the weft yarns of all the fabrics after weaving has larger extension at break than the twisted yarn. This can be due to the weft yarn passes through all the parts of the warping machine and the weft yarn feeding device which will result in the broken fibres [131]. Besides, the weft yarns being in contact with one row of warp yarn in each layer of the structure do not penetrate the entire structure and have few undulations [137]. It can be seen that all curves are coincided, which shows that maximum breaking force of weft yarns after weaving is reduced by 6.2% - 11.8%.

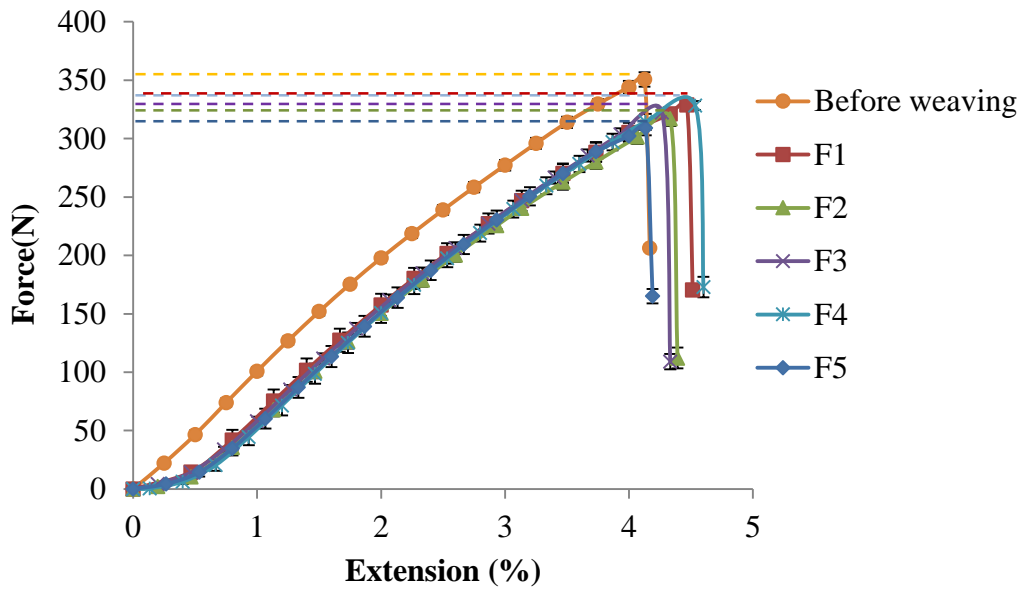
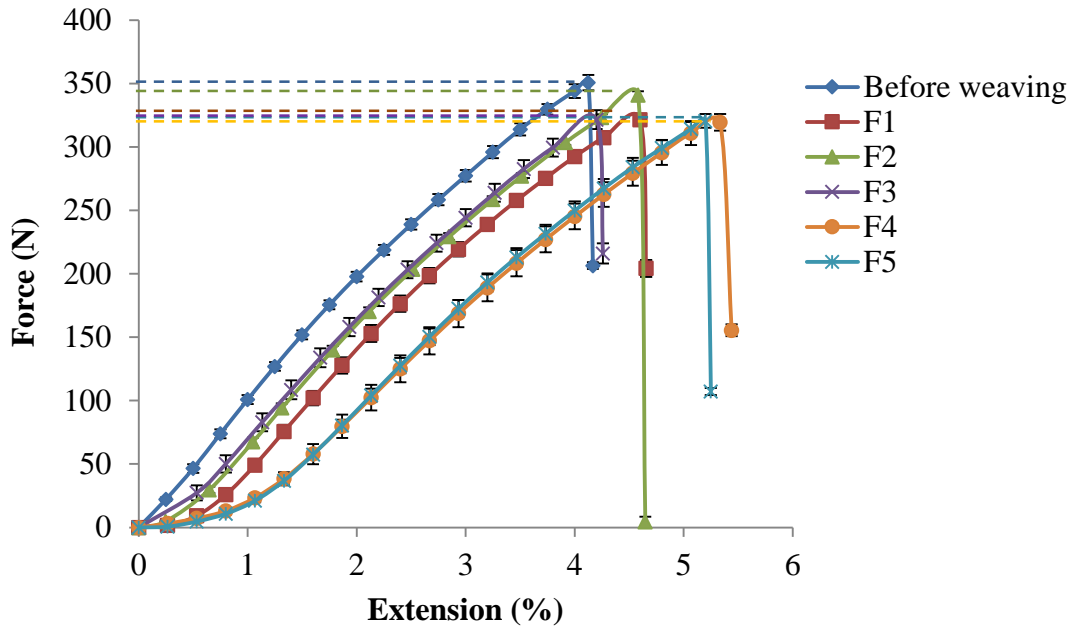
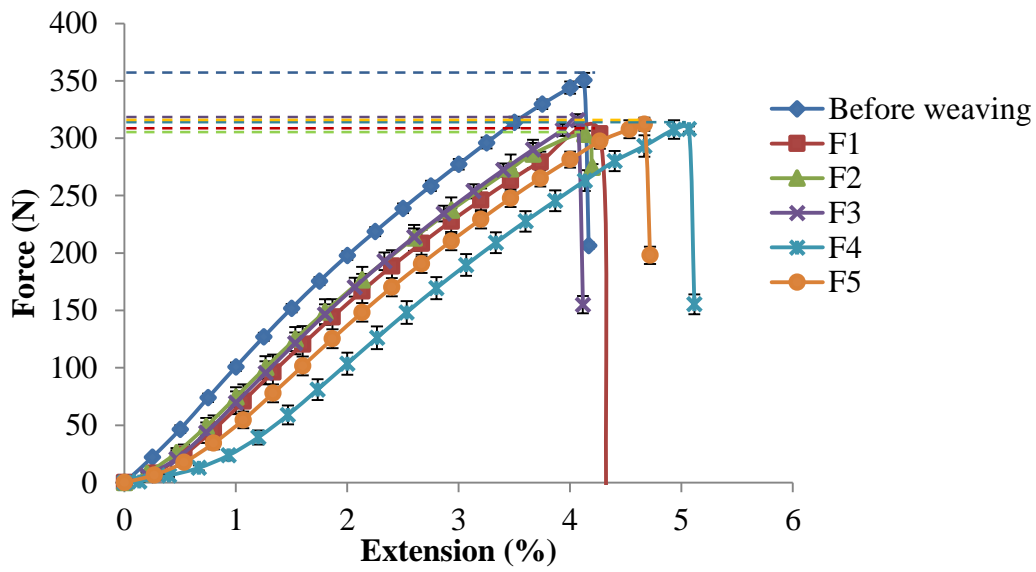


Figure 2-7 Effect of warping and weaving process on the tensile properties of weft yarns.

As shown in Figure 2-8, compared to the yarns after twisting, the binding and stuffer warp yarns of all the fabrics after weaving and extracted from fabrics have larger extension at the break. In terms of the binding warp yarn, the main causes of damage that happened in the warping and picking process that weft yarns was inserted by rapier. The yarn extension of F1, F2 and F3 fabrics are smaller than the F4 and F5 fabrics (Figure 2-8 (a)). Because the binding warp yarns of F1, F2 and F3 fabrics are joined layer by layer, while for F4 and F5 fabrics, the binding warp yarn are joined through the thickness of the fabric and such structures can have many undulations due to the crossing of warp and weft yarns. Moreover, the maximum tensile property of the binding warp yarns after weaving is reduced by 2.8% - 8.9%, and the stuffer warp yarn is reduced by 9.9% - 15.2%. It indicated that the stuffer warp yarns were subjected to higher abrasion damage in the weaving process that the yarn is forced to slide against a large number of components during weaving, such as the warp beams, tensioning devices, heddles, reed and rapier, which produce ultra-small scratches on the fibres.



(a)



(b)

Figure 2-8 Effect of warping and weaving process on warp yarns mechanical properties of 3DWIFs (a) binding warp yarns, (b) stuffer warp yarns.

2.3 Summary of Chapter 2

3DWIFs woven by high-performance multi-filaments yarns are developed and successfully implemented at the modified conventional weaving machine. To reduce their loss of breaking

force during the weaving process, the additional twist of high-performance multi-filaments yarns (50 twists per meter) was considered. The warp yarn tension of 3DWIF weaving process is uneven and an improved method has been introduced and adapted for adjusting the warp yarn tension of 3DWIF during the weaving process. From the technological and technical point of view, this method is very helpful for efficiently manufacturing the 3DWIFs by using conventional weaving technology. Besides, the structure and geometrical properties of the produced impregnated preform have also been compared. Moreover, the three systems' yarns abrasion during the weaving process was also studied. Based on the result, the average breaking force of weft yarns was reduced by 6.2% - 11.8%, and the yarn extension at the break of weft yarns is less than 1%. Compared with the binding warp yarns, the yarn strength degradation of stuffer warp yarns is 9.9% - 15.2% which may due to the friction among the yarns and yarns with the loom machinery part.

Chapter 3 Mechanical behaviour of 3D warp interlock fabrics

3.1 Introduction

The mechanical behaviours of 3DWIFs are still systematically unclear. In terms of such new materials, knowledge and experience are lacked and associated challenges are also emerged to predict and express their material properties. This can be attributed to the complexity of the different parameter combinations of the 3DWIFs. Besides, tensile behaviour analysis has been significant to understand the mechanical properties all the time. Such a study is needed due to the importance to optimise or create new 3DWIFs structures for composite reinforcement. Many parameters are involved in determining the tensile properties of the 3DWIFs. From the literature review, it can be seen that the tensile mechanical properties of 3DWIFs were studied from the following aspects of the materials used [30,76], the fabric structures [79], the weaving parameters [26,77,80,85], and so on. An investigation dedicated to check the effect of structure on the tensile behaviour of 3DWIFs has not been often studied. The design and manufacture of different structures 3DWIFs have been presented in Chapter 2. In this part, tensile properties and physical measurements are performed to understand their mechanical behaviour to their structures linked to the process and product parameters. The influences of the wrapping angles and the binding path in the 3D warp interlock structure are also discussed.

3.2 Materials and experimental set-up

3.2.1 Tensile property characterisation

The tensile tests of the specimen were performed by an INSTRON 5900 tensile testing machine with a 250 KN load cell following standard EN ISO 13 934-1. The rectangular samples with the surface dimensions 300 mm × 50 mm are proposed for the tensile characterisation on the dry fabric scale. To avoid the slippage between the fabric sample and the grippers during the tensile tests, an extra part of adhesive bonding on both ends with 50 mm has been added by using epoxy resin to strengthen the clamped part. As the non-polar and chemical inertness of HMWPE fibres surfaces inherently results in poor adhesion properties with most polymers [138–141], some little holes were made by sharp needles in both clamping fabric zone in the course of the preparation processes as shown in Figure 3-1 to increase the adhesion of the epoxy resin on HMWPE fibres surfaces and finally to ensure zero slippage observed in the test. Five tests for each structure have been done in both warp and weft directions. The nominal length between the two clamps of the tensile bench was 200 mm at a speed of 100 mm/min at room

temperature conditions (20°C and 65% HR). During testing, the force and the extension values were measured and recorded for all samples. Moreover, for each test, the tensile machine was checked and verified to avoid sliding between the sample and the grip.

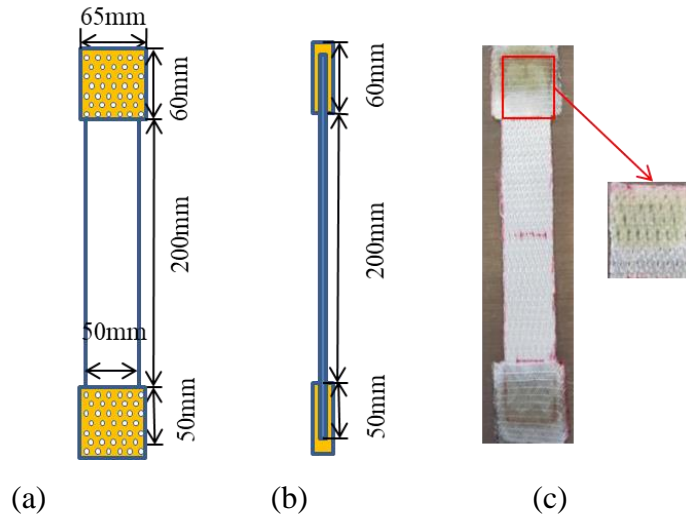


Figure 3-1 Methods of avoiding testing slippage by adhesive bonding on both ends with an extension of 50mm: (a) the front photographic and schematic view; (b) schematic view of side plan; (c) actual operation.

3.2.2 Yarn crimp in the 3DWIFs

The yarn crimp, namely undulations or waviness, was resulted by interacting with other yarns. To analyse the influence of the yarn's crimp on the tensile behaviour of the 3DWIFs, the yarn crimp tests according to ASTM D 3883 are proposed to the yarn samples (both warp and weft yarns) with 10 cm in length. These tests are carried out for ten yarns of each 3DWIF structure carefully extracted from the dry 3DWIF samples. Firstly, the initial length (length with waviness) of the yarn was measured with an accuracy of 1mm which is obtained by measuring the fabric dimension. Then, the yarn was fixed on one end of the crimp tester machine and unbending (straightened) it under 150cN and measuring its length. The waviness of the yarn is expressed as the mean difference between the straightened yarn length and crimped yarn length, as follows:

$$C = \frac{L_s - L_i}{L_i} \times 100 \quad (3-1)$$

where C is the yarn crimp (%), L_i is the length of initial yarn with yarn crimp (mm), L_s is the length of straightened yarn (mm).

3.3 Experimental results and discussions

3.3.1 Yarn crimp in the 3DWIFs

Table 3-1 shows the average crimp values of warp and weft yarns located in different layers for different dry 3DWIFs. Thanks to the identification of the different inter-ply positions of warp yarns as represented in Figure 1-2 of Chapter 1, it is possible to determine the level number of each binding warp yarns; considering its highest position inside the fabric: the level number of each binding warp yarns are inter-ply 0, inter-ply 1, inter-ply 2; the level number of each stuffer warp yarns are inter-ply 1, inter-ply 2, inter-ply 3. It is obvious that the binding and stuffer warp yarns will not have the same yarn crimp values due to their different types of length consumption which can prove that the force-extension curves of binding and stuffer warp yarn have similar trends with little difference in Figure 2-8 of chapter 2. In terms of F1, F2 and F3 fabrics, the binding warp yarn and stuffer warp yarn have similar levels of yarn crimps. This is because that the binding warp yarn and stuffer warp yarn were controlled by two different beams that former one is automatic and latter one is un-automatic. Thus, the actual result is deviated from the theoretical result. But in general, the stuffer warp yarn crimp is lower than the binding warp yarn crimp. Moreover, the weft yarn crimp is larger than both binding warp yarn crimp and stuffer warp yarn crimps in F1 and F3 fabrics. The reason may be that the temples were not used which resulted in the large weft yarn crimp during the weaving process.

It can be noticed that both warp and weft yarns crimp values of F4 fabric are the highest compared to others. However, the yarn crimps of F5 fabric have a great difference between binding (4.4 ± 1.06 %) and stuffer warp yarns (0.95 ± 0.44 %), crimp values of the binding warp yarns are almost 5 times larger than the ones of stuffer warp yarns. The possible two main reasons are the structure of F5 fabric and the yarns let-off difference of two warp yarns beam. The F5 fabric with angle/through-the-thickness structure shows that the binding warp yarns crimp values are higher than the corresponding stuffer binding warp yarns with lower yarn crimp values. It can be seen from the cross-section weft yarns view in Table 2-1 that binding depth and binding step of binding warp yarns in F5 fabric are high. Following the increase of binding depth from F1 to F5, the yarn crimp values of both binding and stuffer warp yarns

generally increase. Because of the larger binding step ($X=4$) and binding depth ($Y=4$) in the structure of F4 and F5 fabrics, these two structures' fabrics show higher yarn crimps than the other three structures' fabrics. The error of average binding warp yarn crimp in F5 fabric is large because of uneven warp yarn tension during the weaving process. The value of stuffer yarn crimps in F4 fabric are large than other fabrics because the stuffer yarn beam is not controlled automatically and there was too much feeding of stuffer warp yarns.

Besides, weft yarn crimp is almost the same for F1, F3, and F4, F5, respectively. The F2 fabric shows a slightly lower degree of undulation in weft tows. This lower crimp in the weft direction for the F2 fabrics does not affect the decreasing trend of total areal weight that decreases with the binding depth of warp tows, from F1 to F5 fabric. The micro-observation of the weft cross-section can highlight the binding warp yarn evolution inside the fabric structure, shown in Table 3-1.

Table 3-1 Average crimp values of all warp and weft yarns for all the 3DWIFs.

No. of fabrics		F1	F2	F3	F4	F5
		Binding warp yarns crimps%				
Warp yarns	Inter-ply 0	0.9±0.8	1.3±0.3	1.0±0.5	5.8±0.6	4.4±1.1
	Inter-ply 1	1.2±0.4	1.5±0.5	0.9±0.6	-	-
	Inter-ply 2	1.2±0.6	1.5±0.5	-	-	-
	Average value	1.1±0.6	1.4±0.4	1.0±0.6	5.8±0.6	4.4±1.1
	Stuffer warp yarns crimps%					
crimps/(%)	Inter-ply 1	0.7±0.3	1.2±0.5	1.3±0.7	4.3±0.6	0.8±0.5
	Inter-ply 2	0.7±0.5	1.2±0.5	0.8±0.5	4.0±0.1	1.3±0.5
	Inter-ply 3	0.9±0.7	1.1±0.4	0.9±0.4	4.2±0.4	0.7±0.3
	Average value	0.8±0.5	1.2±0.5	1.0±0.5	4.2±0.3	1.0±0.4
	Weft yarns	Layer 1	1.2±0.3	0.8±0.5	1.2±0.4	2.0±0.9
Layer 2		1.6±0.3	0.9±0.5	1.4±0.5	1.8±0.5	2.1±0.7
Layer 3		1.8±0.6	0.7±0.3	1.1±0.4	1.8±0.6	2.0±0.7
Layer 4		1.4±0.6	0.6±0.4	1.4±0.6	2.0±0.8	1.7±0.4
Average value		1.5±0.4	0.8±0.4	1.3±0.5	1.9±0.7	2.0±0.5

Figure 3-2 shows the comparison of the single binding yarn cross-sectional shapes of F2 and F4 fabrics. There is a significant difference in the morphology between two binding warp yarns from different fabrics. The binding warp yarns in F4 fabric have important curvature and the wrapping angle is much larger than the one of F2 fabric. By contrast, the binding warp yarns in F2 are almost straight and have a small bend in the fabric, which is in accordance with the results noted in Table 3-1 because the binding warp yarns only interlace between two layers in F2 fabric.

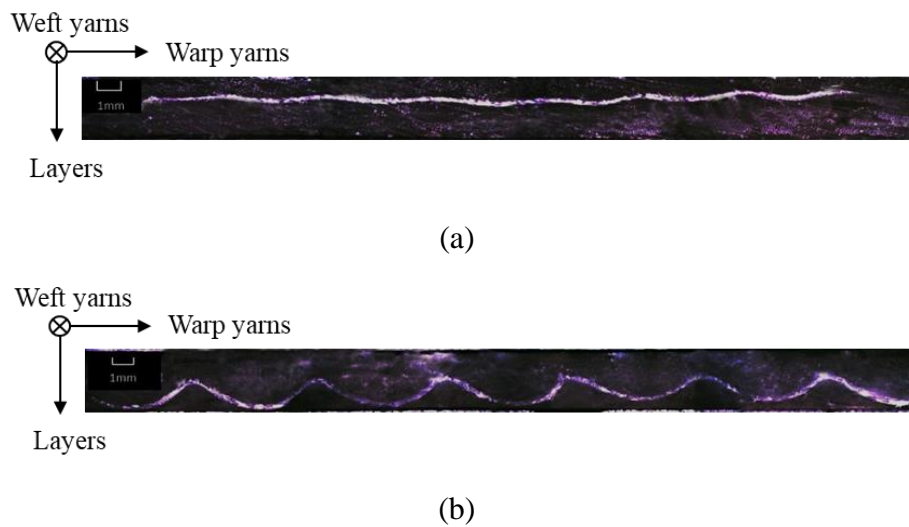


Figure 3-2 Micro-observation of a single binding warp yarn in (a) F2 and (b) F4 fabrics, cross-sectional view.

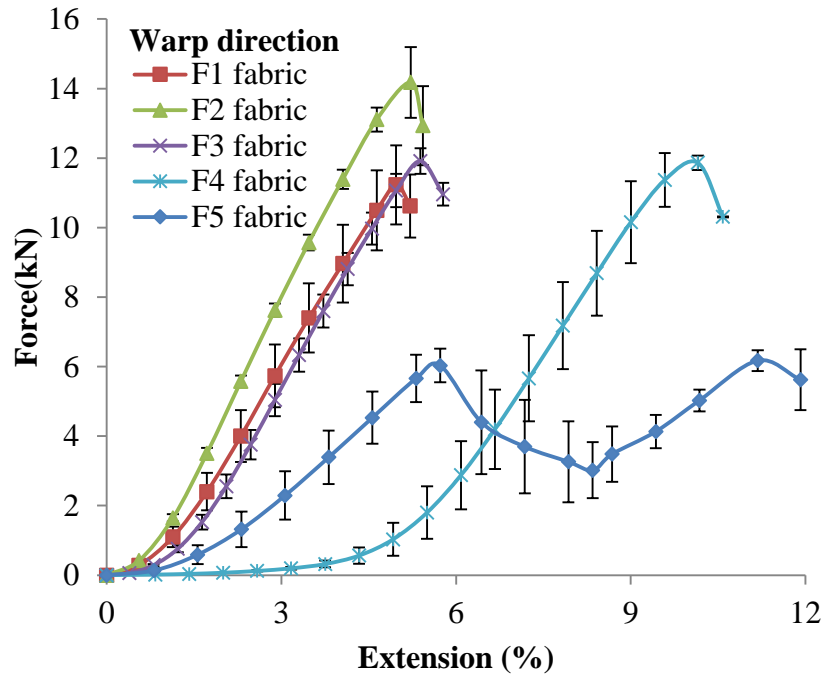
3.3.2 Tensile behaviour of 3DWIFs

The tensile properties of the tested 3DWIFs were measured as a function of both strain and damage accumulation. Figure 3-3 (a) and (b) show a comparison of the typical force-extension response of five 3DWIFs in the warp and weft directions, respectively. As for the tensile behaviour, a non-linear progression can be observed in both the warp and weft directions. The tensile curves can be generally divided into two parts. The first part is concerned with the alignment of yarns in the fabric structure that the extension starts to increase slowly with the small amount of increasing tensile loads. It can be remarked a very important yarns alignment in the tensile process of F4 due to the largest yarn crimps average values (see Table 3-1). The extension of yarns can be observed in the second part; the curves of the F1, F2, F3 and F5

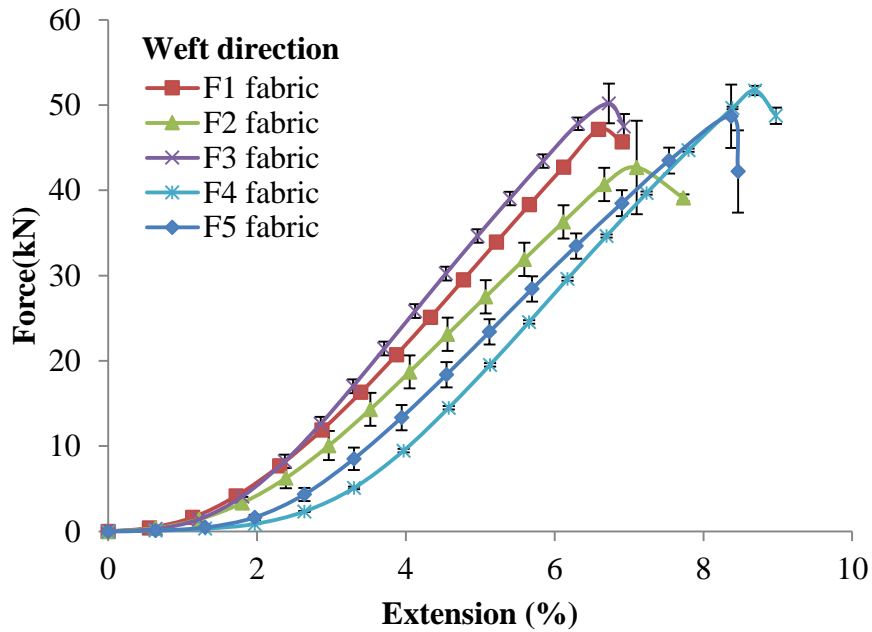
fabrics reveal linear progression where real straightening of yarn occurred with the rapid increase of tensile loads.

In Figure 3-3 (a), the slope of the initial linear region of the F1, F3 and F4 fabrics was very similar. The extension slope is slightly smaller than the one of the F2 fabric but more important than the two slopes of the F5 fabric. The F5 fabric exhibited two peaks in the extension stage in the warp direction, as the average yarn crimp values of binding warp yarns were several times larger than the yarn crimp values of stuffer warp yarns. As presented in the literature [76,77], the 3D-A fabrics have the same typical tensile response (two peaks) in the warp direction. In the F5 fabric structure, the number of binding warp yarns is the same as one of the stuffer warp yarns (25 ends). It leads to an identical peak and the same tensile slope in two extension stages. It is possible that the first load drop occurs exactly and the other part of the yarns moved relatively freely after one part of the warp yarns failed. The first peak indicates the strength of the stuffer warp yarns and the second peak indicates the strength of the binding warp yarns finally aligned after elongation of the 3D fabric structure. However, there were no clear and distinguish peaks in other fabrics since the yarn crimps were similar between the binding and stuffer warp yarns in these fabrics, as shown in Table 3-2.

Compared to the tensile results in the warp direction, the tensile curves in the weft direction of the different 3DWIFs are quite similar. Following a small yarns alignment stage, the linear yarns extension stage reveals a quasi-identical slope. Bandaru et al. [76] reported a similar type of tensile response in the weft direction of 3D angle fabrics. The tensile resistance was generally greater in the weft direction as compared to warp direction in the case of all fabrics due to the main difference between end and pick densities [30]. The weft density was about 4 times larger than warp density. Another reason is that during weft insertion through a shuttle, weft tows do not undergo similar deterioration as warp tows during the weaving process [142].



(a)



(b)

Figure 3-3 Tensile force / tensile extension curves of 3DWIFs in warp (a) and weft (b) directions.

As presented in Table 3-2, the failure strain was different in warp and weft directions. It could be noticed that the value of elongation in the weft direction is higher than the corresponding in the warp direction for all the tested fabrics, except for the F4 fabric, which is due to larger average warp yarn crimp than weft yarn crimps in F4 fabric. The F4 and F5 had higher failure

strain in the warp direction, indicating that higher failure strain can be achieved by the A/T or O/T types of 3DWIFs structures, which means that through-the-thickness structures contribute to the higher breaking strain. The F5 fabric shows the ultimate force of first peak because it has two peaks in the force-extension curve in Figure 3-3. Besides, these two peaks have similar value due to the same number of binding warp yarns and stuffer warp yarns.

Table 3-2 Breaking force (St) and failure value (ϵ) of tensile tests in the warp and weft directions.

	Parameters	F1	F2	F3	F4	F5
Warp	S _t (kN)	11.2±1.1	14.2±1.0	11.9±0.4	11.9±0.2	6.0±0.5
	ϵ (%)	4.97±0.01	5.22±0.01	5.39±0.01	10.15±0.01	5.73±0.01
Weft	S _t (kN)	48.46±0.1	42.7±1.8	50.3±1.8	51.7±0.5	48.7±3.7
	ϵ (%)	6.73±0.01	7.10±0.01	6.68±0.01	8.70±0.01	8.37±0.01

From a comparison of tensile response among these 3DWIFs (Figure 3-3), it was clear that the fabric architecture played an important role in the tensile behavior of fabrics. Table 3-2 shows the influence of fabric structure on the tensile properties including tensile strength and failure strain of different fabrics. F2 fabric shows the highest maximum tensile load in the warp direction and the lowest maximum tensile load in the weft direction. F4 fabric presents a weaker maximum tensile load at the highest strain than the other tested fabrics.

3.3.3 Inter yarn frictions during the tensile test of 3DWIFs

Compared to the weft direction, the tensile behaviour in the warp direction for 3DWIFs is more complex and interesting. During the tensile test in the warp direction, the work made through the clamping force can be described by Eq. 3-2 based on the energy conservation law for purely theoretical discussion in this section. W_m is the work performed by the tensile machine, W_e^B and W_e^S present the work concerning the extension of the binding and stuffer warp yarns, respectively. W_f^B and W_f^S are the work related to the friction effect of the binding and stuffer warp yarns, respectively, in the yarns alignment stage (the inter yarns sliding). Theoretically, the contact surface between the stuffer and weft yarns is very small (Figure 3-4) [76,143]. Consequently, W_f^S can be neglected in Eq. 3-2. Based on the work done by the force which is equal to the product of the force and distance of the object travels in the direction of the force,

the details are developed in Eq. 3-3. The average friction load of single binding warp yarn can be described by Eq. 3-4. Therefore, the average friction load of all binding warp yarns \bar{F}_f can be finally described by Eq. and 3-5.

$$W_m = W_e^B + W_e^S + W_f^B + W_f^S \quad (3-2)$$

$$\int_0^u F_m du = \sum_1^{n_B} \int_{u_B}^u F_e^B du + \sum_1^{n_S} \int_{u_S}^u F_e^S du + \sum_1^{n_B} \bar{f}_f \cdot u_B \quad (3-3)$$

$$\bar{f}_f = \frac{\int_0^u F_m du - \sum_1^{n_B} \int_{u_B}^u F_e^B du - \sum_1^{n_S} \int_{u_S}^u F_e^S du}{n_B \cdot u_B} \quad (3-4)$$

$$\bar{F}_f = n_B \cdot \bar{f}_f \quad (3-5)$$

where u (m) is the global displacement of the fabric (the displacement of the tensile machine clamps); n_B and n_S are the number of binding warp yarns and stuffer warp yarns, respectively; u_B (m) and u_S (m) are the sliding of the binding and stuffer warp yarns, respectively, in the yarns alignment stage; F_e^B (N) is the extension load of a single binding warp yarn; F_e^S (N) is the extension load of a single stuffer warp yarn; \bar{f}_f (N) and \bar{F}_f (N) are the average friction loads during the tensile test on a single binding warp yarn and all the binding warp yarns, respectively; n_B and n_S present the number of binding and stuffer warp yarns, respectively.

W_m is obtained by the data value of force-displacement from tensile test. Besides, the average crimp values of warp yarn of all the 3DWIFs shown in Table 3-1 were also used to determine the start of yarn extension stage. In the initial stage of fabric extension, the warp yarns were straightened at this stage and the main work is done by yarn friction (the compressions between yarns are ignored). W_f^B is calculated by multiplying the number of the binding warp yarns and the friction which is calculated later. In the second stage, when the yarn has started to slide in the fabric, the yarn is extended until the yarn breaks. Thus, W_e^B and W_e^S are obtained by multiplying the number of yarn and the value of force-displacement of average single binding warp yarn and stuffer warp yarn respectively.

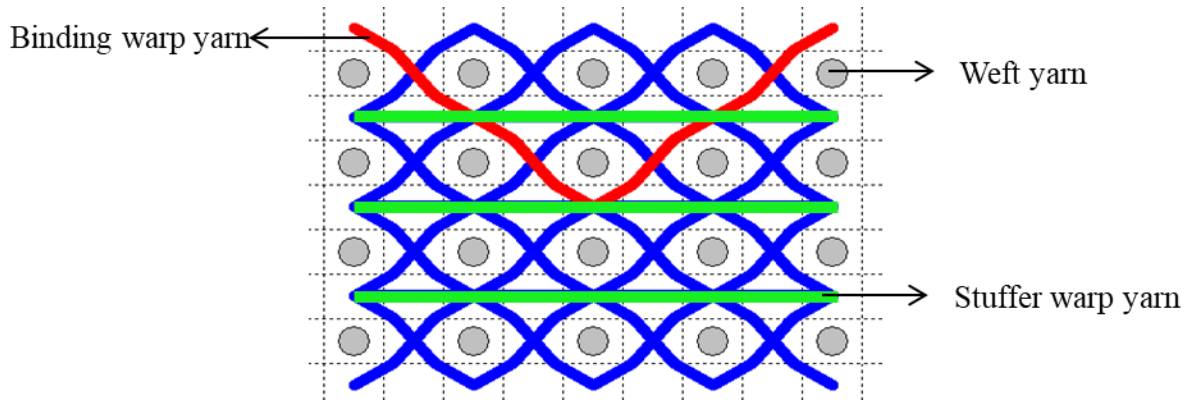


Figure 3-4 Example of the contact surface between stuffer and weft yarns (in the F1 fabric).

Figure 3-5 shows the average friction force (\bar{F}_f) on the binding warp yarns vs. the fabric extension curves for all 3DWIFs samples during the tensile test. The binding warp yarns friction load \bar{F}_f was calculated by the Eq. 3-5 according to the series of force and displacement data as mentioned above. Based on theoretical calculation results in Figure 3-5, it can be noted that the F2 fabric has the highest friction load during the tensile test, which has a good agreement with the tensile results of the fabrics shown in Figure 3-3 (a) that the F2 fabric has the highest breaking force. All the work done by friction force happened before 1.6% deformations except for F4 fabric. The F4 fabric has the largest deformation (4.5%) which is probably related to the largest yarn crimps in the 3DWIF with O-T structure. Therefore, it is clear that the work is done by binding warp yarns friction conducted in the crimp zone, which is displayed at the beginning of the 3DWIFs tensile tests. The trend of average friction load-deformation curves of the binding warp yarns during the tensile tests is similar to those shown in Figure 3-3 (a). The curve increased gradually at the beginning of the tensile test, the binding warp yarns are only in contact with the weft yarns without compression. After that, the weft yarns start to be compressed by binding warp yarns until it reaches the maximum. The binding warp yarns continued to be stretched until the strength reaches the maximum value and the fabrics were broken.

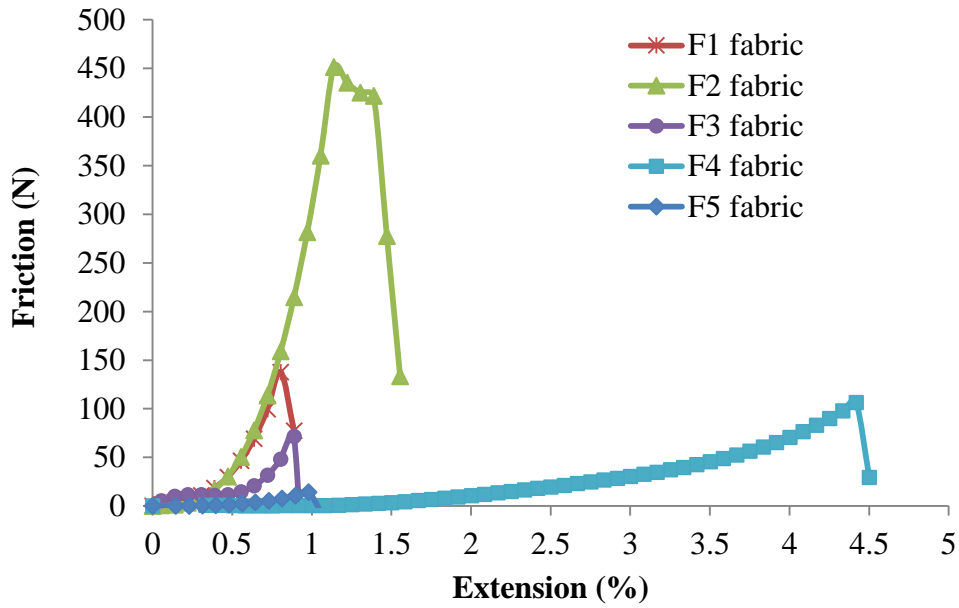


Figure 3-5 Average friction load-extension of the binding warp yarns during the tensile tests of five different 3DWIFs samples.

3.3.4 Geometrical model and the wrapping angle

Yarn interaction at the crossing points is the essential feature of woven fabric [144]. The weave style and yarn interlacing strongly influenced the tensile failure initiation of 2D fabrics [145]. Obviously, the yarn interlacing way that warp yarns cross under and over the weft yarns in 3DWIF is more complicated than in 2D fabrics. The arrangement of the yarn in the fabric can be mathematically described by Peirce's geometrical model [146–148]. The definition of yarn wrapping angle (θ), for the circular cross-sections and the flexible yarns, is shown in Figure 3-6 by using Peirce's geometrical model.

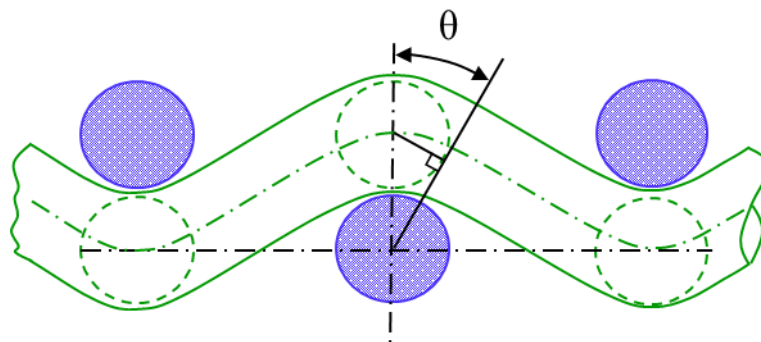


Figure 3-6 The definition of yarn wrapping angle (θ) in plain-woven fabric using Peirce's geometrical model.

In the present study, the yarn interlacing and yarn wrapping angle in 3DWIFs are described based on Peirce's geometrical model for discussing and comparing the binding warp yarn frictions during the tensile test. Figure 3-7 gives an example of a schematic diagram and geometrical model of yarn wrapping angles (θ_i) and linking points among the warp and weft yarns in the F2 fabric. It can be seen from the figure that this shape of the contact area between binding warp and weft yarns is the symmetrical structure. Assuming that the yarn is a cylinder, the yarn diameter (d) in mm can be calculated in the equation below [149]:

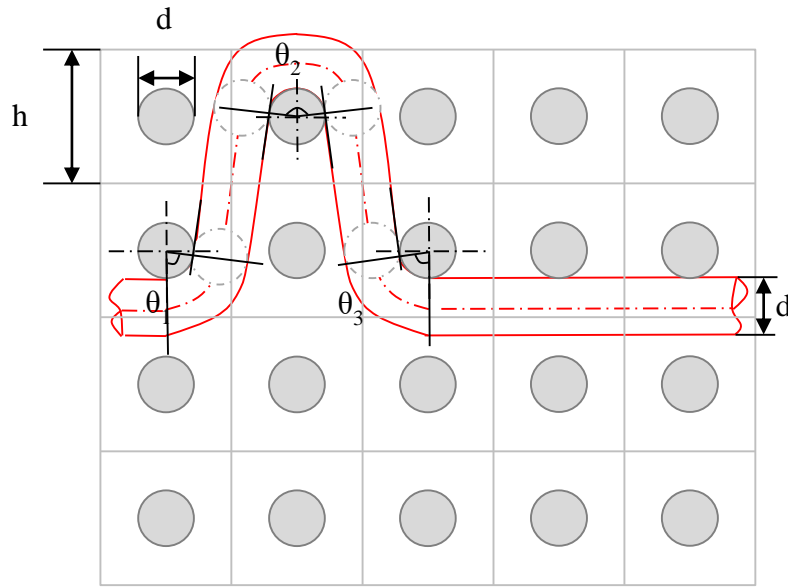
$$d = \sqrt{\frac{4T_t}{\pi\delta 10^3}} \quad (3-6)$$

where the yarn density is δ (g/cm³) and T_t is the linear density of the yarn in Tex.

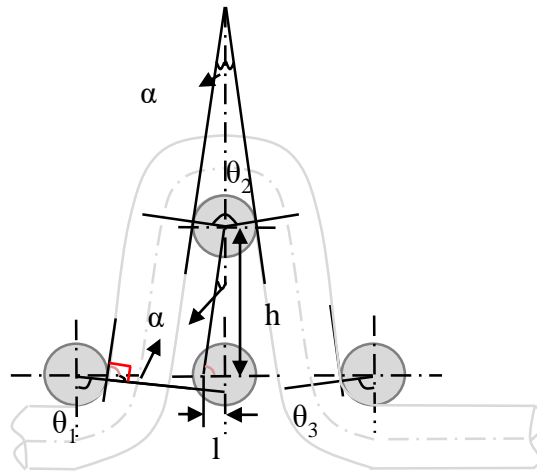
Figure 3-7 (a) represents a unit cell and h presents the height, which is around 1 mm since the weft density is 42 picks/cm and there are about 16 picks weft yarns per unit cell in 4 layers, as shown in Figure 3-7 (a). Therefore, there are some gaps or spaces between the binding warp and weft yarns. As shown in Eq. 3-7, α and θ_1 are the mutual complementary angles, 2α and θ_2 are the supplementary angles. In Figure 3-7 (b), wrapping angle θ_2 is twice larger as θ_1 and θ_3 , where θ_1 and θ_3 are equal to each other. Finally, the wrapping angle θ can be calculated by Eq. 3-8, where l is approximately $d/2$.

$$\begin{cases} \frac{\pi}{2} = \alpha + \theta_1 \\ \frac{\pi}{2} = \alpha + \theta_3 \\ \pi = 2\alpha + \theta_2 \\ \theta = \theta_1 + \theta_2 + \theta_3 \\ \alpha = \arctan \frac{l}{h} \end{cases} \quad (3-7)$$

$$\theta = 2\pi - 4\arctan \frac{l}{h} \quad (3-8)$$



(a)



(b)

Figure 3-7 Schematic diagram (a) and geometrical model (b) of wrapping angles (θ) and linking points among the warp and weft yarns in the unit cell of the F2 fabric.

According to the binding warp yarns interlacing in the fabrics and the geometrical model above, the wrapping angles of the binding warp yarns and the linking points between binding warp and weft yarns in different 3DWIF samples are calculated. The wrapping angle depends mostly on the yarn interlacing and influences directly to the contact surface between binding warp and weft yarns. Table 3-3 shows the wrapping angles and yarn interlacing shape of binding warp yarns in different fabrics per weave repeat. The warp yarn density (10.09 ± 0.13 ends/cm) and weft yarn density (42 ± 1.51 picks/cm) are similar among the tested five fabrics, which proved that all the samples (with the same surface dimensions $200 \times 50 \text{ mm}^2$) in this study have 25

ends binding warp yarns. It showed that the total wrapping angle is the sum of all the repeat unit cells in the fabric. It can be seen that the F2 fabric has the highest wrapping angle than other fabrics. In contrast, the F5 has the lowest wrapping angle. The rank of the total wrapping angle (F2 > F4 > F1 > F3 > F5) is very similar to the friction load discussed in Figure 3-5. The friction effects on the interface between binding warp and weft yarns depend on the normal force and also the contact surface-related directly to the total wrapping angle.

Table 3-3 The wrapping angles between binding warp and weft yarns and the yarn interlacing shapes in different fabrics.

Fabric	F1	F2	F3	F4	F5
Weft cross-Section					
Single binding warp yarn					
Cross-linking shape and wrapping angles (°)	0	80	0	90	0
	90	160	90	0	80
	0	80	0	180	0
	90		90	0	80
			90	0	
Total wrapping angle per unit cell (°)	180	320	180	360	160
Total wrapping angle in fabric (×360°)	656.3	1166.7	437.5	875	388.9

3.4 Summary of Chapter 3

To quantify the influence of binding path upon the strength transfer from tow to 3DWIFs, five different 3DWIFs were designed and manufactured with the same warp and weft densities. As one of the most important mechanical properties, the tensile properties of these 3DWIFs were experimentally characterised in both warp and weft directions. The inter yarn frictions in the tensile tests were analysed. Based on Peirce's geometrical model, the wrapping angles between binding warp and weft yarns in 3DWIF structures were calculated and the influence of these angles on the tensile property was also discussed. It can be noted that the warp binding path influences not only mechanical properties in the warp direction but also in the weft direction. The arrangement of weft tows i.e., their reorganisation and resultant fibre-less voids depend on the warp binding path and weft yarn arrangement. The binding depth of interlocking warp plays an important role in determining the efficiency of the fabric in the loading direction. Moreover, the wrapping angles/total wrapping angle of the 3DWIFs depend on the weave patterns, which are related to the inter yarn friction of 3D fabrics and have an influence on the tensile properties of 3DWIFs. Besides, the results also show that the 3DWIFs manufactured by HMWPE yarns have strong tensile strength which can be considered for further study and explored the stab resistance for protection material.

Chapter 4 An exploration on the stab-resistance of 3DWIFs

4.1 Introduction

Due to the restrictions imposed by firearm control legislation and more commonly used of knives in street fights and muggings [150], stabbings are still a persistent and worrying concern and growing life-threatening assaults to the policemen and security forces are of particular concern in European and Asian countries [2,151]. As stated in the literature review, the 3DWIFs, as soft materials, are essential for a range of applications, including protecting law enforcement and security personnel against stab attacks. Layers of 3DWIFs are connected together by a binding warp yarn to ensure greater cohesion [42,152], preserving the integrity of the entire structure. Besides, 3DWIFs revealed good mouldability and fewer wrinkle formations as well as other good mechanical properties [12], which can also be used as female body armour [13].

This chapter first describes the investigation of the classical stab resistance characterisation test that concerns a single-pass stabbing which was used in all of the relative studies. According to the references [153], the victims are suffering not only the single-pass stab wound but also repeated stabs, which might directly result in death. Repeated stabs or double stabs might occur to the same body armour at the same locations, which, to the authors' knowledge, have not been thoroughly investigated in the literature. Therefore, a unique methodology is proposed for characterizing the repeated stab resistance of HMWPE 3DWIFs as polymeric protection materials, which supplements the lack of testing methods on the classical stab test. Moreover, the results of single-pass stab vs. double-pass stab test response of multi-ply 3DWIFs, were compared.

4.2 Research methodology

The stab resistance test of the 3DWIFs specimens was conducted on a drop tower impact test machine according to the UK standard: HOSDB Body Armour Standard (2017) [154]. Figure 4-1 shows the schematic of a stab test device used in the present study to characterize the stab resistance. The principle of drop-weight impact [155] was used, as shown in Eq. 4-1. In order to establish the falling height required to generate stab energy, the formula outlined within Eq. 4-2 was arranged.

$$E_p = mgh \quad (4-1)$$

$$h = \frac{E_p}{mg} \quad (4-2)$$

where E_p is potential energy, m is the mass of the knife with the holder in kg, g is the gravitational acceleration and h is the falling height.

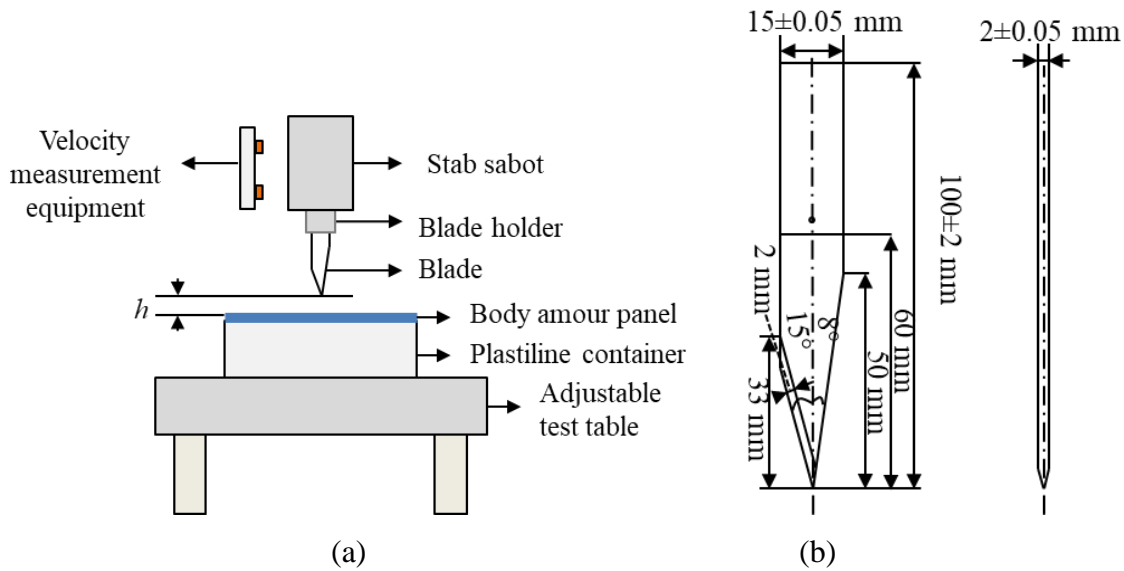


Figure 4-1 Schematic of a stab test device (a) General view and (b) Details of the stab blade.

The kinetic energy of the impactor can be adjusted by varying the height h , which is measured as the distance between the tip of the blade and the surface of samples laid on the Plastiline[®] clay, as shown in Figure 4-1 (a). The drop-weight m is 2.11kg which is the total mass of the system including stab sabot, blade holder and blade, Figure 4-1(a). HOSDB/P1/B sharpness blades shown in Figure 4-1 (b) were used in the test following the UK standard [154]. For ensuring the steady conditions, each knife was used a maximum of 10 times since the effect of repeated use of test blades is seen to be relatively small [156]. Besides, the Roma Plastiline[®] in the container was manipulated to avoid air gaps before the tests. Once the striker was located at the corresponding initial height to achieve the desired stab energy, it dropped in a free-falling process. The preliminary tests showed that with a falling height according to the standard of 1.16 m for the potential energy of 24 J, the knife penetrated all structures and the differences among them could not be observed. To find out differences between the different structures fabrics, tests were performed under the energy of 2.5 J in this research. Note that this energy is

lower than that considered in the standards of personal protection analysis; this is because, in this work, the multiple plies of 3DWIFs are analysed under low-velocity stab test and not on a real vest. To achieve the protection required by the standard, the improvement in fabric density and the number of layers can strongly affect the stab resistance [157,158]. Reiners [156] found that after evaluating the penetration depth there is no significant difference in the results between the sample sizes and there is no significant influence of the pretension onto the results. Specimens in this research had a size of 100 mm × 100 mm. In order to imitate the human body temperature for the practical application, the Plastiline[®] clay were warmed up to the temperature of 37.5 ± 0.5 °C before tests. According to the standard, tests were repeated three times for each sample [154]. Table 4-1 shows the conditions for stab resistance testing.

Table 4-1 The conditions for drop tower testing.

Parameters	Value
Strike energy	2.5 J
Drop mass (m)	2.11 kg
Drop knife type	HOSDB/P1/B
Drop height (h)	121 mm
Gravitational acceleration (g)	9.81 m/s ²
Dimension of the specimen	100 × 100 mm ²

4.2.1 Single-pass stabbing test

The conventional stabbing test concerns the stab-resistant characterization through the single-pass stabbing experiments. The ply orientation of the fabric panels (angle α) can be described by X (0°), Y (90°), Z orthogonal coordinate system, which depends on the angle α formed by the fabric rotating counter-clockwise and X-axis (weft yarn direction), (Figures 4-2 (a) and 4-2 (b)). Wang et al. defined that [159], when all the plies (all warp yarns in the fabric panel) are in the same direction, the panel is defined as aligned fabric panels. When the panels are oriented in different directions, the panel is defined as an angled fabric panel. As shown in Figure 4-2 (a) as an example, the schematic of four-ply fabric panel was made up of four single-ply 3DWIFs. When the blade is parallel to the weft yarn in four plies aligned fabric panels, the stab angle is 0° and it was marked as [0]₄ as shown in Figure 4-2 (a); on the contrary, when the blade is parallel to the warp yarn, the stab angle is 90° and it was marked as [90]₄. The panels

are oriented in different directions like [0/22.5/45/67.5], as shown in Figure 4-2 (b). For aligned fabric panels, the fabrics are stacked counter clockwise from the bottom to the top with incensement of the number of plies. In this study, single and multi-plyies of 3DWIFs are prepared and laminated as aligned stacked fabric panels and angled stacked fabric panels.

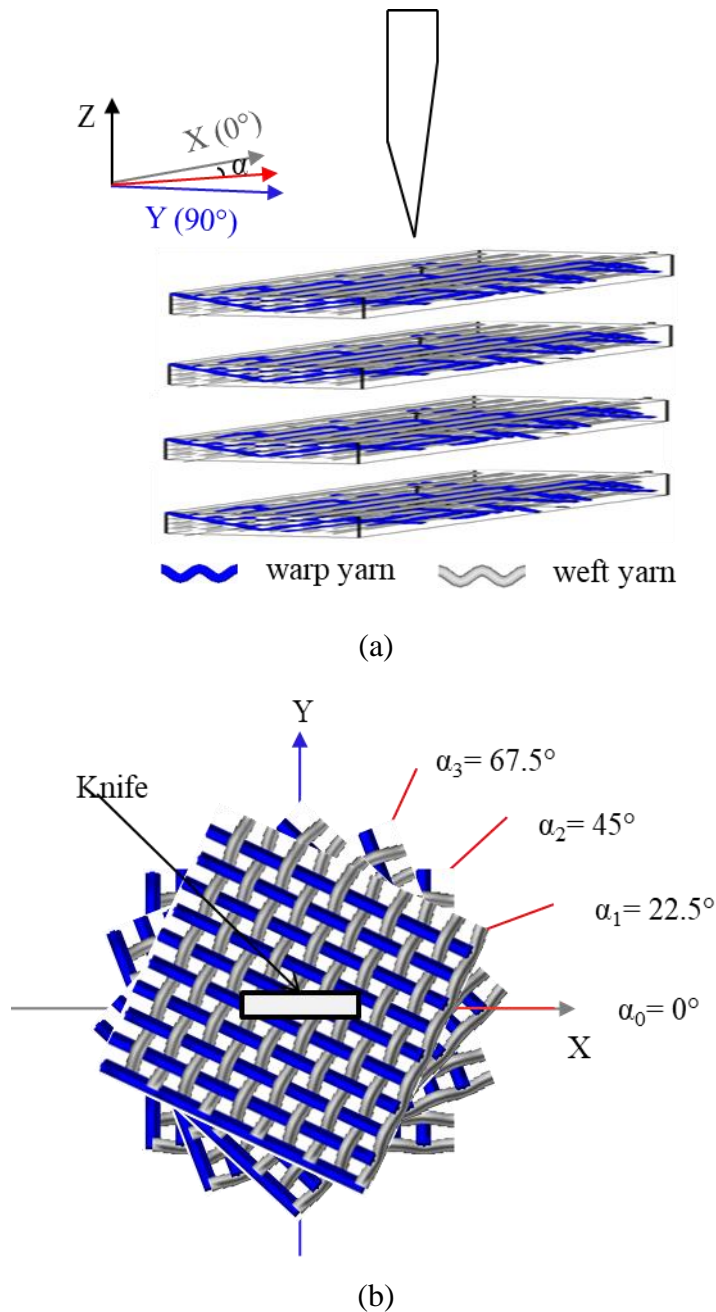


Figure 4-2 Schematic of the coordinate system of the ply orientations panels for the stab test: (a) aligned panels [0]4; (b) angled panels [0/22.5/45/67.5].

To quantify the stabbing deformation in both single-pass and double-pass stabbing tests, three stages of knife attack have been identified [9,120,160,161] and described in Figure 4-3. Stab-resistant materials and bulletproof materials have similar functions for protecting the human body from harmful projectiles. However, the mechanism of stab-resistant behaviour and bulletproof behaviour are not similar in dynamic behaviour and reponse of the protective material [2]. According to the low velocity of the impact of the blade, stab-resistant materials should simultaneously be able to stop penetration by sharp point and cutting by blade edge [160–163]. It is commonly accepted that textile stabbing involves three different steps: the initial indentation step, the second cutting step caused by a knife-edge, and the third step leading to the destruction of the assembled fibre bundle, as it is explained in a recent work of Hejazi et al. [164].

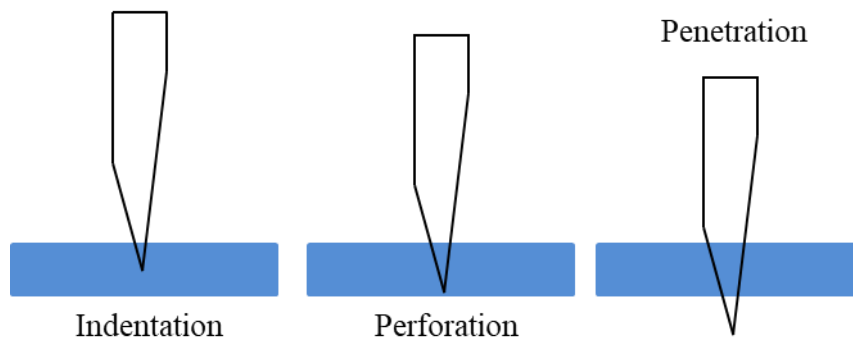


Figure 4-3 An illustration of the three stages of interaction between a knife and armour.

4.2.2 Double-pass stabbing test

As presented previously, most of the research studies are done on single-pass stabbing test which means that the material only was stabbed by the knife for one time. While when the first stab is failed or un-penetrated, the attackers will try the second time to attack the victim that they perhaps rotate their wrist which resulted in the different stab angles. According to this issue, double-pass stab test was proposed to simulate the multi-angle stabs.

Figure 4-4 shows schematically the single-pass stabbing experiments. The unclamped specimens were located on the top of a Plastiline[®] container and were aligned to face the stab in the centre of the sheets. The X (0°), Y (90°), Z orthogonal coordinate system is used in describing the stab angle (θ) of the fabric panels. One, three and six plies of 3DWIFs are

prepared and laminated. Since the blade is fixed in the machine, the fabric panel is rotated counter-clockwise to change the relative position of the blade and the fabric. For example, when the blade is parallel to the weft yarn, the stab angle is 0° .

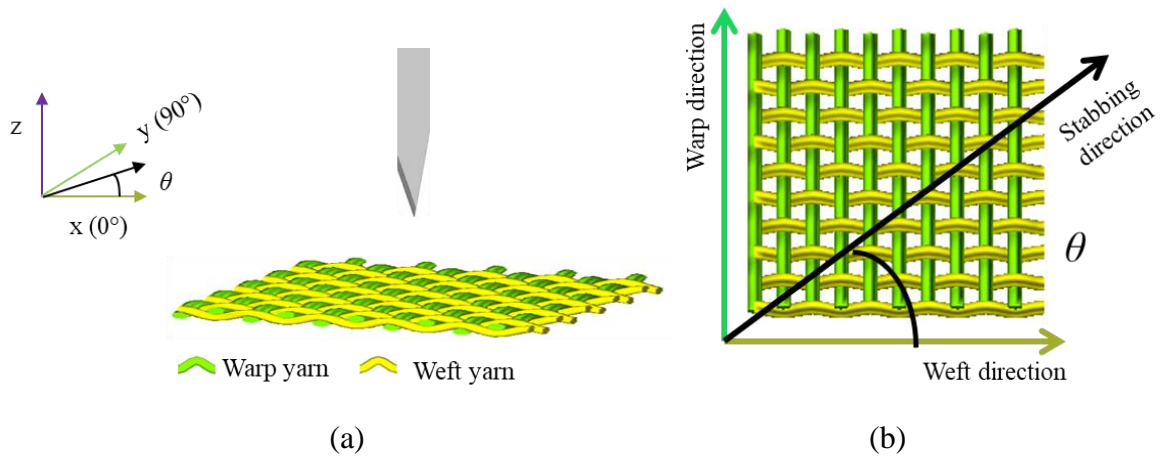


Figure 4-4 A schematic showing the coordinate system of fabric panel (a) 3D schematic diagram, (b) 2D schematic diagram.

The double-pass stabs with the same energy level as the single-pass stab will be proposed to study the effect on the stab resistance of the different architectures. Compared to the classical single-pass stabbing test, the double-pass stab test was done onto the specimen at the same location with the same blade and energy. As shown in Figure 4-5 (a) and (b), the blades are perpendicular to warp and weft yarns respectively in two passes. Moreover, compared to the first pass and keeping the same energy, the stab angle was changed in the second pass stab to simulate the multi-angle stabs (see Figure 4-5 (c) and (d),). It is because that the victim can be possibly stabbed in the same location but never through the same stab direction (with the same stab angle) considering the movement of the assailant and victim itself.

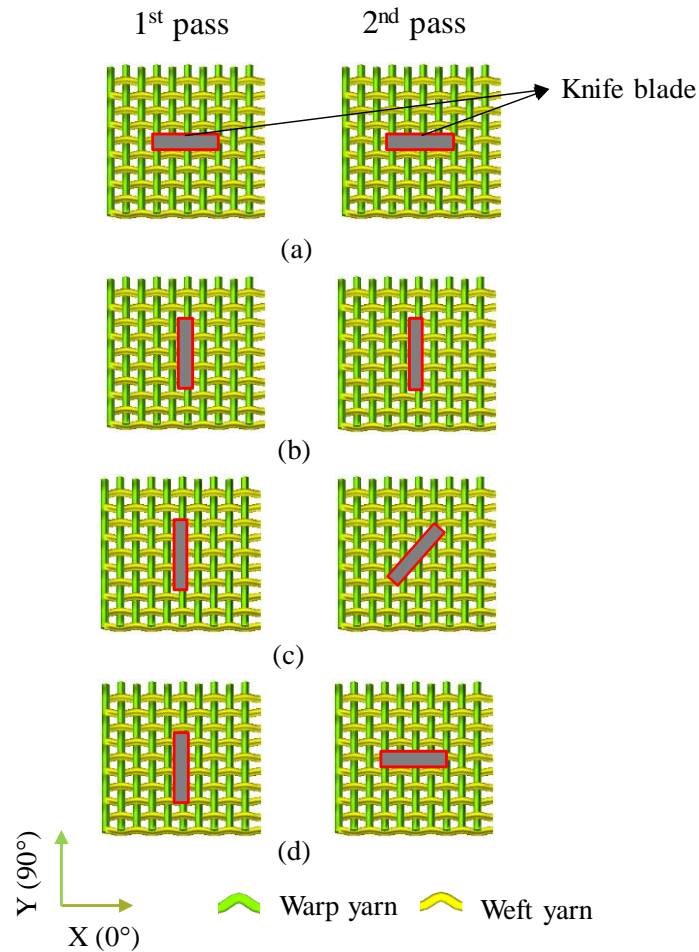


Figure 4-5 Double-pass stabbing tests (a) $0^\circ/0^\circ$; (b) $90^\circ/90^\circ$; (c) $90^\circ/45^\circ$; (d) $90^\circ/0^\circ$.

4.2.3 Measurement of the stabbing deformation

The knife-edge impact on the body protection armour brings out damages or fractures of the specimen that can be delineated in terms of the penetration depth and the number of fabric layers [112]. The stabbing depth can be divided into two parts as shown in Figure 4-6 (a): the depth of penetration (DOP) and the depth of trauma (DOT). The distance between the top tip and the surface of the fabric print mark in the silicone mould is defined as the DOP, which quantifies specially the stabbing trauma. Compared to the DOP, the DOT presents the distance between the surface of the fabric print mark and the bottom of the trauma. To accurately measure and analyse the DOP and DOT, the 3D scanning moulding is proposed in the present study as shown in Figure 4-6 (b) and 4-6 (c).

The RTV 181 poly-condensation silicone as a very resistant elastomer was used to recover prints of the complex shapes of the blade into the Plastiline[®] (see Figure 4-6 (b)). The silicone

with a density of 1.25 g/cm^3 was mixed with the catalyst at the ratio of 20:1. The silicone compound was filled into the trauma to obtain the prints of deformation. It is important to force out the air, by using the vacuum oven, to make sure that there are no air bubbles that emerge inside the silicone prints. Once the silicone print is obtained shown in Figure 4-6 (b), it can be scanned by a 3D scanner and then measured by SOLIDWORKS shown in Figure 4-6 (c). The 3D shape of the stabbing deformation can be observed and the DOP and DOT can be measured directly with errors less than 0.01 mm. The surface damaged area, as shown in Figure 4-6 (d), can be measured and compared based on the silicone prints directly. Moreover, the stab resistance was determined by the DOP of the blade beyond the 3DWIFs.

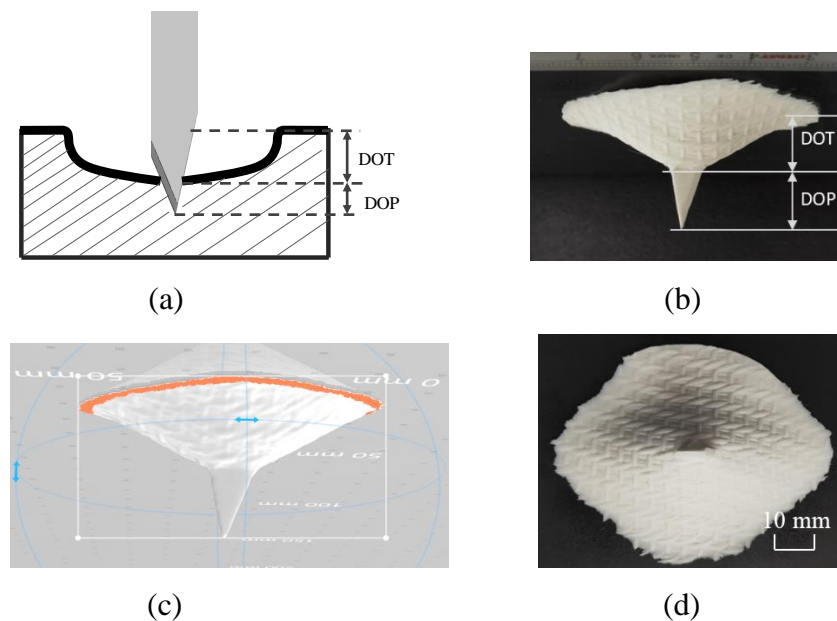


Figure 4-6 The stabbing deformation: (a) Definition of the DOP and DOT, (b) Silicone print of trauma, (c) 3D scanning and (d) Surface damaged area of silicone print.

4.2.4 Image-analysis of fabrics' deformation after stabbing test

The Structure From Motion as image analysis methodology is used to characterise the fabric deformation after the stabbing tests. As described in the study of Shen et al. [165], a stack of photographs, taken around the sample from different angles, were matched by the 3D location of features. Post-processing of 3D point-cloud of the sample via the Structure From Motion method is essential to remove some noise points and improve the quality of modelling with the help of the CloudCompare software. The size of the generated point-clouds was calibrated to

real dimensions. Then the differences between two point-clouds from before and after the stabbing test respectively based on Hausdorff distance can be computed [166]. The comparative example between real sample and model of F4 fabric was shown in Figure 4-7. The absolute distance in the Z direction (H) between two compared point-clouds (the measured points between before and after the stabbing test) is shown in Figure 4-7 (c).

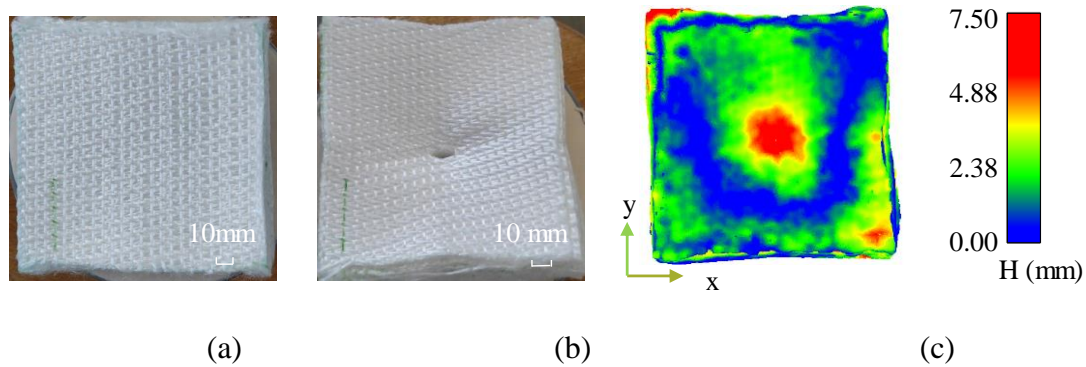


Figure 4-7 Comparative example between real samples and model, (a) real sample before stab test, (b) real sample after double stab $90^{\circ}/0^{\circ}$, (c) sample model after double stab $90^{\circ}/0^{\circ}$.

4.3 Experimental results and discussion

4.3.1 Single-pass results

4.3.1.1 Effect of fabric design on stab resistance

Figure 4-8 shows the DOP after the single-pass stabbing tests of different samples. A clear difference can be observed among the five architectures and different laminated plies against the knife (P1) impactor. The DOP of the impact knife into the backing material tends to decrease with the increase of panels number, this phenomenon can be confirmed by the study of Tien et al. [112]. No significant difference of DOP can be noted in the single-pass stabbing with one-ply fabric with stab angle of 0° . It is obvious that the five fabrics are penetrated completely by the blade and then the blade stopped to penetrate due to the knife handle, which is 60 mm from the tip of the blade and that was blocked by the fabrics. Therefore, the DOP is approximately equal to the length of the exposed blade for one-ply fabric. Following the increase in the number of plies, the DOP value is reduced. It confirms that the increase in fabric

plies has more effect on decreasing the penetration depth. Moreover, the smaller DOP can be observed in F4 and F5 fabrics than the other three samples (F1, F2, and F3 fabrics).

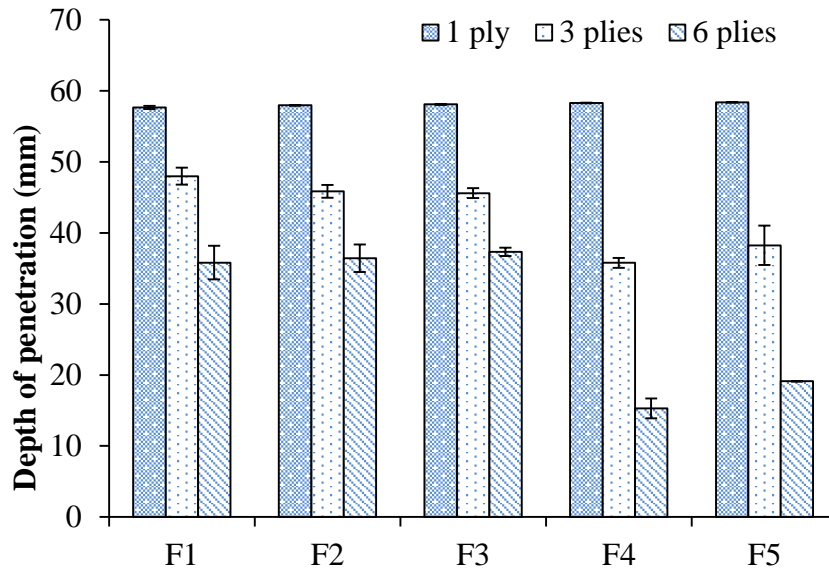


Figure 4-8 DOP of different aligned panels: 1 ply [0], 3 plies [0]3, 6 plies [0]6.

Although no obvious trend can be noted for the depth of trauma (DOT), it always remains at a weak level for F4 and F5 fabrics (as shown in Figure 4-9). Moreover, the asymmetrical V-shaped knife blade has the only one-side cutting edge with 33 mm length which is lower than the DOP value of all the fabric panels, except the six plies F4 and F5 fabrics with the stab angle of 0°. It is probably due to the effect that all the preforms are well penetrated to bring out an important DOP.

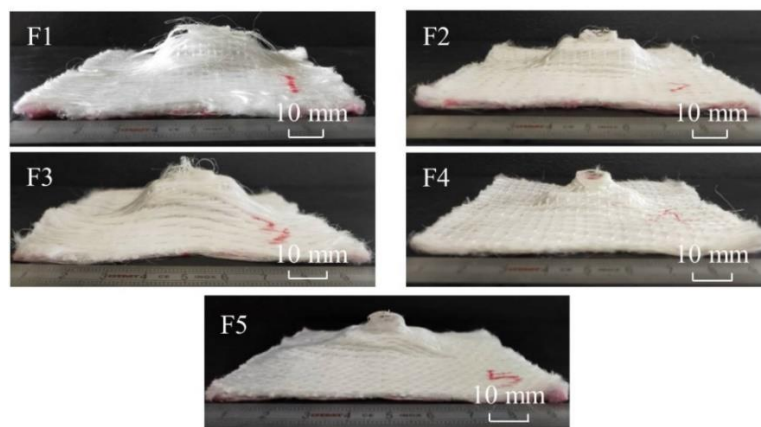


Figure 4-9 Observation of the stabbing deformation on the bottom surface in the single-pass stabbing test with 1 ply fabric panel.

The DOP per unit thickness is figured out (Figure 4-10) to analyse the influence of fabric thickness on the single-pass stab resistance. Regarding the single-layer samples (1 ply), as the DOP in each stabbing test is superior to 60 mm (the maximum value can be measured by the stab test device, discussed in Figure 4-8), the DOP per unit thickness is directly related to the fabric thickness. Thus, the DOP per unit thickness for 1 ply fabric shows different trend among these five structures compared with the counterpart of 3 plies and 6 plies. F4 and F5 fabrics have more important DOP per unit thickness than other fabrics due to their low layer height. By contrast, the influence of fabric thickness on the stab resistance can be reflected well in the stabbing of multilayered samples. An increase in thickness does make a qualitative difference to the results of DOP, F4 fabric with a low thickness (1.6 mm) has the same or smaller DOP per unit thickness compared to the other fabrics, which indicates a better stab resistance for the F4 fabric structure.

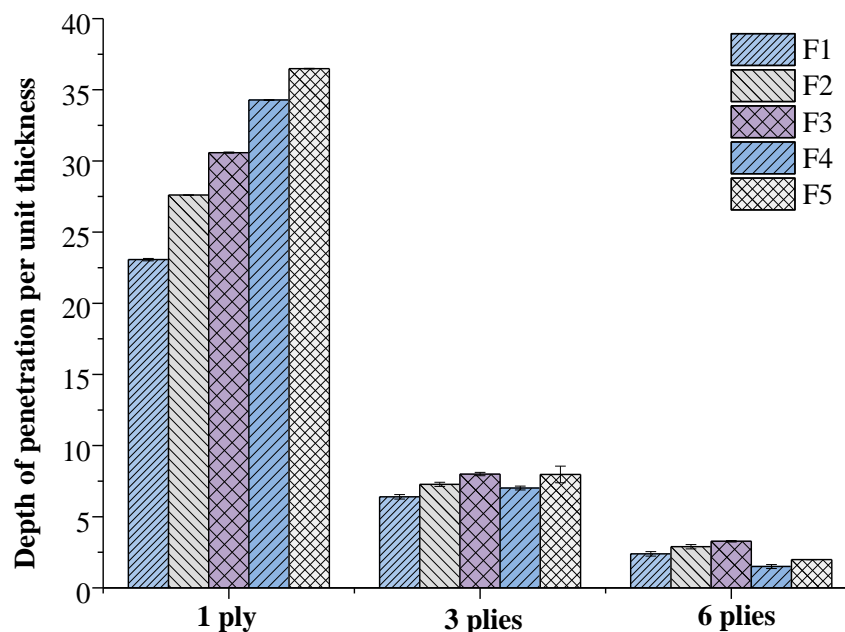


Figure 4-10 DOP per unit thickness in stabbing tests with the stab angle of 0°.

The stabbing deformation of the single-pass with the stab angle of 90° was carried out. The comparison with 0° stab angle is figured out for the preforms with 6 plies (Figure 4-11). Regarding the F1, F2, and F3 fabrics, the stabbing deformation (DOP) is smaller through 90° than 0°. By contrast, this stabbing deformation is identical in 0° and 90° which can be observed by the damaged area with stab angle of 0° and 90° (Figure 4-12). Although the sample exhibits

almost four times larger weft yarn density than the warp yarn density, the advantage of stab resistance through 90° is not significant than 0° which might be due to the structures of 3DWIFs. From the perspective of the thickness direction of the fabric, all the fabrics have four layers of weft yarns, which indicate that the weft yarns density in each layer of the 3D structure is approximately equal to the warp yarns density. Thus, the gap between the warp and weft yarns in each layer of the 3D structure is theoretically equal. This result shows that the yarn density is not the main influent factor. In our previous study [84], the weft yarns crimps are lower than the binding warp yarns crimps. Higher yarn crimps could result in a tighter fabric structure which prevents the knife blade from penetrating the yarn gap. As for the lower weft yarn crimps, it is difficult for the knife blade to stab on all the yarns near the blade and some yarns are likely to be forced out rather than cut. Compared to the F1, F2 and F3 architectures, the DOP is significantly lower for F4 and F5 fabrics in both 0° and 90° stabbing, in particular for F4 fabric (Figure 4-11). The F4 and F5 architecture exhibits the highest stab resistance against penetration when compared to the other panels due to their tighter fabric structure (Through-the-thickness interlock structure), as the densely-multi-layered or closely-spaced laminated preforms can dissipate the energy of an impact [167].

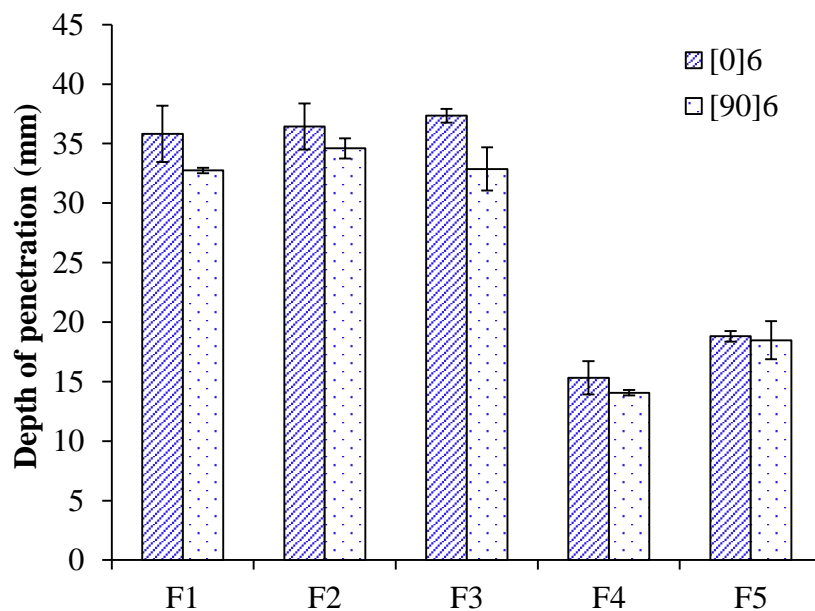


Figure 4-11 Comparison of DOP of 6 plies laminates from different fabrics in aligned panels $[0]_6$ and $[90]_6$ respectively submitted to stabbing tests.

The damage morphologies of 6 plies panels are displayed in Figure 4-12, which demonstrates stab damage areas of the F4 and F5 fabrics are lower than that of the F1, F2 and F3 fabrics. As shown in Figure 4-12, the dominant failure mechanism is fibre cutting in the middle of the stab position. While some fibres/yarns of F1, F2 and F3 fabrics were also extended and slipped rather than broken. The binding type of through-the-thickness causes tighter interlock structures than the binding type of layer-to-layer. Besides, in our previous work [84], the binding depths of binding warp yarns from these 3DWIF structures are lower than F4 and F5 fabrics, which indicated that F1, F2, and F3 structures were fairly loose. Then, in the second stage, i.e. cutting caused by a knife-edge, when there is no more space present for the yarns to extend further, the knife was almost locked up and started to cut the yarns. Comparatively speaking, the edges of cutting areas from F4 and F5 fabrics are relatively smooth. In the third step, F1, F2, and F3 fabrics were damaged with more assembled fibre bundles under the same drop-weight impact energy. It can be proved by the damage observations of the stabbing deformation on the bottom surface of 6 plies fabric panels after single-pass stabbing tests in the stab angle of 0° and 90° (Figure 4-12).

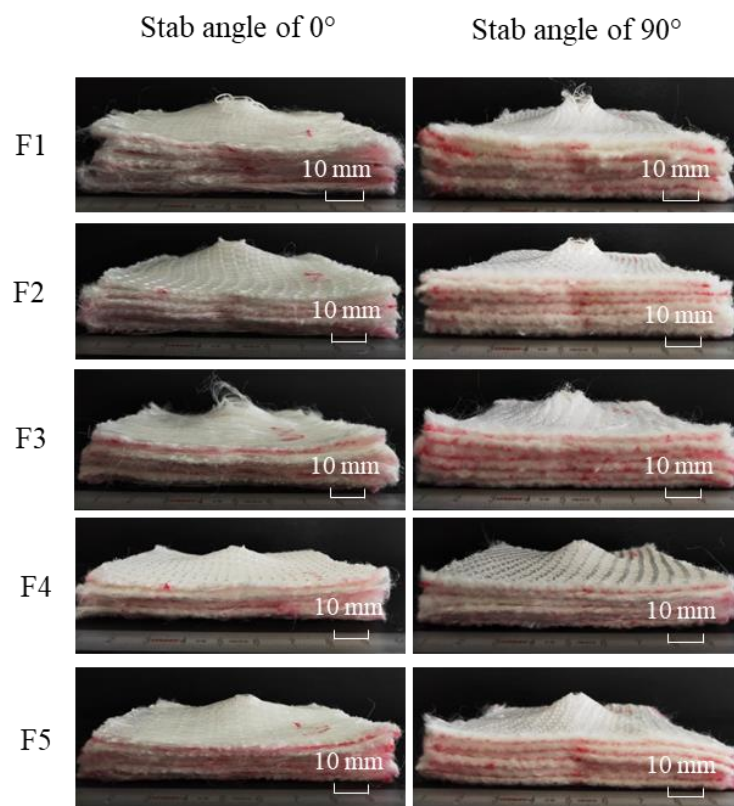


Figure 4-12 Damage morphologies of the stabbing deformation on the bottom surface of 6 plies fabric panels after single-pass stabbing tests in stab angle of 0° and 90° .

Figure 4-13 shows the silicone prints of aligned panels $[0]_6$ and $[90]_6$ stabs respectively, which illustrates the stab impact-induced fabric deformation from the impact centre to the boundaries. The blade resists to by the strained warp and weft yarns which constitute two directions. In previous studies, three stages of a knife attack have been identified, like indentation, perforation, and further penetration [9,161]. It means that in the initial indentation and perforation step, the fabrics occur with different deformations. In general, compared to the surface damaged area between aligned panels $[0]_6$ and $[90]_6$, the value of them are close to each other as shown in Figure 4-14. The surface damaged area of F4 fabric panels $[0]_6$ and $[90]_6$ are smallest. But, as shown in Figure 4-13 (a), it can be seen that the fabric deformation of all the fabrics in warp yarn direction is smaller than in weft yarn direction and the shape of surface damaged area is close to be rhomboid after aligned panels $[0]_6$ stab. The differences between the F1 and F3 fabrics with A-L structure versus other architectures can be observed from the deformation prints, where the deformations distribute from the stab impact centre along with weft yarns direction compared to other architectures. As for other structures, the deformations distribute from the stab impact centre along with both warp and weft yarns directions. In Figure 4-13 (b), when the aligned fabric panels $[90]_6$ were penetrated, the shape of surface damaged area is close to elliptical. But, overall, the deformation of all the fabrics in warp yarn direction is smaller than in weft yarn direction when aligned fabric panels were penetrated by aligned panels $[90]_6$. By comparing with other architectures, although the warp yarn density is lower than weft yarn density, the F4 fabric has the smallest deformation difference between warp and weft yarns directions, which may due to the dense fabric architecture and less yarn slippage before penetration. As a result, the F4 fabric with O-T structure had a better stab resistance and can distribute the stab force evenly with a less damaged area due to the relatively compact fabric structure.

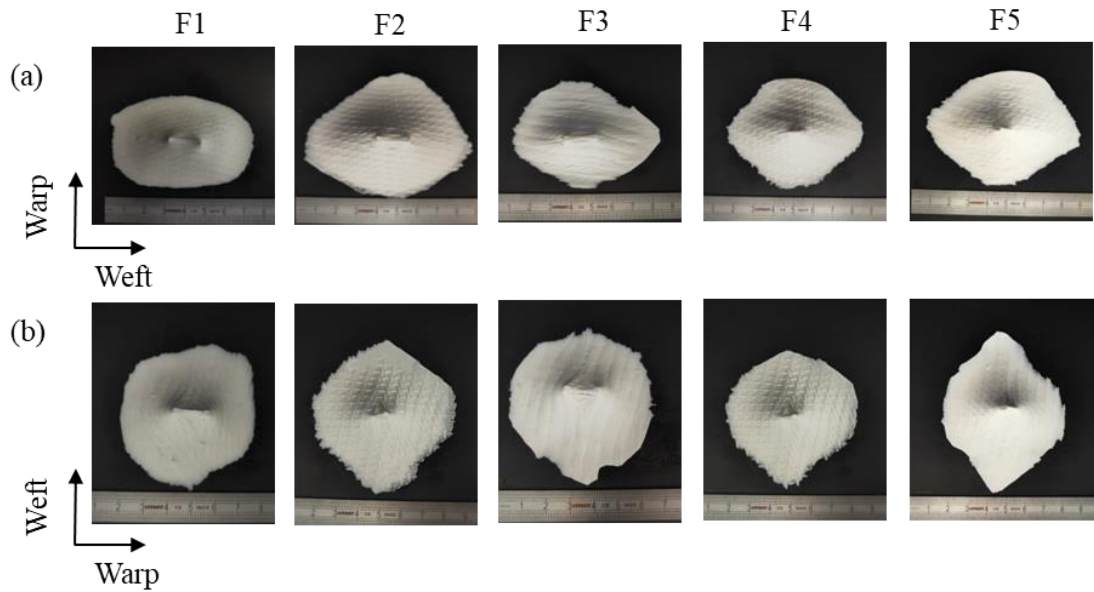


Figure 4-13 Silicone prints of 6 plies aligned fabric panels after stab tests: (a) aligned panels $[0]_6$ and (b) aligned panels $[90]_6$.

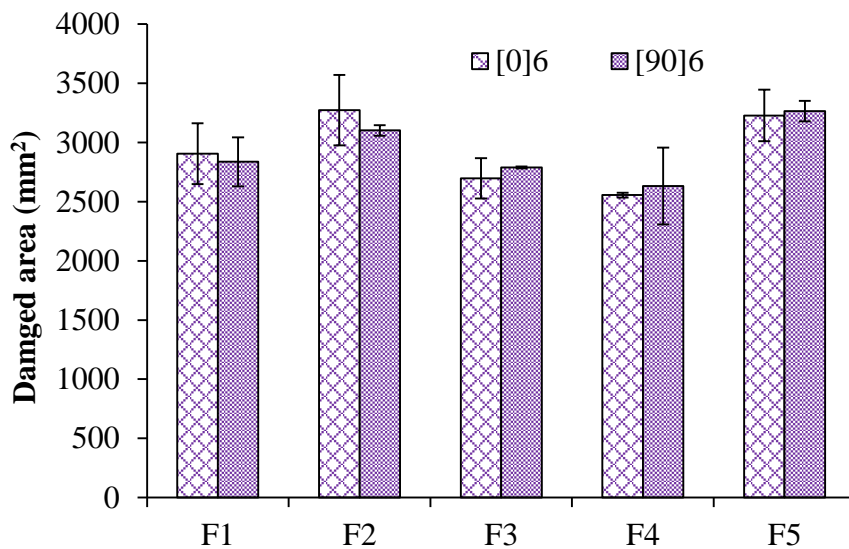


Figure 4-14 Surface damaged area after stab tests of 6 plies aligned fabric panels $[0]_6$ and $[90]_6$.

In order to have a better understanding and a global evaluation of stab resistance of different 3DWIFs, a single radar chart diagram is plotted and presented in Figure 4-15. Six main indicators of different 3DWIF structures (thickness, areal density, fibre weight fraction, and DOP with stab angle of 0°) are chosen. It can be noticed that F4 and F5 fabrics have smaller DOP values with less thickness and areal density, which shows that these two fabrics

(Orthogonal /Through-the-thickness and Angle /Through-the-thickness structures) have better stab resistance with lighter weight and less thickness. It can be also observed that F4 fabric (purple line in Figure 4-15) covers the smaller area than F5 fabric. In F4 and F5 fabric structures, the Z-yarns (binding warp yarns) run through the thickness direction to hold the stuffer warp yarns and weft yarns together to form a quite stable and tighter structure, which can absorb energy more efficiently compared to other interlock structures. Compared to F4 and F5 structures, the differences are the yarn crimps and yarn wrapping angles per unit cell of binding warp yarns that placed through the thickness direction to hold the weft yarns as shown in our previous study [84]. F4 fabric with orthogonal interlock structure has larger yarn crimps and yarn wrapping angles per unit cell, which might contribute to increase the yarn frictions and dissipate a portion of the total energy during the stabbing. Consequently, in single-pass stabbing, the F4 fabric with O-T structure shows the most desirable stab resistance performance.

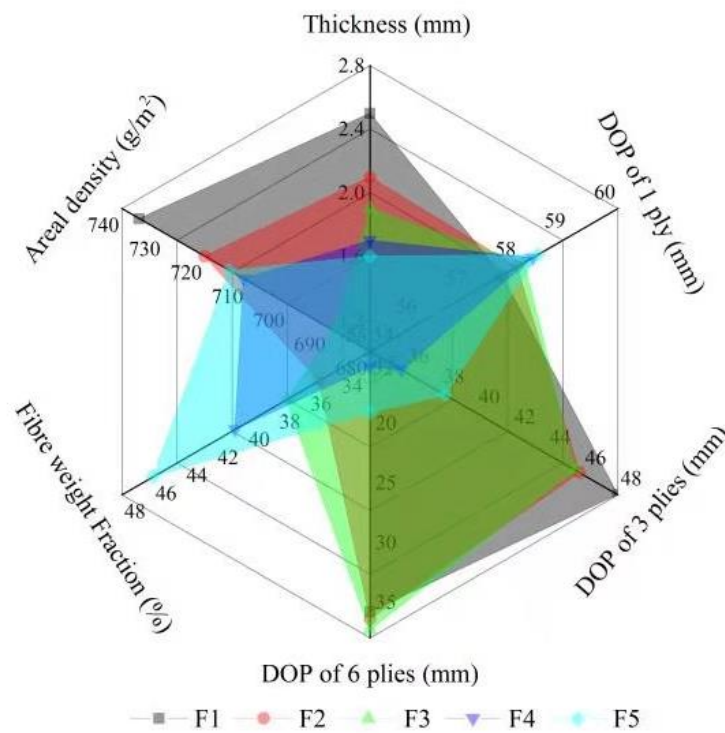


Figure 4-15 Summary of different parameters from different fabrics.

4.3.1.2 Effect of ply orientation on stab resistance

As discussed in the previous section, multiple plies of high-performance fabric are required to get enough protection against high-velocity impact. The stacking of multiple plies fabrics to make a single panel can be done in different ways. According to the research of Usman Javaid

et al. [168], the differences between the stab resistance at different penetration angles can be linked to the orientation and availability of yarns under the knife edge. In Figure 4-16 (a), the knife-edge traveling (K) for cutting yarns at different penetration angles is shown with colorful dotted lines. In this study, the 3DWIFs are unbalanced due to the weft density which is about 4 times higher than the warp density. In Figure 4-16 (b) and 4-16 (c), four layers of weft yarns can be seen from the 3D structure, which means that the weft densities in each layer are 10 picks/cm the same as the warp yarn density (10 ends/cm). Only the yarns cut by the knife are considered and the width of the blade is assumed as the same for each panel at each ply. There are five possibilities concerning the knife travel (K) for each consecutive yarn cutting, as shown in equations:

$$K_{\alpha} = D_{warp}d \cos \alpha + D_{weft}d \sin \alpha \quad (4-3)$$

$$K_{\alpha} = d \cos \alpha + 4d \sin \alpha \quad (4-4)$$

$$K_0 = d \quad (4-5)$$

$$K_{22.5} = d \cos 22.5^{\circ} + 4(d \sin 22.5^{\circ}) \approx 2.45d \quad (4-6)$$

$$K_{45} = d \cos 45^{\circ} + 4(d \sin 45^{\circ}) \approx 3.54d \quad (4-7)$$

$$K_{67.5} = d \cos 67.5^{\circ} + 4(d \sin 67.5^{\circ}) \approx 4.08d \quad (4-8)$$

$$K_{90} = 4d \quad (4-9)$$

where d is the width of the knife ($0 < d \leq 15\text{mm}$); the thickness of the blade has been ignored; K_{α} , K_0 , $K_{22.5}$, K_{45} , $K_{67.5}$ and K_{90} are the distance of knife travels when penetration angles are α , 0° , 22.5° , 45° , 67.5° and 90° respectively, D_{warp} is the warp density which is 10 ends/cm, D_{weft} is the weft density which is 40 picks/cm.

Therefore, when the penetration angles are 0° , warp yarns resist to knife cutting; when the penetration angles are 90° , weft yarns resist to knife cutting; when the penetration angles are 22.5° , 45° , and 67.5° , both warp and weft yarns offer the resistance simultaneously, although more resistance is offered by a yarn that is cut near to its transverse direction.

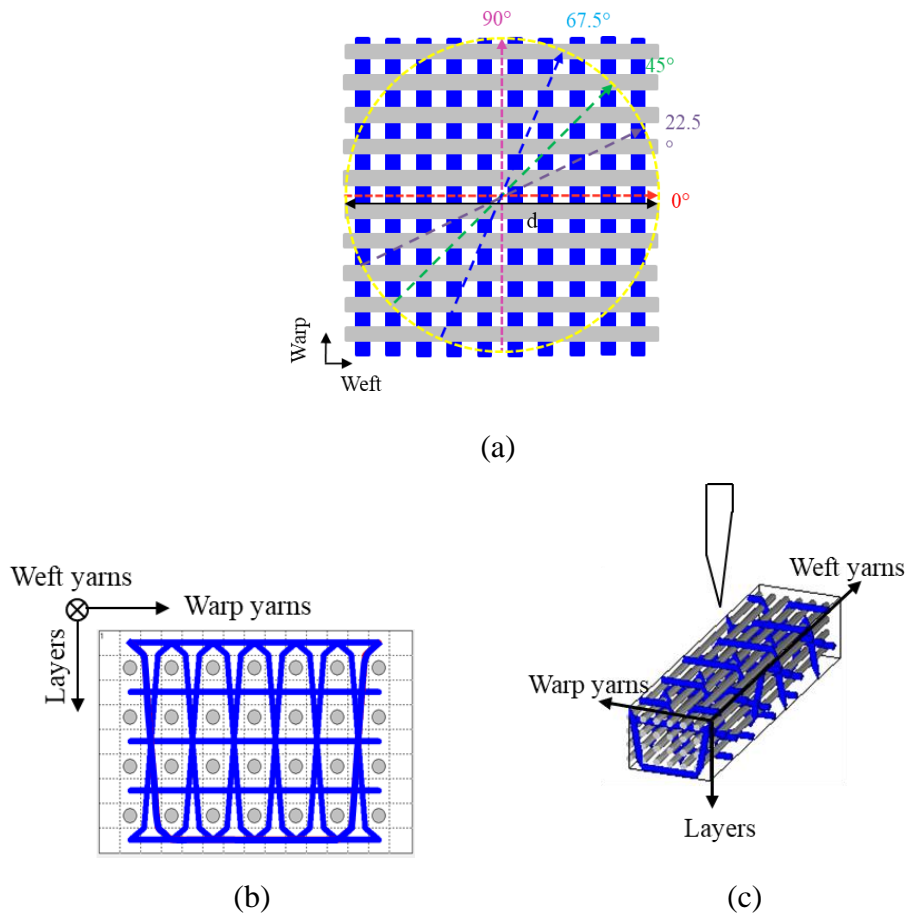


Figure 4-16 (a) Illustration of the path, knife-edge travels at different penetrating angles; (b) cross-section weft yarns view of F4 fabric, and (c) 3D view of F4 fabric.

Figure 4-17 shows the DOP of the 6 plies panels in different ply orientations via the stab resistance test with the same impact energy. In the case of the aligned multi-ply fabric panels, the panel construction with ply orientation of $[90]_6$ shows the lower DOP value by comparing with the ply orientation of $[0]_6$, which is same as the result shown in Figure 4-11. As shown in equations (3-9) above, the knife travel distance $K_{[90]_6}$ has the largest value, which means that more yarns are cut under the penetration angle of 90° at the same plies of panel. Although the knife travel distance $K_{[0]_6}$ has the lowest value, the DOP values are not the largest compared with other ply orientations. The main reason is that the warp yarns have larger yarn crimps than weft yarns. Perhaps it is helpful to improve the inter yarn friction during stab test. In the case of the angled multi-ply fabric panels, the panel construction with the layering sequence of $[0/22.5/45/67.5/0/22.5]$ generally shows lower DOP values than the layering sequence of $[0/22.5/45/67.5/0/0]$ which has the highest DOP value. It is supported by the above conclusion from Figure 4-14 that both warp and weft yarns offer stab resistance simultaneously and the

layering sequence of [0/22.5/45/67.5/0/22.5] provides more resistance because of the larger knife travel distance $K_{22.5}$ at the penetration angle of 22.5° for the last ply of fabric panel. Besides, no matter the ply orientation of fabric panels is aligned or angled, the structure of F4 fabric still shows the lowest DOP value, which confirms again the above results that F4 fabric architecture has the best stab resistance. In general, the angled fabric panels have higher DOP value under stab impact, while there is no obvious benefit of angled fabric panels in stab resistance properties for 6 plies panels fabrics. Therefore, the DOP does not decrease when the fabric panel is constructed with angled plies which demonstrate that stab resistance may not only be related to the knife travel distance (K) of different ply orientation but also be relevant to the yarn crimps difference.

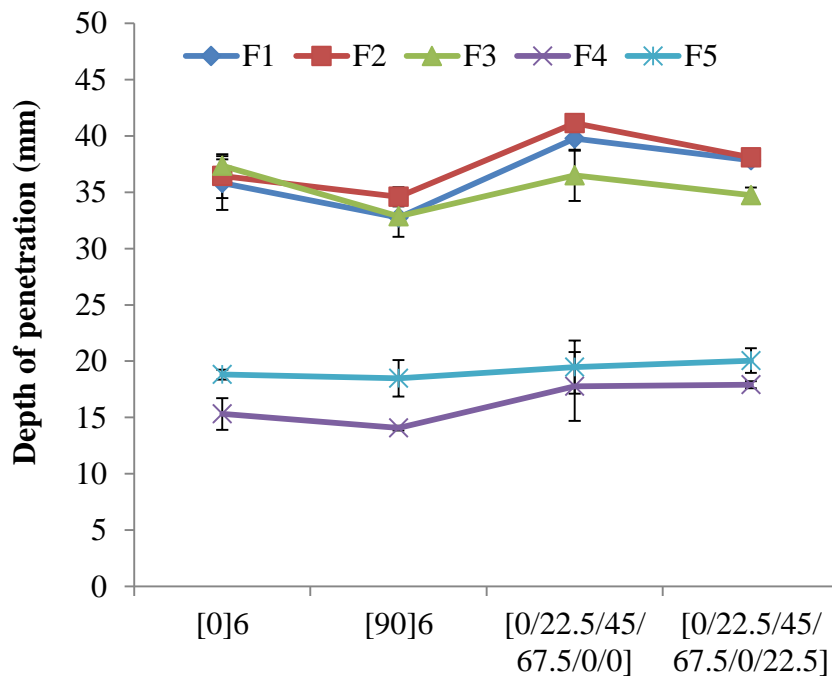


Figure 4-17 Comparison of DOP from 6 plies panels in different ply orientations.

To further verify the above results, the relatively symmetrical stacking sequences [0/22.5/45/67.5]₂ were proposed in eight plies panels of F4 fabric according to the Ref. [159]. In Figure 4-18, it reveals again that the panel construction with an aligned panel [90]₆ ply orientation shows the lowest DOP value. The result indicates again that the DOP does not decrease when the fabric panel is constructed with angled plies. It shows a different conclusion in Wang et al. [159] that the panel [0/22.5/45/67.5]₂ shows the best impact performance of the

panels compared that plain woven fabrics almost always show an orthotropic material behaviour arising from the structural arrangement. The main reason is that the warp density and weft density of the unbalanced fabric has a big difference in this study. Even though the knife travel distance $K_{[0]_8}$ is lower than $K_{[0/22.5/45/67.5]_2}$, the DOP values are close to each other for these two different ply orientation panels. Thus it is hard to make the conclusion which ply orientation has a better advantage to stab resistance between $[0]_8$ and $[0/22.5/45/67.5]_2$. Aligned panels $[90]_8$ have the best stab resistance among these three different ply orientation panels and there is a small tiny difference of stab resistance between aligned panels $[0]_8$ and angled panels $[0/22.5/45/67.5]_2$ when it has increased to 8 plies panels.

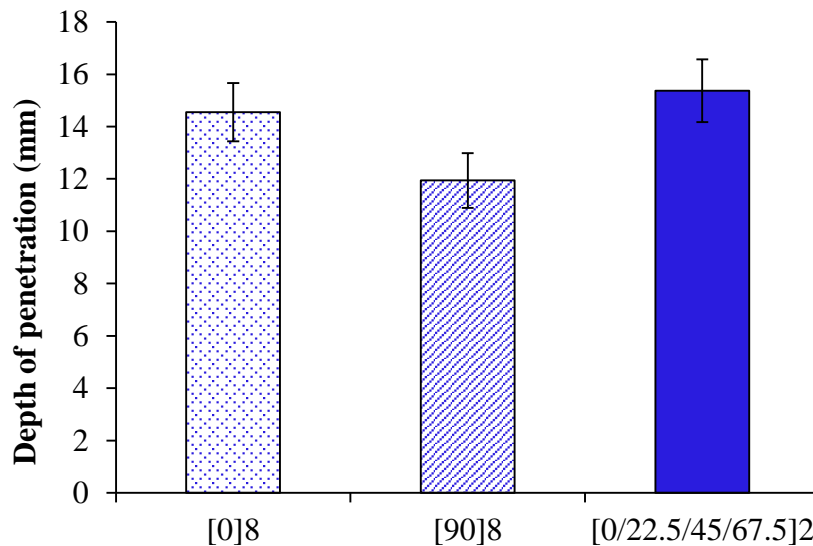


Figure 4-18 DOP of 8 plies panels in different ply orientations of F4 fabric.

By comparison, the surface damaged areas of 8 plies F4 fabric panels are about the same size, as shown in Figure 4-19. However, the surface damaged areas of 8 plies F4 fabric panels after stab impact show difference shapes among three stacking sequences, as shown in Figure 4-20. The stab impactor resists to the strained warp and weft yarns, which constitute only two directions in aligned $[0]_8$ and $[90]_8$. The shapes of surface damaged areas are close to be rhomboid. In the $[0/22.5/45/67.5]_2$ targets, additional directions contribute to the stab resistance, which is the same as Gürgeç et al. [169] stated that the impact energy is distributed through different straining paths and thereby increasing the energy absorption resistance. From the surface damaged area point of view, it tends to be central symmetrical and is roughly circular of angled fabric panels $[0/22.5/45/67.5]_2$ compared to other panels, as shown in Figure 4-20

(c). This is because as the different fabric layers are oriented along different axes, the assembly approaches isotropy. Post stab impact, the formed pyramid has a quadrilateral base because of the two principal axes along which the diagonals of the base align. Hence, if there are more than two sets of perpendicular axes, as in the case of a multi-layered fabric with angle ply orientation, the base may tend to be circular, so that the pyramid approximately becomes a cone and hence, the energy absorption increases [159].

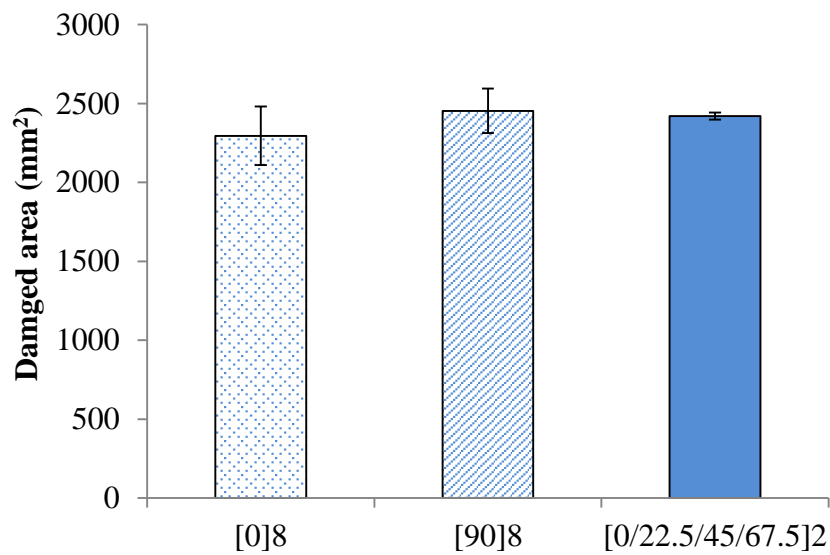


Figure 4-19 Damaged area of 8 plies fabric panels of F4 fabric after stab tests of [0]₈, [90]₈, and [0/22.5/45/67.5]₂.

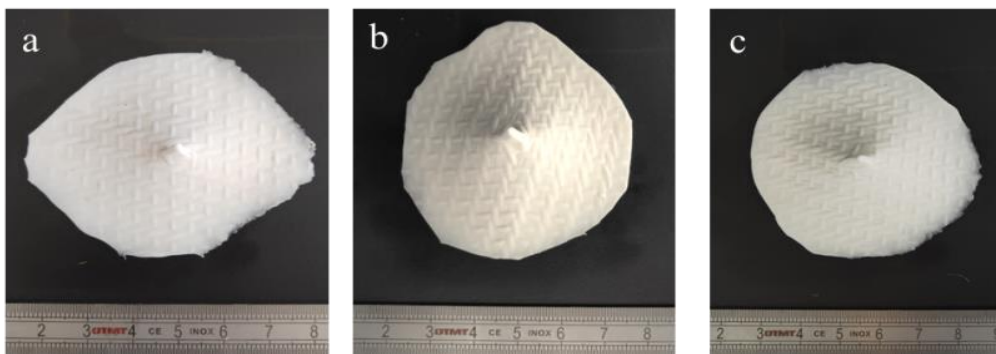


Figure 4-20 Silicone prints of 8 plies fabric panels of F4 fabric after stab tests: (a) [0]₈; (b) [90]₈, and (c) [0/22.5/45/67.5]₂.

In order to perform a further comparison of different ply orientation of stacking sequences of stab resistance differences among aligned panels $[0]_{16}$, $[90]_{16}$ and angled panels $[0/22.5/45/67.5]_4$, 16 plies panels in different ply orientations of F4 fabric were tested. Figure 4-21 shows the results of the DOP for each panel. According to the results, aligned panels $[0]_{16}$ differ from aligned panels $[90]_{16}$ and $[0/22.5/45/67.5]_4$. It shows that aligned panels $[90]_{16}$ and $[0/22.5/45/67.5]_4$ are not penetrated when the panels increase until 16 plies. The ply orientation of stacking sequences panel $[0/22.5/45/67.5]_4$ has better stab resistance than panel $[0]_{16}$ of F4 fabric with O-T structure. Concerning the knife travel (K) for each consecutive yarn cutting, as shown in equations (5-8), the knife travel distance $K_{[0]_{16}}$ is much lower than $K_{[0/22.5/45/67.5]_4}$ that less yarns were cut by the knife blade in the fabric stacking sequences panel. In general, when the number of plies increases, the main influent factor is the knife travel. Besides, the change of ply orientation in fabric stacking sequences panel of $K_{[0/22.5/45/67.5]_4}$ is not conducive for the blade to penetrate into the gaps of the fabric which means that more yarns are effectively cut. Therefore, both the knife travel distance and yarn crimp differences may be the impact factors on the final stab resistance of different ply orientations panels.

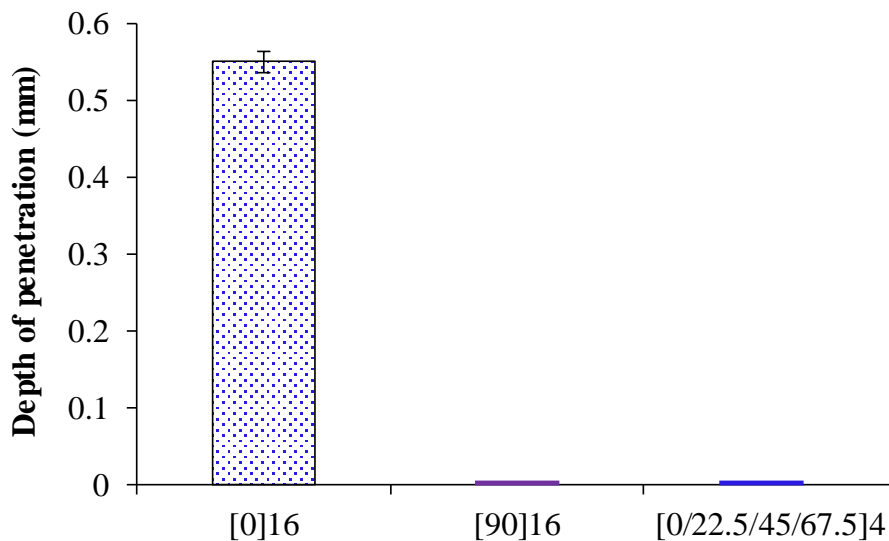


Figure 4-21 DOP of 16 plies panels in different ply orientations of F4 fabric.

4.3.1.3 Effect of fabric plies

As shown in Figure 4-22, the relationship between the DOP value and the number of fabric plies from different structures fabrics is found which can be obtained by curve-fitting the measured data. The change of fabric plies is significantly related to the dynamic stab resistance.

It can be seen that, the DOP of the impact knife into the backing material tends to linearly decrease with the increase of plies number. It reveals similar results as the study of El Messiry et al. [117] that when the number of plies increases, the impact energy is more absorbed by the cumulative amount of layers, so that the DOP of the impact knife into the backing material decreases. By contrast, in the case of less number of fabric plies, the DOP values of F1, F2, and F3 fabrics have a similar trend and decline relatively slow with the increase of fabric plies number, while the DOP values of F4 and F5 fabrics have a similar trend and decline relatively rapidly with the increase of fabric plies number. The result indicated that, within a certain number of fabric plies, the stab resistance increases with an increasing number of fabric plies.

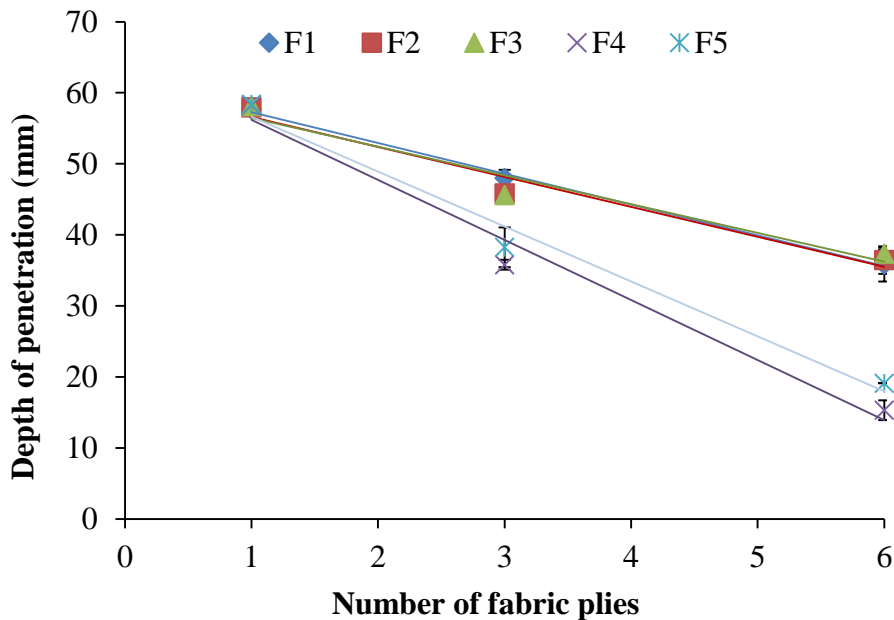


Figure 4-22 DOP of different fabrics stabbed with the 0° angle configuration as related to the number of plies.

Moreover, the relationship between DOP and number of fabric plies is further discussed with the increase of more number of fabric plies. As can be seen in Figure 4-23, there is an obvious non-linear relation between DOP and the number of layers of F4 fabric structure. As the number of fabric plies increases, the DOP starts to drop suddenly, while the decline gradually becomes less noticeable as the number of layers increases to the zero value of DOP. It indicates that the increase of the number of fabric plies can significantly enhance its stab resistance performance, but when it reaches a certain number of layers, the effect of the number of fabric plies is limited

and cannot improve stab resistance performance. Dynamic stab resistance had linear relation to the number of fabric plies with fewer fabric plies, but dynamic stab resistance showed a parabolic relationship generally with the increase of much more fabric plies until it reaches its limits.

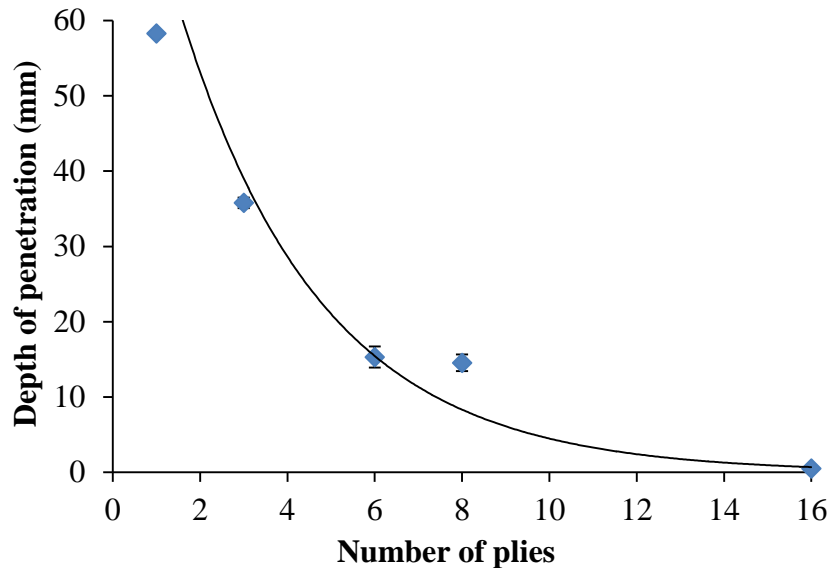


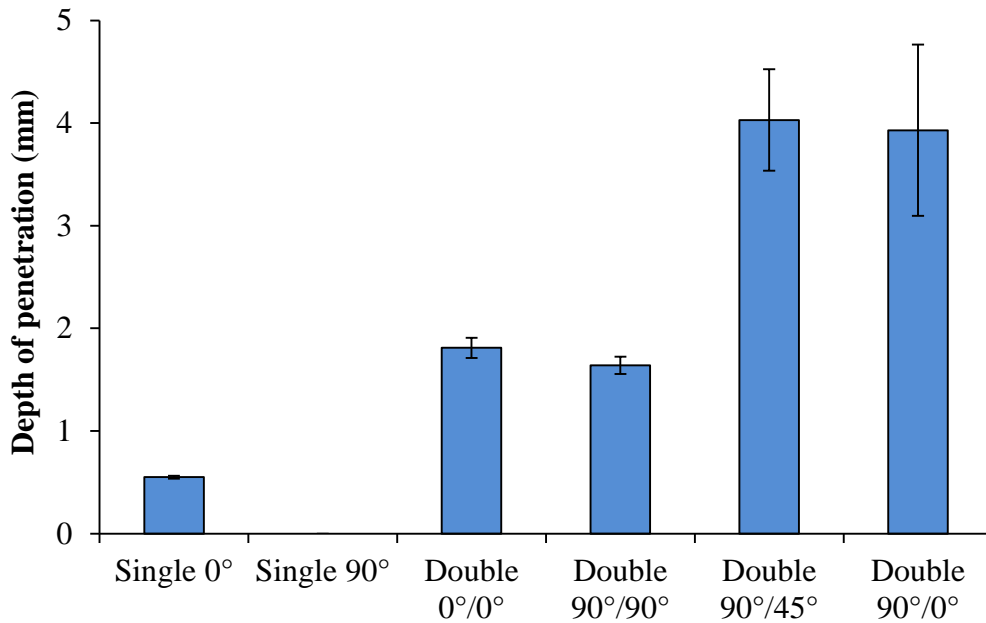
Figure 4-23 DOP of F4 fabrics stabbed in the angle of 0° as related to the number of plies.

4.3.2 Double-pass results

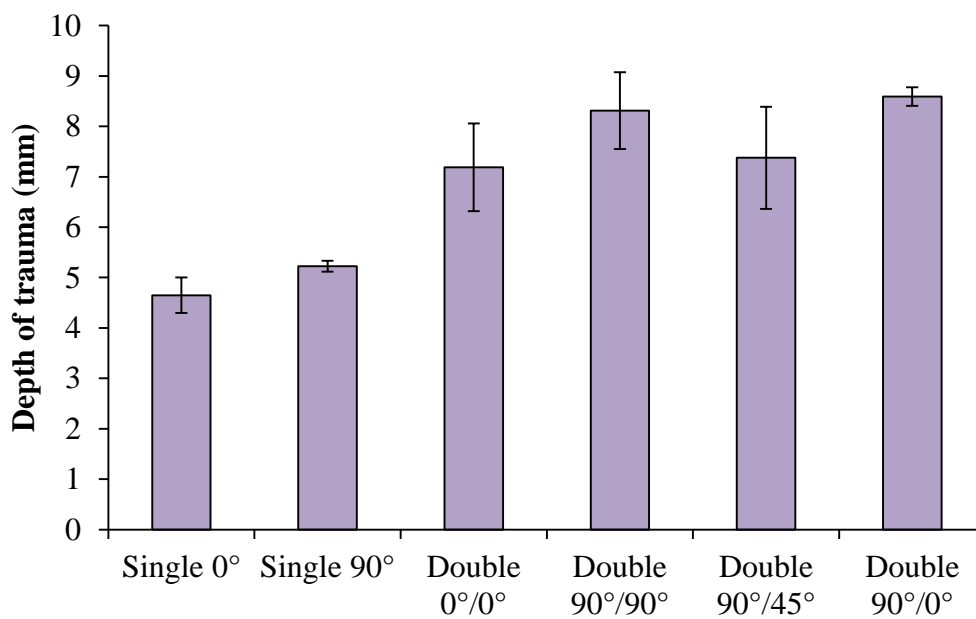
Based on the single-pass stabbing results, the study of the double-pass and multi-angle stab resistance is focused on the F4 architecture. The repeated stabbing should be experienced in the condition in which the perforation or small penetration occurs in the first pass (see Figure 4-6). Consequently, the panels of sixteen F4 plies are chosen to achieve the investigation. Figure 4-24 (a) shows the DOP in double-pass stabbing tests with different stab angles (as mentioned in Figure 4-5) and the comparison with the single-pass ones through stab angle of 0° and 90° , respectively. No penetration is observed for the single-pass in stab angle of 90° , which indicates that the P1 blade impactor was blocked and could not penetrate the specimen. Regarding the single-pass in stab angle of 0° , the specimen is penetrated with 0.5 mm depth due to the larger value of weft yarn density (42 picks/cm) than the warp yarn density (10 ends/cm). Therefore, cutting in warp direction (in stab angle of 0°) is easier than in the weft direction (in stab angle of 90°), the effect of the yarn density on the stab resistance is obvious in this case.

From the stabbing results, it can be remarked that the panel of sixteen F4 plies has a great anti-stabbing performance in single-pass condition but not in certain double-pass ones. Compared to the single-pass results, the DOP has a large increase in double-pass stabbing, particularly in double-pass with stab angles of $90^\circ/45^\circ$ and double-pass with stab angles of $90^\circ/0^\circ$ tests. A very similar DOP can be obtained in double-pass with stab angles of $90^\circ/45^\circ$ and double-pass with stab angles of $90^\circ/0^\circ$ stabbings, this DOP is two times to the ones in double-pass with stab angles of $0^\circ/0^\circ$ and double-pass with stab angles of $90^\circ/90^\circ$ conditions. Therefore, the better condition occurs when the stab angles are identical in the first and second passes.

In addition, the double-pass with stab angles of $90^\circ/90^\circ$ shows relatively better stab resistance compared to the double-pass with stab angles of $0^\circ/0^\circ$. Besides the influence of the yarn density in warp and weft directions, of orthogonal interlock architecture, some warp yarns are deeply bent from one surface to the other, thus preventing slippage of the yarns in the structure while weft yarns follow a smoother evolution. It is obvious that DOT increases in double-pass stabbing than the single-pass one. By contrast with the DOP, the DOT in different double-pass stabbings remains quasi the same level considering the measurement errors (see Figure 4-24(b)). The knife blade causes the compressive yielding of the fabric surface during the first stage of indentation (Figure 4-3). Hosfall [161] showed that indentation theory appears to give good agreement with the perforation resistance of sheet materials penetrated by knives. The similar phenomena, in this case, could be supported by an indentation mechanics reviewed by Tabor [170] that, for pyramidal or conical indenters, the plastic zone size is constant relative to the indentation size. In this study, the same knife blades were used with the same tip angle. Therefore, there is a slight difference of DOT values in different double-pass stabbings which showed that it might also be related to the frictional interaction with the fabric panels.



(a) DOP values



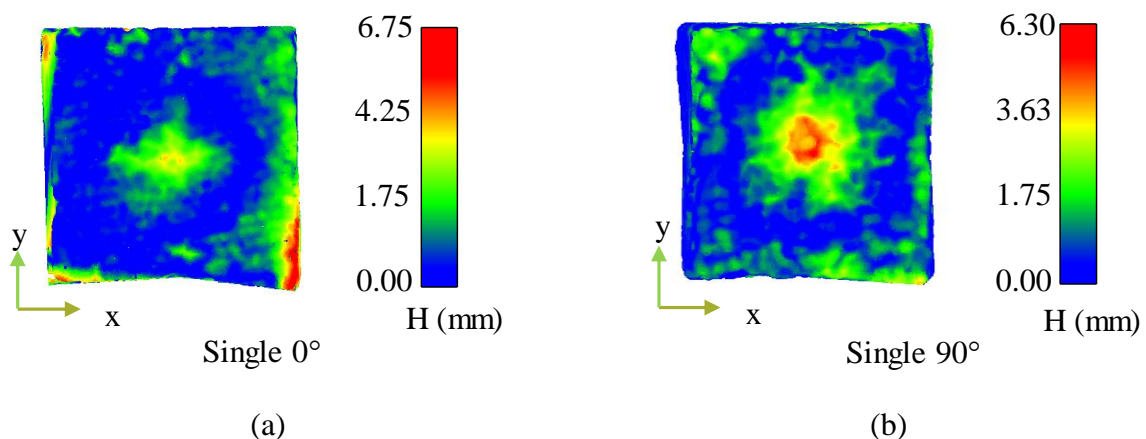
(b) DOT values

Figure 4-24 Stabbing deformation after double and multi-angles stabbing and comparison with the single-pass ones.

It was shown in the above experiments that the double-pass stabbing with the stab angle of 0°/0° and 90°/90° shows a relatively better stab resistance compared to the ones with stab angle of 90°/0° and 90°/45°. These phenomena are probably related to the fabric deformation after stabbing. Figures 4-25 (a) – (f) show the contour plots of the deformation patterns from the top

view of sixteen plies F4 fabric after single-pass and double-pass stabbing with the different stab angles. The X and Y axis show the 0° and 90° directions, respectively.

Figures 4-25 (a) and 4-25 (b) present the deformed fabrics after the single-pass stabbing (as same as the first pass in the double-pass stabbing). This kind of deformation can be attributed to the fabric structure with tightening yarns that dissipate the impact energy and stop the penetration of the knife blade. Regarding the double-pass stabbing (after the second pass in the double-pass stabbing) with 0°/0° and 90°/90° shown in Figures 4-25 (c) and 4-25 (d), the deformation map is similar compared to the one after the single-pass (Figures 4-25 (a) and 4-25 (b)), as the stab angle is not changed between the first and second passes. When the second pass test fabric stabbed with the same stab angle and impact energy, the deformed fabric after the first pass stabbing, with tightening yarns and structure, can resist maximum to another impact during the second pass stabbing. In this case, it can be called the deformed state after the first pass stabbing as the “locking” structure. Therefore, it is hard for the knife blade without changing the stab directions to penetrate such kind of deformed and locked fabric unless the impact energy increases enough to unlock the “locking” structure. It is why the low DOP is observed in 0°/0° and 90°/90° double-pass stabbing tests as shown in Figure 4-24 (a). By contrast, when the angle of the second pass stabbing is changed in the double-pass test (e.g. 90°/0° or 90°/45° double-pass stabbing test), the deformation map is strongly modified (see Figures 4-25 (e) and 4-25 (f)) compared to the single-pass stabbing. The changed angle brings out an impact in another direction and consequently leads to other deformed yarns and structure during the second pass stabbing. The “locking” state after the first stabbing is destroyed. Thus the knife blade continues to penetrate and the DOP is bigger compared to the case without changing the stab angle (see Figure 4-24 (a)).



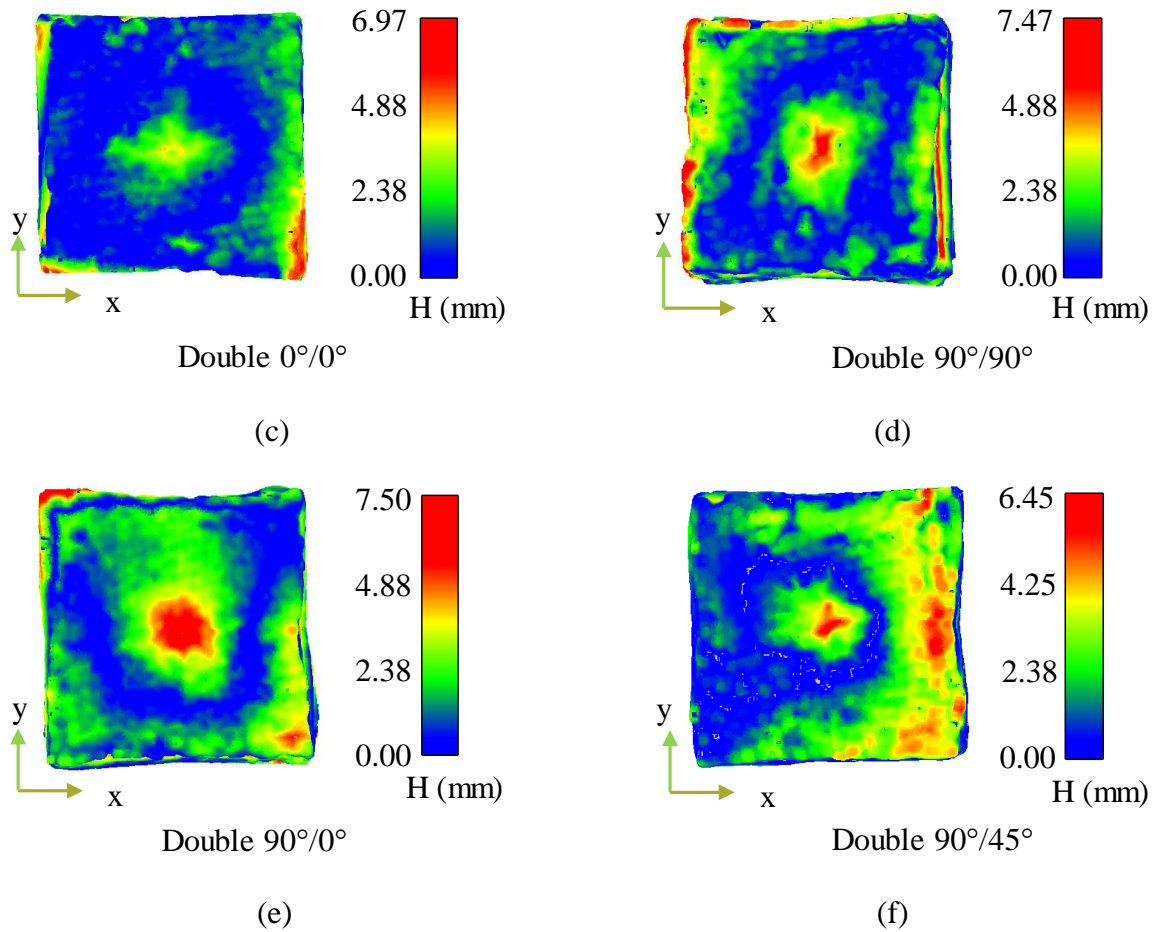


Figure 4-25 Sixteen plies F4 fabric patterns from the top view after single-pass and double-pass stab with the different stab angles: (a) single 0°, (b) single 90°, (c) double 0°/0°, (d) double 90°/90°, (e) double 90°/0°, (f) double 90°/45°.

The second stab was carried out by the same blade since a sharp and pointed edge of a weapon remains rigid and unaffected by the impact event [171]. For the double-stabbed specimens, the trauma shape can reveal important information about the nature of the damage occurred due to the two times stabs. The observation of the bottom surface after different stabbing tests for sixteen F4 plies is shown in Figure 4-26. As proved in Figure 4-15 (a), no or very small penetration presents in single-pass stabbing, quasi no structural damage can be noted in Figures 4-26 (a) and 4-26 (b). In double-pass stabbings of 0°/0° and of 90°/90° (Figures 4-26 (c) and 4-26 (d)), the shapes of damage are very similar looking like a square-circle one, which is smaller than the structure damages in double-pass stabbings of 90°/0° and of 90°/45° (Figures 4-26 (e) and 4-26 (f)). Moreover, the structure damages with the “triangular” shape in double-pass 90°/0° stabbing and with the “Y” shape in double-pass 90°/45° stabbing are more fatal

from the point of view of personal body protection. It confirms again that in stabbing test the favorable condition is no change of the stab angle in the different pass. Consequently, in the real condition in which the change of the stab angle can not be controlled due to the movement of the assailant and victim, the multiaxial balance architecture may be a good solution.

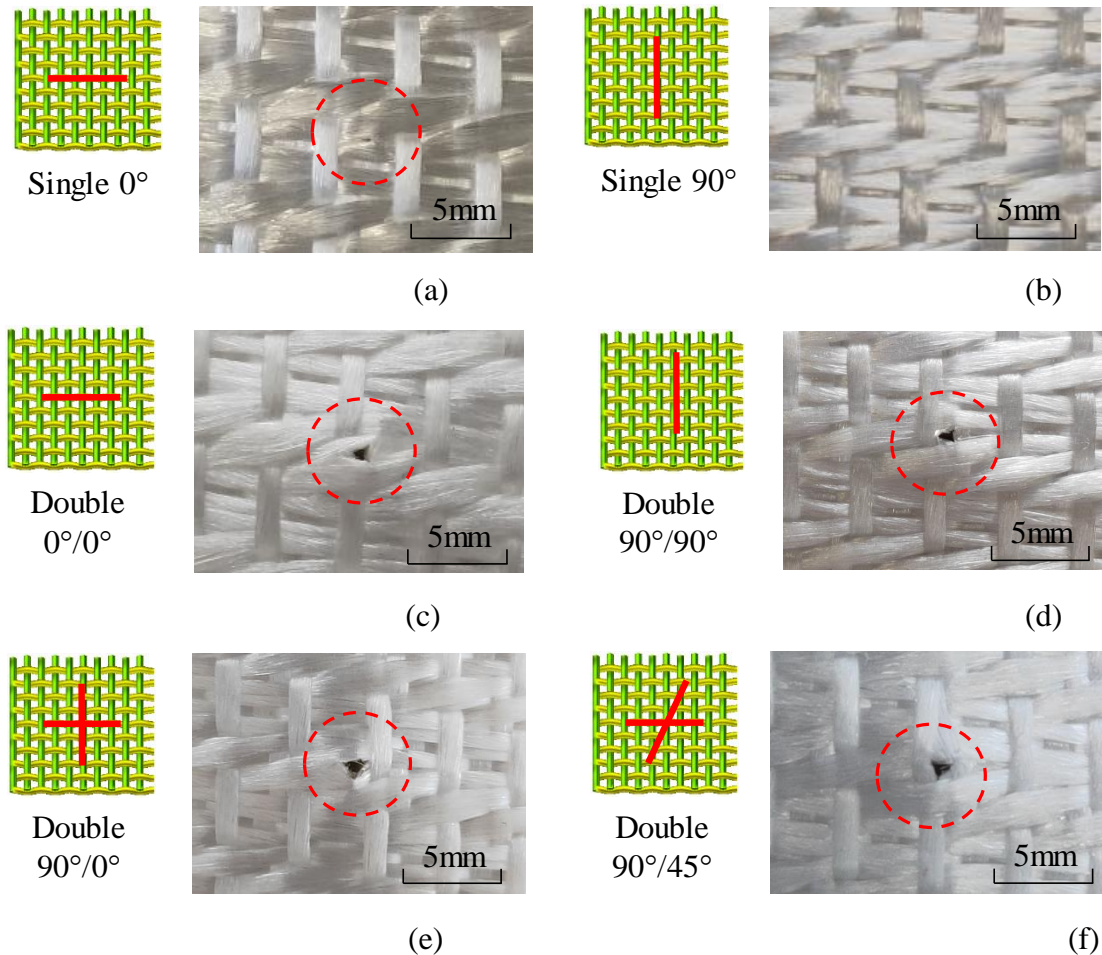


Figure 4-26 Observation of the damage morphology from bottom surface of sixteen plies fabric panel after different double-pass stabbing tests.

4.4 Summary of Chapter 4

This chapter successfully prepared a systematic comparison of 3DWIFs for resisting against dynamic stab attacks. The stab resistance experiment was performed with HOSDB/P1/B sharpness blades on the HMWPE fabrics, to measure the depth of penetration and the printed fabric deformation by the silicone.

Classical single-pass stab test of the different fabric structures were stabbed with the same impact energy at the same location for one time. It was observed that F4 fabric with Orthogonal-Through-the-thickness interlock structure reveals the most favourable stab resistance compared to other structures and the stab resistance in weft direction is higher than that in the warp direction. It can be highlighted that the main structural parameters of the 3DWIF as the binding warp yarns architecture have revealed the orthogonal-through-the-thickness as the best candidate for stabbing protection. Besides, the orientation of plies significantly affects the stab resistance of the multi-ply fabric panels after stab impact. The distance that the cutting knife travelled to cut consecutive yarns was different from the change in knife penetration angle that, to some extent, affected the stab resistance. It indicated that the angled panels do not always increase the stab resistance of 3DWIF compared with the aligned panel since the warp and weft densities are not the same. When the number of plies has reached a certain limit, the ply orientation is conducive to improve the stab resistance performance of the fabric panel. It can be concluded that the increase in fabric plies has some effects on decreasing the trauma and perforation values. To satisfy protection level 1 of the HOSDB standard (penetration depth < 7 mm), the 3DWIF should be with much more plies of the fabric panel. But there are limited benefits to improve stab resistance performance after over a certain number of fabric plies.

Compared to the classical single-pass stabbing, the double-pass stabbing with different stab angles is proposed and analysed in the present paper to respond more appropriately to the personal body protection problem. In order to find an optimized 3DWIF, five different warp interlock architectures were studied. These 3DWIFs, differing in fabric architectures, areal weight, fibre weight fraction, and thickness, were manufactured with the same types of fibres and in the same lab using the same dobby loom. All the specimens were stabbed with the same impact energy. The depth of penetration (DOP) and the depth of trauma (DOT) are measured by 3D scanning. It is observed from the comprehensive evaluation radar chart that the HMWPE fabric with the Orthogonal/Through-the-thickness (O/T) structure reveals better stab resistance compared to other main 3D warp interlock structures. This is due to the through-the thickness binding type and higher binding depth of binding warp yarns than other fabrics. The measurement results of DOP in double and multi-angle pass stabbing provide that the stab resistance in 90° (perpendicular to the weft yarns) is higher than that in other directions. The double and multi-angle pass stabbing results highlight also that the better condition occurs when the stab angles are identical in each pass. The repeated stabbing resistance is quite

essential in real-life applications. Future research could focus on the selection of more advanced high-performance polymer/composite fabrics. Also, the multiaxial balance Orthogonal/Through-the-thickness (O-T) interlock fabric will be developed and analysed to improve the repeated-stab resistance.

Chapter 5 Pre-deformed stab resistance of multi-ply 3DWIF

5.1 Introduction

Soft body armour, commonly used by both police and militaries, must be adapted to the shape of human body for ensuring effective protection [172], which offers protection from typical handguns and small, lower speed shrapnel fragments [173]. Despite the growing trend of females joining the law enforcement police and military services across the world for the last few decades, they still use the body armour designed for males which paid no attention to female unique curvilinear body shape between men and women. Compared with male body armour, the problems in manufacturing the female body armour lie in the curvaceous shape of the female body [6]. Consequently, new design of body armour is necessary to increase protection and improve comfort for women [174]. Moreover, forming, as a commonly used technique, is helpful to achieve a complex shape of dry fibre textile preforms, which is suitable for moulding the human shoulder or female breast in the application of body armours. This technique can provide not only better stab protection but also accommodate their curvilinear upper torso for better comfort, flexibility and fitness. There is great potential for some traditional textile methods to be properly utilized in modern soft body armour through new design and engineering methods. However, the stab resistance of female body armour is rarely studied in the literature.

Precious research about the conventional single-pass stab resistance of different structures of 3DWIFs has been discussed in Chapter V, which proved that orthogonal-through-the-thickness (O-T) interlock structure has a good stab resistance under the same experimental conditions compared with other structures. Hence, in this study, a new test has been proposed, named pre-deformed stab-resistance test, and has been conducted to simulate some parts of the human body wearing body armour, for example, female breast or shoulders, that are attacked by stabbing under wearing body armour. Pre-deformed stab-resistance property is the combination of several deformations, for example, formability, shear property, stab resistance property, etc. It was explored for simulating the stab resistance of the shoulder or female breast that might improve the level of protection. In this study, the comprehensive deformation behaviour of F4 fabric (single $[0^\circ/90^\circ]$ ply and a $[-45^\circ/45^\circ]$ ply) is to be examined with hemispherical forming devices. The influence of the shear angle on the stab resistance of fabric panels is investigated at different target locations based on the forming test result. Furthermore, the pre-deformed stab-resistance tests of aligned and angled fabric panels in three different locations after the hemispherical forming process are carried out and the experimental results are compared.

5.2 Experimental set-up

5.2.1 Sample preparation

In our previous study, the results showed that the 3DWIF with O-T structure reveals the best stab resistance under the classical stab test. Two material configurations were studied before stab stage; hemispherical forming tests of a single $[0^\circ/90^\circ]$ ply and a single $[-45^\circ/45^\circ]$ ply, as shown in Figure 5-1 (a) and (b). The size of the tested individual preforms was $280 \text{ mm} \times 280 \text{ mm}$, with a thickness of $1.7 \pm 0.1 \text{ mm}$.

The schematic description of the different fabric ply types by two cutting methods with a single $[0^\circ/90^\circ]$ ply and a single $[-45^\circ/45^\circ]$ ply respectively, as shown in Figures. 5-1 (a) and (b). The hemispherical forming tests of these two fabric plies were studied before the stab stage. The size of samples was $210 \text{ mm} \times 210 \text{ mm}$, with a thickness of $1.7 \pm 0.1 \text{ mm}$. The average thickness of the specimens was precisely determined using an electromagnetic sensor thickness measuring apparatus based on the standard NF EN ISO 5084.

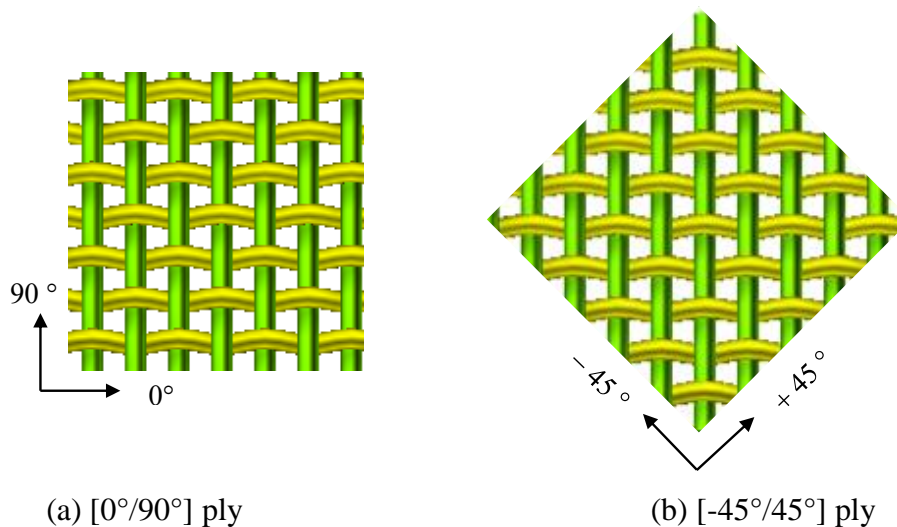


Figure 5-1 Schematic description of the different fabric ply types by two cutting methods.

Two different types of sample panels systems, each consisting of eight plies fabrics with O-T structure, as shown in Figure 5-2 (a) and (b) respectively, have been prepared. The aligned fabric panel was marked as $[0^\circ/90^\circ]_8$. The fabrics of angled panel marked as $[(0^\circ/90^\circ)/(\pm 45^\circ)]_4$ were placed after rotating counter-clockwise direction from bottom to up. The different plies within the sample number of fabric panels were prepared without stitching yarns. The stacking

sequence of the aligned fabric panel and the angled fabric panel are respectively $[0^\circ/90^\circ]_8$ and $[(0^\circ/90^\circ)/(-45^\circ/45^\circ)]_4$.

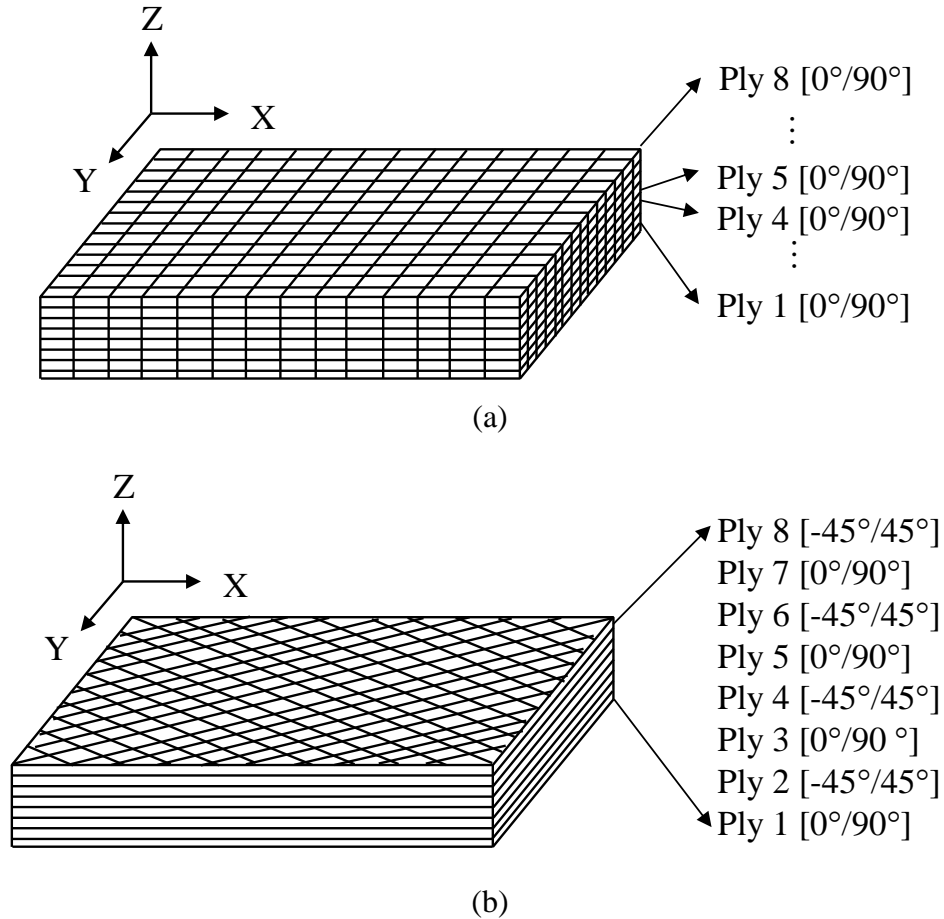


Figure 5-2 Ply orientation in the specimens (a) aligned fabric panel and (b) angled fabric panel.

5.2.2 In-plane shear

The relationship between the shearing angle and load was studied using the experimental bias-extension test. As illustrated in Figure 5-3, rectangular specimens of $210 \times 70 \text{ mm}^2$ (aspect ratio is 3) were tested on a MTS Criterion Testing Systems. Samples providing a gauge length of 210 mm were clamped onto the machine in such a way that the warp and weft directions of the yarns are oriented initially at $\pm 45^\circ$ to the direction of the applied tensile force. All of the bias-extension tests are performed at a constant speed of 50 mm/min up to the termination at first failure signs and repeated at least three times. The shear angle was measured directly by an optical measurement in the pure shear zone A during the test. Moreover, there is a limited shear angle, called 'shear-locking angle' [175], that the wrinkling will appear over this value [107].

The distance d between the two red points a and b from the same binding warp yarn are measured for determining the shear-locking angle.

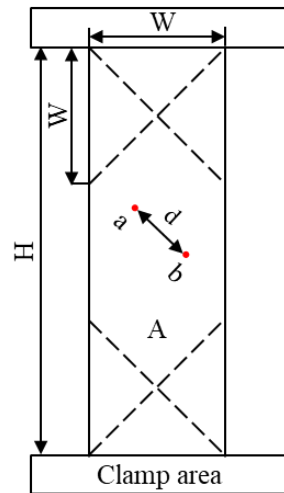


Figure 5-3 A rectangular specimen of fabric with clamp area.

5.2.3 Stab test apparatus

The test apparatus, which was adapted to the UK standard of HOSDB Body Armour Standard (2017) [154], was used for the stab resistance investigation. The stab experiments with the energy of 3.5 J, the drop height 0.169 m and 2.11 kg in mass were carried out, with HOSDB/P1/B sharpness blades which have the total length of 100 mm, the cutting edge length of 33 mm, and the blade thickness of 2 mm [176]. During the test, the direction of the blade does not change. Roma Plastiline[®] moulding clay was used as the backing material, because it is cheap, readily available, and attained higher deformation with time compared to other backing materials [177]. It was heated for 5 hours until the temperature reaches 37.5 ± 0.5 °C before tests to imitate human body temperature. As shown in the previous chapters, the distance between the top tip of the fabric print and the surface of the fabric print mark in the silicone mould is defined as the depth of penetration (DOP). The 3D scanning moulding is proposed by 3D scanner to accurately measure and analyse the DOP.

5.2.4 Testing procedures and methods

The motive for this section is to explore the pre-deformed stab-resistance tests with the same energy level on the three different locations and study the location effect on the stab resistance. pre-deformed stab-resistance tests are conducted to simulate some parts of the human body, for

example, female breasts or shoulders which are attacked by stabbing. Compared to the classical stab test, pre-deformed stab-resistance tests were carried out the same machine, but the specimens are not in the flat shape, because many parts of the human body have certain radii rather than being completely flat.

As shown in Figure 5-4 (a) and (b), the tested fabric panel prepared, with $0^\circ/90^\circ$ yarn orientation and the other with $\pm 45^\circ$ yarn orientation (Figure 5-1), was put in the centre between the upper transparent plate (with a round hole of 110 mm diameter in the centre) and the surface of the mould with a hemispherical groove. Then the fabric panel was stamped with the same force by the punch with same punching height (50 mm). For research purposes, to simulate the female breasts, we preferred to use a hemispherical shaped punch with a diameter of 100 mm to resemble the women's body shape of average size ((90B) bra size). The forming process is finished inside the mould directly. The control of the wrinkle during the formation in the process will be discussed in section 5.3.2. Then the pre-deformed fabric panel was stabbed with different locations, as shown in Figure 5-4 (c). It can be noticed that the stabbing direction is opposite to the practical application of body armours for female breasts. This test method focused more on the study of the deformed fabric with curved shape subjected to stab in different places, which has big difference with the stab resistance test for flat fabric. This method is applied for the following reasons. Firstly, it is the material deformation recovery after the forming process and some parameters will recover from its initial dimension, for example, punching height, material drawing-in, in-plane surface shear angle [178]. Secondly, the influence of gravity is small in this case due to the fact that the fabric is embedded in the groove after deformation. Thirdly, it can reduce the possibility of damage when the samples were removed to the stabbing machine after forming. Finally, this method shows the advantage when the thickness of the fabric panel was quite larger than the space between the punch and blank holder of the forming machine. The stab locations will be selected based on the forming results for mimicking the injuries in different positions of the female breast by a knife blade. Each test was repeated at least three times.

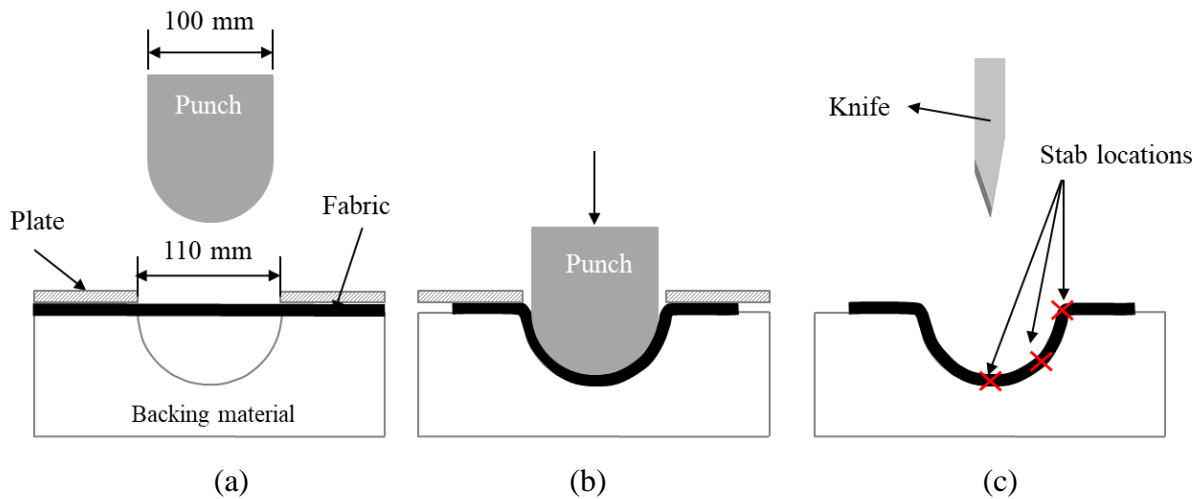


Figure 5-4 The steps of the experiment (a) Preparation of forming, (b) Forming (c) pre-deformed stab-resistance test.

These testing procedures and methods were applied for the following reasons. The cloth on human body is a non-clamped state, to be consistent with the actual situation and simulate the real stab attack, the edge of test samples were un-clamped for the pre-deformed stab resistance tests. Then, there is the material deformation recovery after the forming process and some parameters will recover from its initial dimension, for example, punching height, material drawing-in, in-plane surface shear angle [178]. Besides, it is easy for the fabric panel to keep the deformation with hemispherical groove. Moreover, the influence of gravity is small in this case due to the fact that the fabric is embedded in the groove after deformation. It can also reduce the possibility of damage when the samples were removed from the stabbing machine after forming. In addition, this method shows the advantage when the thickness of the fabric panel was quite larger than the space between the punch and blank holder of the forming machine.

Besides, the pre-deformed stab-resistance experiments were divided into two parts, the first part focused on describing the deformation of $[0^\circ/90^\circ]$ and $[-45^\circ/45^\circ]$ single-ply respectively. Comparisons were made by observing the resulting draw-in of the fabric and shear angles developed in the fabric after stamping. The second part focused on the stab resistance of multi-ply fabric panels at different locations after hemispherical forming tests. The locations were chosen based on the shear angle distribution, including the area with no deformation, with maximum deformation and in-between area. The same impactor and the same energy were used for tests.

5.3 Results and discussion

5.3.1 Shear-locking angle measurement

The shear-locking angle can be graphically determined by using these shear compliance curves suggested by Scouter [179] (see Figure 5-5). It can be seen that the force versus shear angle curve is approximated by two straight segments with a low slope for the first part and a stronger slope for the second beginning at the shear-locking angle (around 30°). In the stage of the shear-locking angle, the yarns are in contact with their neighbours. When the shear angle exceeds the shear-locking angle, the yarns interfere and wrinkle occurrence out of plane [175,180] and yarns become in contact with their neighbours and are laterally compressed, first partially then completely [181].

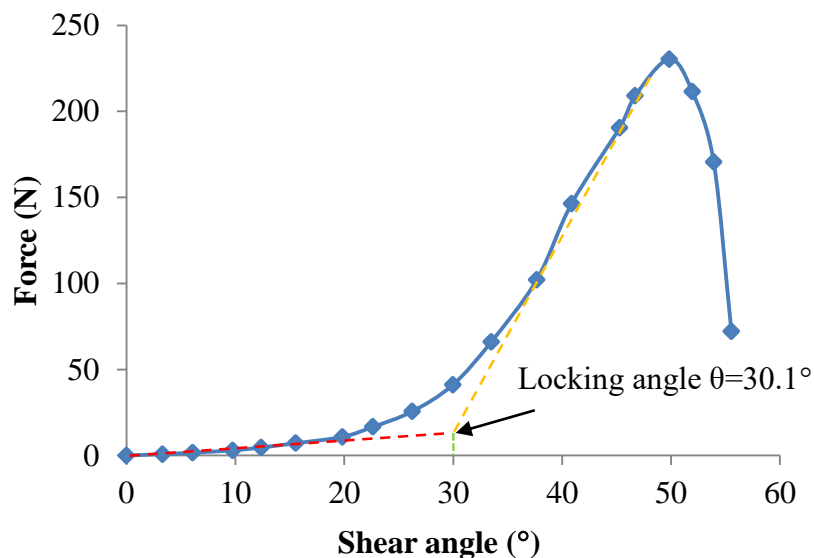


Figure 5-5 Graphical determination of shear locking-angle resulting from bias-extension tests.

Figure 5-6 shows the distance d of two red points at macro-scale of the bias-extension test at the displacement of 0 mm and 31mm respectively. The distance d between the two red points has been measured by Image J software which shows that the distance d remains the same during the period of 0-31mm displacement. The shear angle is 30° at this moment that is not exceeded, which proved the shear locking angle shown in Figure 5-5.

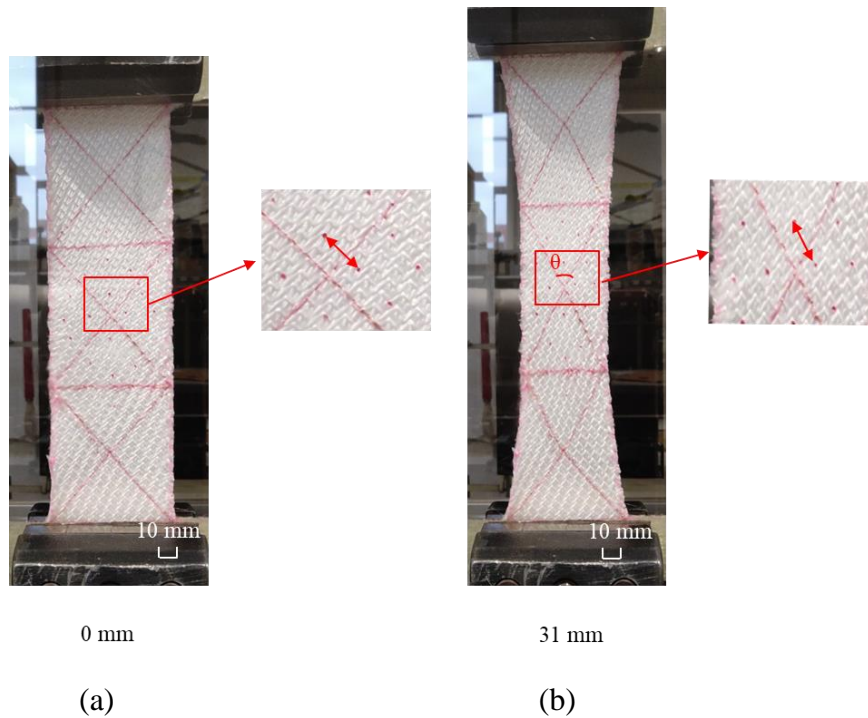


Figure 5-6 The distance d of two red points at macro scale of bias-extension test at displacement of (a) 0 mm (b) 31mm.

5.3.2 Deformation of fabric panel

The material draw-in, treated as a global characteristic exclusively for fabric deformability, can be defined as the amount of material flow in the draping process along the contour from the undeformed position to the deformed one [182]. 3DWIFs with $[0^\circ/90^\circ]$ and $[-45^\circ/45^\circ]$ ply orientation (Figure 5-1) were formed by hemispherical punch with the same experimental conditions. Figure 5-7 indicated the deformed 3DWIFs after hemispherical forming test. Comparing Figure 5-7 (a) and (b), the two cases have quite different deformed profiles and local shear angles distribution, which proved that fibre orientations have a significant effect on 3DWIF forming. The edges of $[-45^\circ/45^\circ]$ yarn orientation samples expand outward, while for $[0^\circ/90^\circ]$ yarn orientation samples, their edges contract inward. To quantify the formability, the material draw-in and surface shear angles by optical measurement were used to be the indicator of the extent of global deformation.

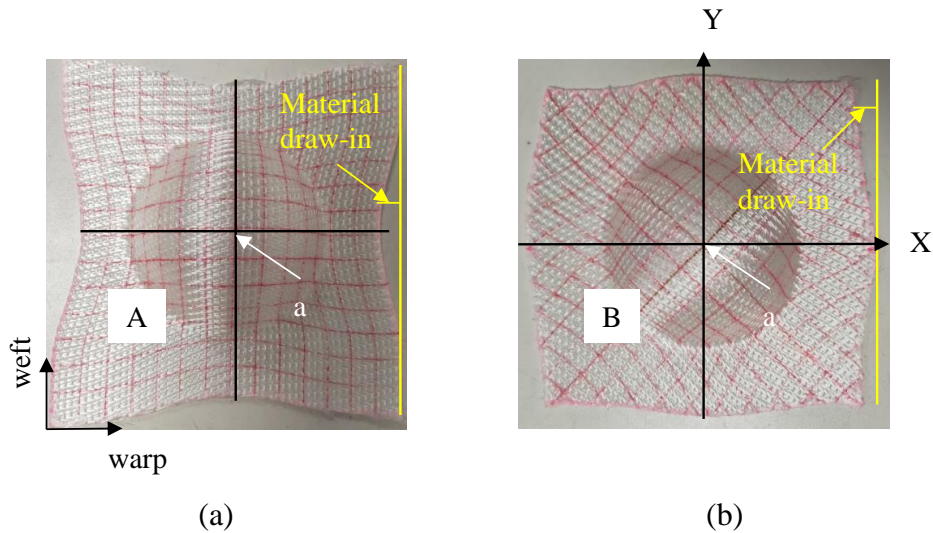


Figure 5-7 Deformed 3DWIF after hemispherical forming test, (a) single $[0^\circ/90^\circ]$ fabric ply and (b) single $[-45^\circ/45^\circ]$ fabric ply.

In this section as the deformed preform after forming was approximately symmetric, the measurement data was obtained as the mean values of two diagonal sides and, for better accuracy, the same sample tests were repeated three times. Material draw-in of single $[0^\circ/90^\circ]$ fabric ply in the warp and weft directions are shown in Figure 5-8. The maximum value is slightly higher in the warp direction for single $[0^\circ/90^\circ]$ fabric ply. Material draw-in of single $[-45^\circ/45^\circ]$ fabric ply in the warp and weft directions are shown in Figure 5-9, which has revealed completely different draw-in distribution in $\frac{1}{4}$ zone B compared with single $[0^\circ/90^\circ]$ fabric ply.

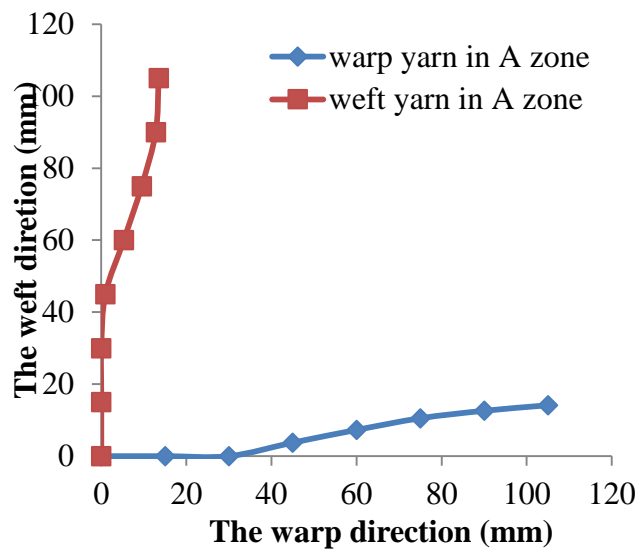


Figure 5-8 Material draw-in of single $[0^\circ/90^\circ]$ fabric ply in warp and weft directions (distribution in $\frac{1}{4}$ zone A of the deformed ply).

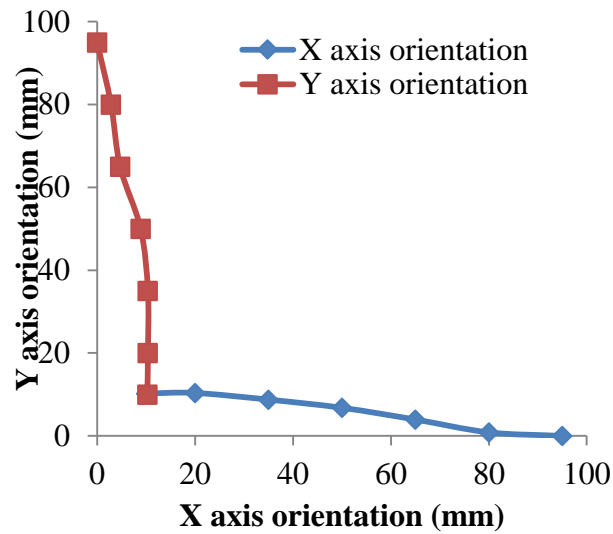
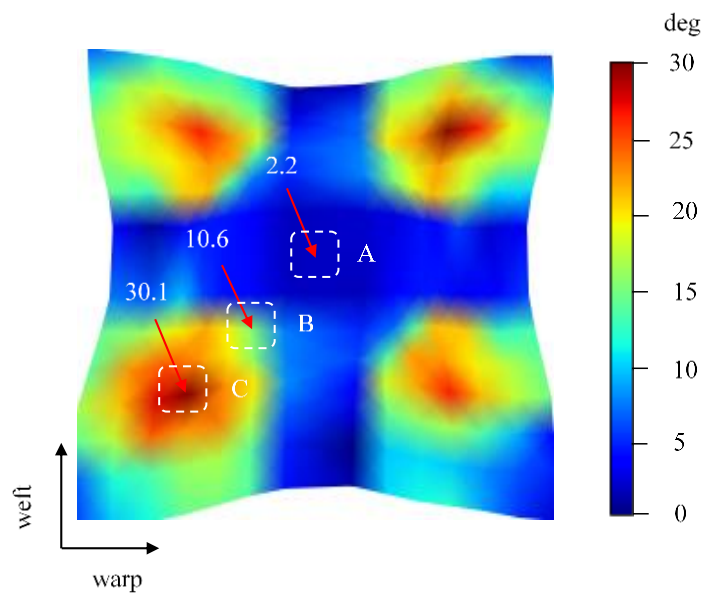


Figure 5-9 Material draw-in of single $[-45^\circ/45^\circ]$ fabric ply in warp and weft directions (distribution in $\frac{1}{4}$ zone B of the deformed ply).

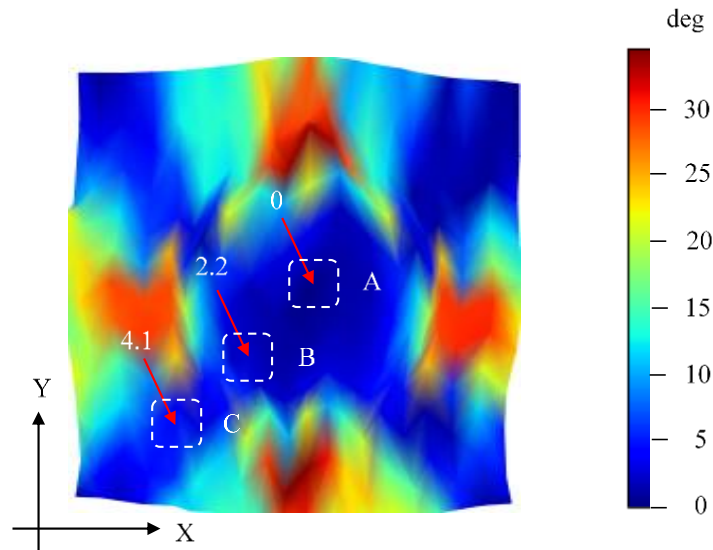
Furthermore, the global shear angle distribution is compared. Shear angle, defined as the variation of the fibre intersection angle between warp and weft yarns, is one of the most important properties that determine how a fabric will behave when subjected to a wide variety of complex deformations. In particular, large in-plane shear could be necessary to obtain the required shape [183]. In this study, the data visualization was conducted using the open-source Matplotlib version 3.3.3 [184], which is a 2D graphics package used by Python for application development, interactive scripting, and publication-quality image generation across user interfaces and operating systems. The distributions of shear angle are significantly effected during forming test and affect each other within zones of interest, as well as on global scale. With the help of the data visualization method, the shear angle distribution after forming test of single $[0^\circ/90^\circ]$ ply and $[-45^\circ/45^\circ]$ ply respectively are obtained, as illustrated in the Figure 5-10 (a) and (b). Woven fabric relies on shearing between weft and warp yarns to accommodate large deformation needed in the forming process. We notice that these shear angle values are large along the diagonal line for $[0^\circ/90^\circ]$ fabric and along the median line for $[-45^\circ/45^\circ]$ fabric. But along the median lines of $0^\circ/90^\circ$ and along the diagonal lines of $\pm 45^\circ$ the angular distortions are very small $< 8.5^\circ$ and 5.7° respectively.

Wrinkles were found in none of the fabrics during the forming test. Nevertheless, the onset of wrinkling is related to achieving a critical shear angle [185]. In Figure 5-10 (a), the distributions

of the shear angle on the symmetry line of the cross centre (weft and warp yarn directions) are minimum (less than 10°) and very smooth. Besides, the centre position is almost zero. Shear angles reach their maximums in directions of diagonal directions ($\pm 45^\circ$ directions). There is no wrinkling occurs within the main deformation zone 3 which has the largest shear angle distribution area compared with the zone 1 and zone 2. This is due to wrinkling will occur when the shear angle exceeds the shear-locking angle [186] (around 30°), as shown in Figure 5-5. The maximum shear angle for the $[0^\circ/90^\circ]$ ply is about 30.1° and 36.4° for the $[-45^\circ/45^\circ]$ ply. Large gradients exist in region of four corners for the shear angle distribution in Figure 5-10 (a). In Figure 5-10 (b), although the maximum shear angle is a little larger than the shear-locking angle, the wrinkles does not been found in the area with largest shear angle. Because the wrinkle onset does not depend solely on the shear angle and the other strain energies also play a role [187]. Besides, the blank holders shown in Figure 5-4 create tensions that decrease or suppress wrinkling in the useful part.



(a)



(b)

Figure 5-10 Comparison of the shear angle distribution of single ply fabric after deformation: (a) $[0^\circ/90^\circ]$ ply; (b) $[-45^\circ/45^\circ]$ ply. (For interpretation of the references to color in this figure legend, the reader is referred to the web version of this article.)

5.3.3 Stab resistance properties after deformation

5.3.3.1 Definition of stab location

As described in Section 5.2, the pre-deformed stab-resistance tests of 3DWIF panels are tested to resemble the stab of frontal female body contour. When body armor adapted to the female body shape is stabbed by a knife blade, the results may vary depending on the exact location of the stab. Each location corresponds to a particular yarn structure and a local deformation of the woven structure. The stab location, therefore, poses questions about the fabric behaviour in the 3DWIF stab impact. Based on the results of a hemispherical forming test of single $[0^\circ/90^\circ]$ and $[-45^\circ/45^\circ]$ fabric plies, pre-deformed stab-resistance test was conducted at three different locations on the deformed fabric panels with eight layers plies as shown in Figure 5-11. For the location A in Figure 5-11 (a), the shear angle of the vertex is close to 0° and it means that almost no shear deformation take place at this position. The location C, with the largest shear angle, were determined where has the highest deformation in Figure 5-11 (c), and the location of the middle area (see Figure 5-11 (b)) were determined in the midpoint point which is between the centre location and locking angle area. In this section, the stab resistance of targets made

of 3DWIFs with different target systems and locations will be enlightened. The influence of the shear angle on the stab resistance of fabric panels will also be investigated.

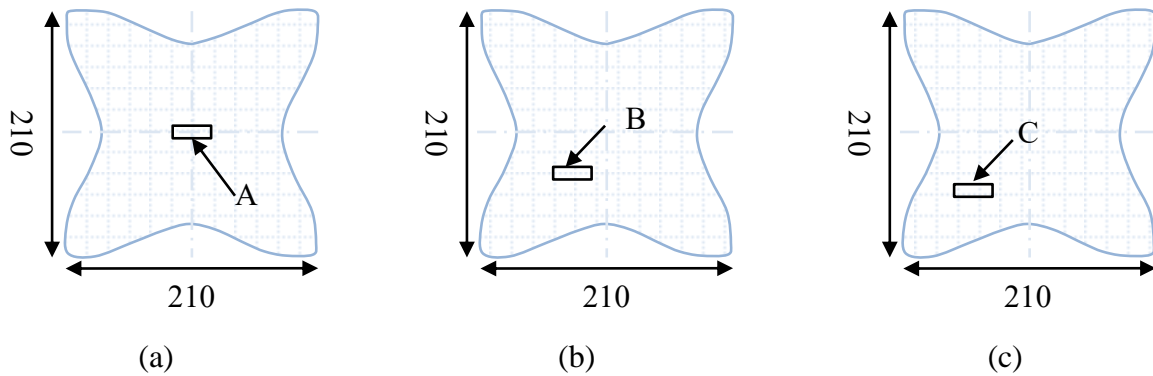
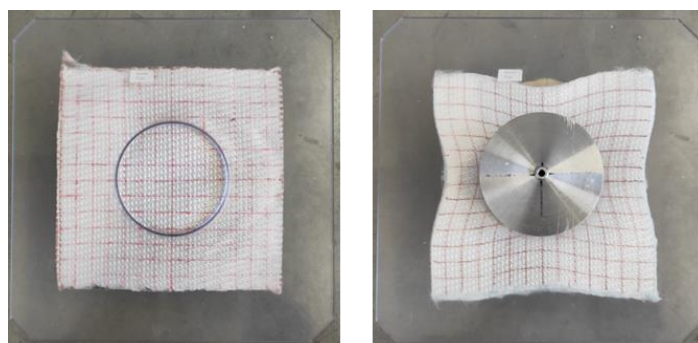


Figure 5-11 Schematic of: (a) In the centre location, (b) In the middle area and (c) In the locking area (dimensions in mm).

5.3.3.2 Pre-deformed stab-resistance test

In the stabbing experiment, the impact energy as mentioned earlier is lower than the required energy in the standards of personal protection analysis. To find out differences between the different structures of fabrics, tests were performed under the energy of 3.5 J in this paper. In order to study the influence of fabric stacks on deformed 3DWIF panels, two different fabric patterns as shown in Figure 5-1, i.e. $[0^\circ/90^\circ]$ ply and $[-45^\circ/45^\circ]$ ply, were chosen to form aligned fabric panel and angled fabric panel. For each panel, the pre-deformed stab-resistance test of three stab locations, as shown in Figure 5-11, i.e. in the centre location (A), in the middle area (B) and in the locking area (C), were employed. Top view of before forming tests and stabbing tests after deformation of the same aligned fabric panels are shown in Figure 5-12. The transparent plate used here is benefit for the deformation of the fabric panel before pre-deformed stab-resistance test.



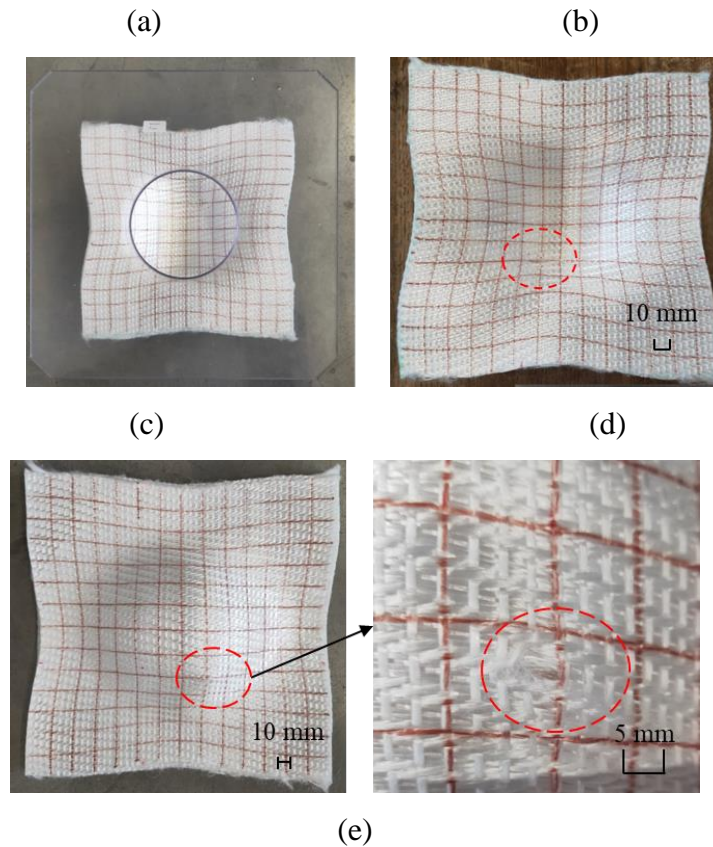


Figure 5-12 Example pre-deformed stab-resistance tests (a) Preparation, (b) Preforming of fabric panel, (c) Deformed fabric panel, (d) Stabbing on the deformed fabric panel, (e) Bottom of fabric panel after pre-deformed stab-resistance tests.

5.3.3.3 Influence of ply orientation

The stab resistance of two different deformed stacking sequences ($[0^\circ/90^\circ]_8$ and $[(0^\circ/90^\circ)/(-45^\circ/45^\circ)]_4$ with the same number of plies in each orientation has been studied. Figure 5-13 shows the depth of penetration of aligned and angled fabric panels at different locations. All the fabric panels were penetrated under the same stab energy. From the DOP point of view, there is an obvious difference in DOP value for both aligned and angled fabric panels from different stab locations. This result indicates that the stab location plays a significant role in the 3D fabric panels' performance.

In the case of $[0^\circ/90^\circ]_8$ aligned fabric panels, the DOP was decreased with the increase of shear angles in different locations, as shown in Figure 5-13. These results show that the centre location of aligned fabric panels is the most vulnerable position against stab. This may be due to the increase of shear angle, to some extent, which is helpful for the increase of fabric density,

and can make more yarns be efficient for preventing the blade to penetrate the fabric during the stabbing process.

In the case of $[(0^\circ/90^\circ)/(-45^\circ/45^\circ)]_4$ angled fabric panels, although the shear angle in the location of C is small and near to 0° for single $[-45^\circ/45^\circ]$ ply, it can be observed that the fabric which is stabbed in location C has also the minimum DOP value compared to other stab locations, as shown in Figure 5-13. It may be due to the fact that the weft yarn density is higher than warp yarn density. When the angle of fabric panels changed, more weft yarns will be cut by the blade. Besides, the angled fabric panels have some additional yarns in the two directions $(-45^\circ/45^\circ)$, which can reduce the possibility that the blade penetrated through the gap of the yarns. Moreover, concerning location A and B of angled fabric panels, the former DOP value is smaller than the latter. It indicated that the stab resistance of the fabric in the middle location is less significant than that in the fabric center stab impact because the impact location of the fabric is near the edges, the extension of the deformation pyramid is limited in the warp direction, and weft yarns are easily pulled out in this direction.

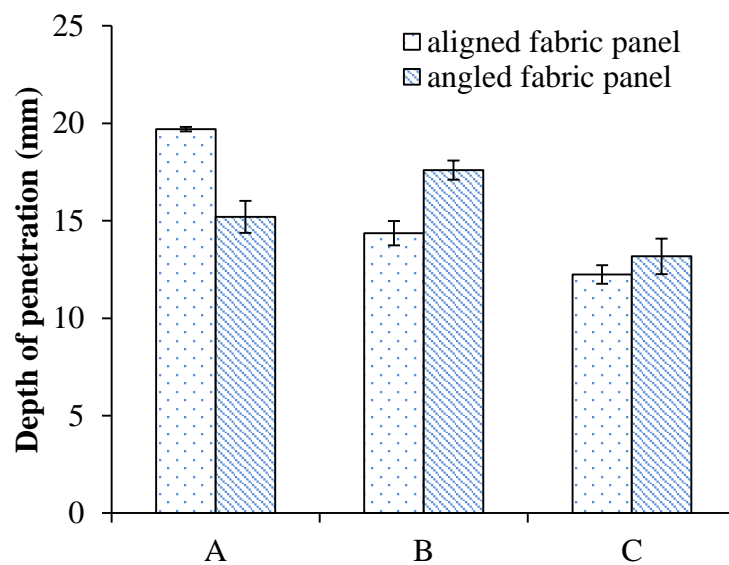


Figure 5-13 Depth of penetration of aligned and angled fabric panels at different locations.

5.3.3.4 Influence of stab location

Figure 5-14 compares the damage morphologies of fabric specimen of $[0^\circ/90^\circ]_8$ aligned fabric panels after the experimental stab test in different locations. Considering the partially enlarged view (Figure 5-14 (b)), the primary yarns (both weft and warp) in the back face of the fabric

are cut by the sharp blade edges. All the fabric targets have been penetrated primarily due to fiber failure and all fabric panels show little or no evidence of windowing from the side view (see Figure 5-14 (c)). Besides, it is obvious that the stab damaged area of the fabric specimen stabbed in location C is much larger than that of in locations A and B (Figure 5-14 (b)). The improvement of the stab strength is mainly due to the shear-locking angle which is helpful to reduce the gap between yarns [175] in location C. As the fabric is deformed, the density of warp and weft yarns per unit area increases, and that prevents the knife from continuing to penetrate the fabric panel. Thus, the depth of penetration is smallest. Besides, as shown in the side view of Figure 5-14 (c), it is clear to see that the yarns in the location C are completely cut off by the sharp edge of the knife. The sample stabbed in the location C appears to show a permanent, residual hole in the fabric layer that persisted when the knife was removed. By contrast, the sample stabbed in locations A and B shows no residual hole. While some of the secondary direction yarns in location A are pulled out and pushed as the knife penetrates [3]. It can be noted from the fabric specimen stabbed in location A and B that the deformation of fabric panels are smaller than the fabric specimen stabbed in location C (see Figure 5-14 (c)).

As shown in Figure 5-14 (c), DOT value (26.3 mm) in location C is larger than the DOT value in location A and B which is almost zero. It indicates that knife causes greater fabric deformation in the location C compared with the cases in location A and B via stabbing with the same stab energy. Besides, it shows that most of the energy is absorbed by the fabric panel and, therefore, the DOP is smaller by stabbing in the location C. The reason is that shear-locking angle appears in the location C, which results in tighter fabric panel and the yarns in this area can lock the knife and prevent the knife blade from perforating further during the penetration process.

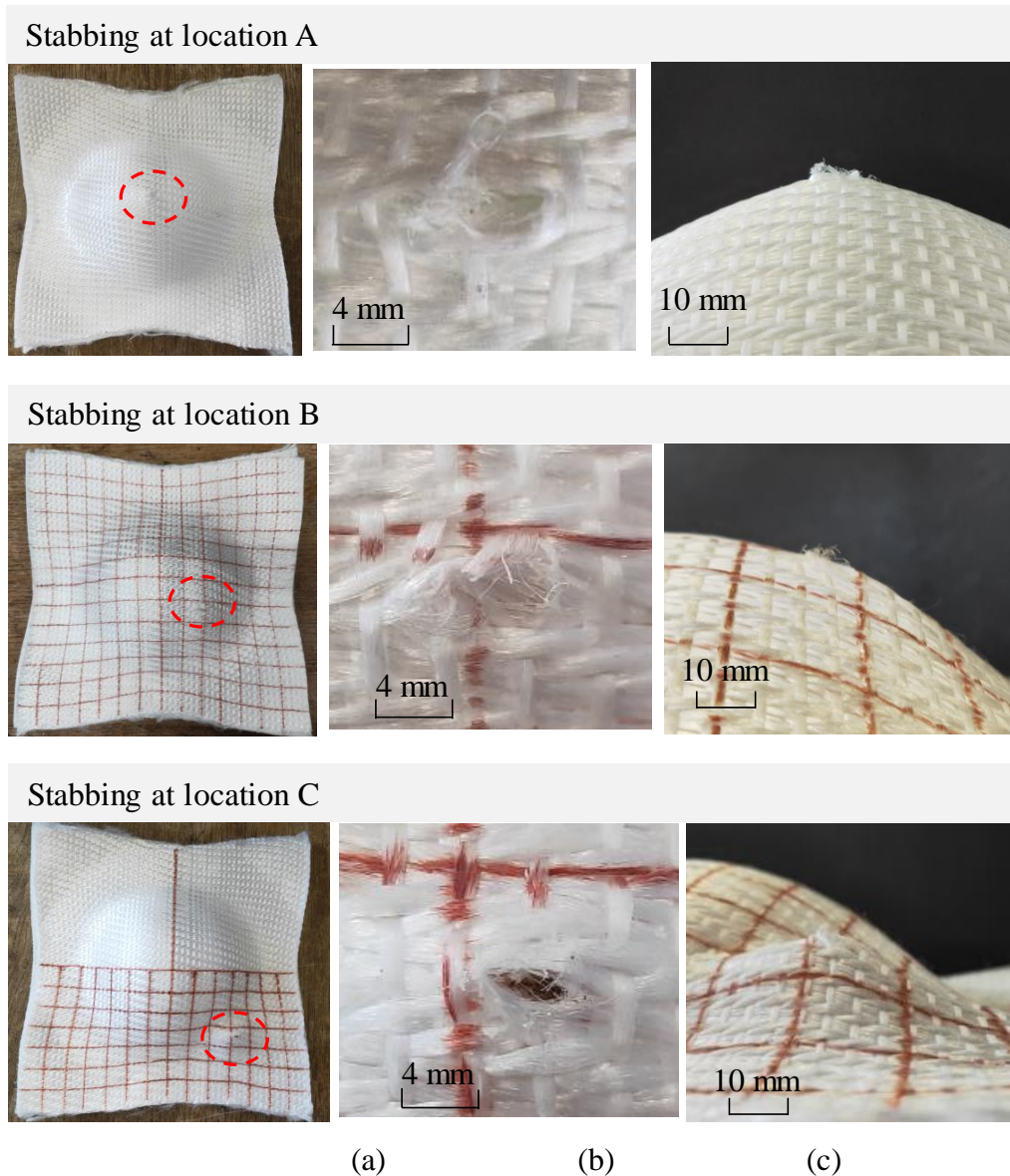


Figure 5-14 Damage morphologies of $[0^\circ/90^\circ]_8$ aligned fabric panels after the experimental stab test: (a) Overview; (b) Partial enlarged view; (c) Side view.

Figure 5-15 displays the damage morphologies of fabric specimen of $[0^\circ/90^\circ, -45^\circ/45^\circ]_4$ angled fabric panels after the stab test. During the stab tests, whether it was aligned or angled fabric panels, all the fabric panels were perforated. Local tearing strength of fibres is exceeded by the impact force, and therefore, the fibres are cut [3]. The fibres are not dishevelled and the cut is clear in locations B and C, see Figure 5-15 (b). Besides, the samples stabbed in the location B and C appear to show a permanent, residual hole in the fabric layer after the knife was removed. In contrast, the sample stabbed in location A shows no residual hole. The longitudinal fibers are mainly cut and transversal yarns are not completely damaged. It shows that the penetrator

pushes the fibres aside without cutting them which was defined as a windowing mechanism by Mayo et al. [188]. The fabric specimen stabbed in locations A and B that the deformation of fabric panels are smaller than the fabric specimen stabbed in location C which is similar to the results shown in aligned fabric panels.

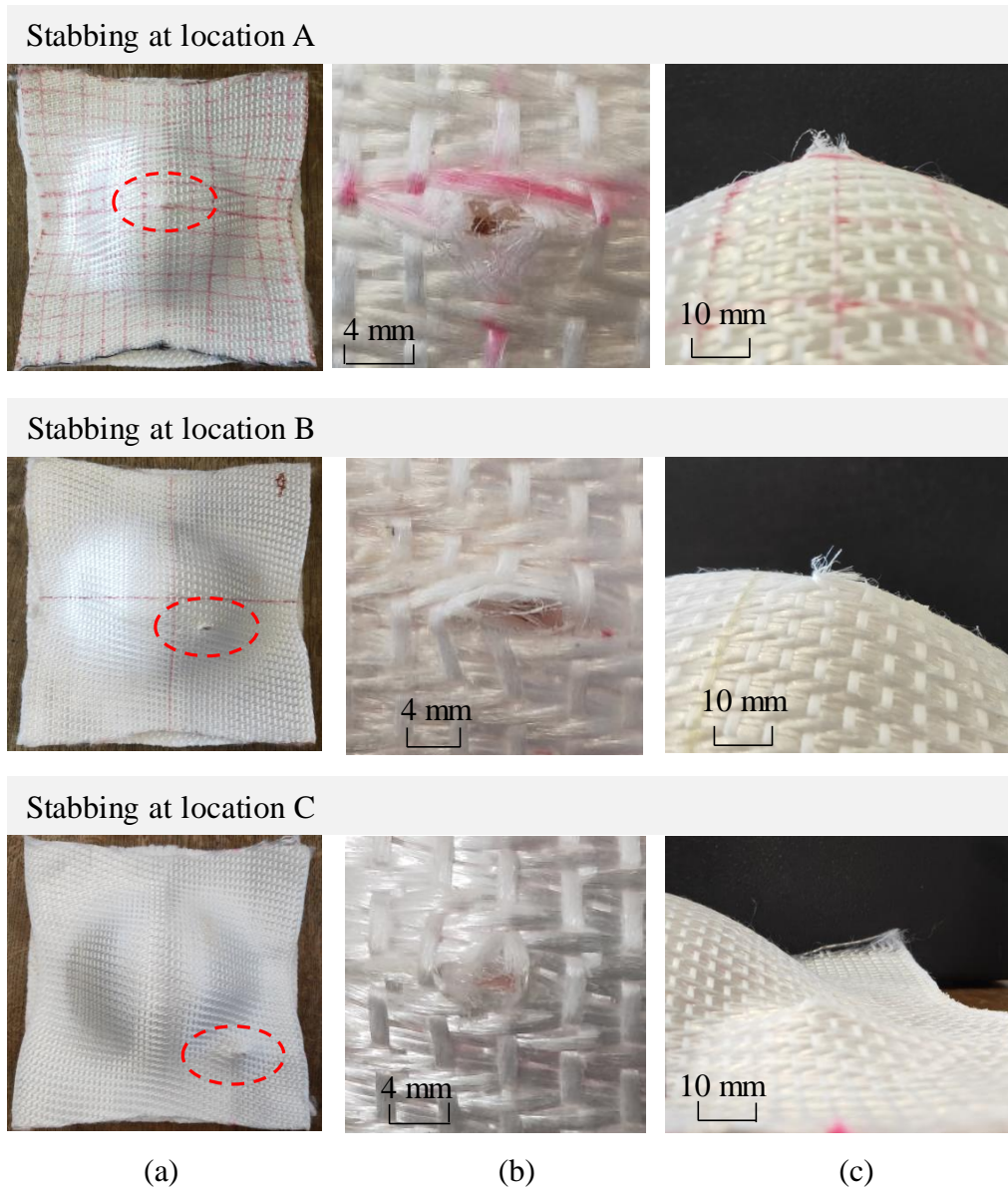


Figure 5-15 $[(0^\circ/90^\circ)/(-45^\circ/45^\circ)]_4$ angled fabric panels after the experimental stab test: (a) Overview; (b) Partial enlarged view; (c) Side view.

In Figure 5-15 (b), the trauma width in the location A is smaller than the corresponding one in location B. The first reason is that the yarns are highly symmetrical and evenly distributed in four directions ($0^\circ/90^\circ/\pm 45^\circ$) in angled fabric panels which can absorb more impact energy

compared with the aligned fabric panel, which showed good agreement with the study of Wang et al. [3]. The second reason is that the knife penetrated in the centre which is the point of intersection of yarn from four directions of fabric panel. As shown in Figure 5-15 (c), in $[0^\circ/90^\circ, -45^\circ/45^\circ]$ 4 angled fabric panels, it is similar with the $[0^\circ/90^\circ]$ 8 aligned fabric panels that the DOT (18.5 mm) of fabric panel stabbing in location C is larger than the DOT stabbing in location A and B which is also around 0. It shows that the locking-shear angle is indeed, to a large extent, conducive to improving stab resistance.

5.4 Summary of Chapter 5

This research has explored the pre-deformed stab-resistance property of the 3DWIF with O-T interlock structure after the hemispherical forming process to resemble the female body shape of 90B bust size. Two different initial orientations (single $[0^\circ/90^\circ]$ ply and a $[-45^\circ/45^\circ]$ ply) of fabric yarns were selected which produced very interesting results when observed from the point of views of shearing of the fabric yarns and of the material draw-in along the contours of woven fabrics with hemispherical forming devices. The two cases show quite different deformed profiles and local shear angles distribution, which proved that fibre orientations have a significant effect on 3DWIF forming.

Three stab impacts locations at the fabric centre, at the middle of the deformed place and at the area with largest shear angles were chosen based on results of the forming process. The stab resistance of aligned and angled fabric panels in these three different locations after the hemispherical forming process was investigated and the experimental results were compared. The results show that the effect of stab localization on the fabric behaviour is significant and the stab resistance in the location with large shear angle of both deformed fabric stacks ($[0^\circ/90^\circ]$ 8 and $[(0^\circ/90^\circ)/(-45^\circ/45^\circ)]$ 4) is the best in the studied cases compared with other locations.

General conclusion

Conclusion

The present study aims at engineering design different 3DWIFs for protective application. The objectives set out for this PhD research are (a) to characterise the geometric and structural parameters of these structural fabrics; (b) to experimentally focus on the mechanical property of the different fabrics, tensile property were discussed and compared; (c) to work out a relatively good structure of 3DWIFs for the protective application based on the selected fabric type, stab resistance property had been explored, including single-stab resistance and double-stab resistance properties; (d) to introduce the pre-deformed stab resistance, the study of the deformed fabrics with curved shape were stabbed in different places.

The main achievements of the research are concluded as follows:

- 1) 3DWIFs woven by high-performance multi-filaments yarns (50 tpm) are successfully implemented at the modified conventional weaving machine and introduction of individual dropper on each yarn has been helped to adjust the warp yarn tension of 3DWIF during the weaving process.

Five different 3DWIFs were designed and manufactured in the same warp and weft densities. Moreover, the yarns degradation during the weaving process of the three systems was also studied. Based on these result, the average tensile strength of weft yarns was reduced by 6.2% - 11.8%, and the deformation at break of weft yarns is less than 1%. Compared with the binding warp yarns, the yarn strength degradation of stuffer warp yarns is 9.9% - 15.2% which may due to the friction among the yarns and yarns with the loom machinery part.

- 2) The warp binding path influences not only mechanical properties in the warp direction but also in the weft direction and increasing binding depth i.e. crimp amplitude of interlocking warp tows reduces the breaking strength of the fabric in the warp direction.

The inter warp yarn frictions in the tensile tests were analysed. Based on Peirce's geometrical model, the wrapping angles between binding warp and weft yarns in 3DWIF structures were calculated and the influence of these angles on the inter yarn friction was also discussed. The arrangement of weft tows i.e., their reorganisation and resultant fibre-less voids depend on the warp binding path. The binding depth of interlocking warp plays an important role in determining the efficiency of the fabric in the loading direction. Moreover, the wrapping

angles/total wrapping angle of the 3DWIFs depend on the patterns of weave, which are related to the inter yarn friction of 3D fabrics and also have an influence on the tensile properties of 3DWIFs.

- 3) The fabric with orthogonal-through-the-thickness interlock structure reveals the most favourable stab resistance compared to other structures and the stab resistance in weft direction is higher than that in the warp direction.

A systematic comparison of 3DWIFs for resisting against classical dynamic stab attacks has been successfully performed with HOSDB/P1/B sharpness blades on the HMWPE fabrics. It can be highlighted that the main structural parameters of the 3DWIF as the binding warp yarns architecture have revealed the orthogonal-through-the-thickness as the best candidate for stabbing protection. Besides, the orientation of plies significantly affects the stab resistance of the multi-ply fabric panels after stab impact.

The distance that the cutting knife travelled to cut consecutive yarns was different from the change in knife penetration angle that, to some extent, affected the stab resistance. It indicated that the angled panels do not always increase the stab resistance of 3DWIF compared with the aligned panel since the warp and weft densities are not the same. When the number of plies has reached a certain limit, the ply orientation is conducive to improving the stab resistance performance of the fabric panel.

- 4) The measurement results of DOP in double and multi-angle pass stabbing provide that the stab resistance in 90° (perpendicular to the weft yarns) is higher than that in other directions. The double and multi-angle pass stabbing results highlight also that the better condition occurs when the stab angles are identical in each pass.
- 5) The effect of stab localization on the fabric behaviour is significant and the stab resistance in the location with large shear angle of both deformed fabric stacks ($[0^\circ/90^\circ]_8$ and $[(0^\circ/90^\circ)/(-45^\circ/45^\circ)]_4$) is the best in the studied cases compared with other locations.

Two different initial orientations (single $[0^\circ/90^\circ]$ ply and a $[-45^\circ/45^\circ]$ ply) of fabric with O-T interlock structure were selected, which produced very interesting results when observed from the point of views of shearing of the fabric yarns and of the material draw-in along the contours of woven fabrics with hemispherical forming devices. Two cases have quite different deformed profiles and local shear angles distribution, which proved that fibre orientations have a

significant effect on 3DWIF forming. Three stab impacts locations at the fabric centre, at the middle of the deformed place and at the area with largest shear angles were chosen based on results of the forming process. The stab resistance of aligned and angled fabric panels in three different locations after the hemispherical forming process was investigated and the experimental results were compared.

Perspectives

Based on the work done in the present research, a number of projects are possible to be continued.

- The design of these fabrics would be beneficial for the optimisation of the 3DWIF's architecture and improve the protection level of soft protective materials.
- The stab resistance of deformed fabric in different size could be discussed for different body shapes.
- A systematic study of the failure mechanisms of the 3DWIF under stab impact would be helpful for understanding the superiority of different structures.
- A yarn-level finite element model can be assumed as an interesting approach in analysing the stab resistance response of different structures.
- The energy absorption by the fabric panels can be investigated for further comparison of different structures.

REFERENCES

- [1] Allen G, Audickas L, Loft P, Bellis A. Knife crime in England and Wales. vol. SN4304. 2019.
- [2] Decker MJ, Halbach CJ, Nam CH, Wagner NJ, Wetzel ED. Stab resistance of shear thickening fluid (STF)-treated fabrics. *Compos Sci Technol* 2007;67:565–78. <https://doi.org/10.1016/j.compscitech.2006.08.007>.
- [3] Rodríguez-Millán M, Álvarez-Díaz A, Aranda-Ruiz J, Álvarez-Díaz J, Loya JA. Experimental analysis for stabbing resistance of different aramid composite architectures. *Compos Struct* 2019;208:525–34. <https://doi.org/10.1016/j.compstruct.2018.10.042>.
- [4] Yadav R, Naebe M, Wang XG, Kandasubramanian B. Body armour materials: from steel to contemporary biomimetic systems. *RSC Adv* 2016;6:115145–74. <https://doi.org/10.1039/c6ra24016j>.
- [5] David NV., Gao XL, Zheng JQ. Ballistic resistant body armor: Contemporary and prospective materials and related protection mechanisms. *Appl Mech Rev* 2009;62:1–20. <https://doi.org/10.1115/1.3124644>.
- [6] Chen XG, Yang D. Use of 3D Angle-Interlock Woven Fabric for Seamless Female Body Armor: Part 1: Ballistic Evaluation. *Text Res J* 2010;80:1581–8. <https://doi.org/10.1177/0040517510363187>.
- [7] Mawkhlieng U, Majumdar A, Laha A. A review of fibrous materials for soft body armour applications. *RSC Adv* 2019;10:1066–86. <https://doi.org/10.1039/c9ra06447h>.
- [8] Hassim N, Ahmad MR, Ahmad WYW, Samsuri A, Yahya MHM. Puncture resistance of natural rubber latex unidirectional coated fabrics. *J Ind Text* 2012;42:118–31. <https://doi.org/10.1177/1528083711429144>.
- [9] Nayak R, Crouch I, Kanesalingam S, Ding J, Tan P, Lee B, et al. Body armor for stab and spike protection, Part 1: Scientific literature review. *Text Res J* 2018;88:812–32. <https://doi.org/10.1177/0040517517690623>.
- [10] Karahan M, Kuş A, Eren R. An investigation into ballistic performance and energy absorption capabilities of woven aramid fabrics. *Int J Impact Eng* 2008;35:499–510. <https://doi.org/10.1016/j.ijimpeng.2007.04.003>.
- [11] Chen XG. *Advances in 3D Textiles*. Cambridge: Woodhead Publishing, 2015.
- [12] Li MR, Wang P, Boussu F, Soulat D. A review on the mechanical performance of three-

- dimensional warp interlock woven fabrics as reinforcement in composites. *J Ind Text* 2020;0:1–50. <https://doi.org/10.1177/1528083719894389>.
- [13] Abteu MA, Boussu F, Bruniaux P, Loghin C, Cristian I. Engineering of 3D warp interlock p-aramid fabric structure and its energy absorption capabilities against ballistic impact for body armour applications. *Compos Struct* 2019;225:1–15. <https://doi.org/10.1016/j.compstruct.2019.111179>.
- [14] Shi WF, Hu H, Sun BZ, Gu BH. Energy absorption of 3D orthogonal woven fabric under ballistic penetration of hemispherical-cylindrical projectile. *J Text Inst* 2011;102:875–89. <https://doi.org/10.1080/00405000.2010.525815>.
- [15] Alubel Abteu M, Boussu F, Bruniaux P, Loghin C, Cristian I. Ballistic impact mechanisms - A review on textiles and fibre-reinforced composites impact responses. *Compos Struct* 2019;223:110966. <https://doi.org/10.1016/j.compstruct.2019.110966>.
- [16] Bilisik K. Two-dimensional (2D) fabrics and three-dimensional (3D) preforms for ballistic and stabbing protection: A review. *Text Res J* 2016;87:2275–304. <https://doi.org/10.1177/0040517516669075>.
- [17] Chen XG, Zhou Y. 6-Technical textiles for ballistic protection. *Handb. Tech. Text.*, 2016, p. 169–92. <https://doi.org/10.1016/b978-1-78242-465-9.00006-9>.
- [18] Bogetti TA, Walter M, Staniszewski J, Cline J. Interlaminar shear characterization of ultra-high molecular weight polyethylene (UHMWPE) composite laminates. *Compos Part A Appl Sci Manuf* 2017;98:105–15. <https://doi.org/10.1016/j.compositesa.2017.03.018>.
- [19] Nguyen LH, Lässig TR, Ryan S, Riedel W, Mouritz AP, Orifici AC. A methodology for hydrocode analysis of ultra-high molecular weight polyethylene composite under ballistic impact. *Compos Part A Appl Sci Manuf* 2016;84:224–35. <https://doi.org/10.1016/j.compositesa.2016.01.014>.
- [20] da Silva LF, Lavoratti A, Pereira IM, Dias RR, Amico SC, Zattera AJ. Development of multilaminar composites for vehicular ballistic protection using ultra-high molecular weight polyethylene laminates and aramid fabrics. *J Compos Mater* 2019;53:1907–16. <https://doi.org/10.1177/0021998318815959>.
- [21] Brandt J, Drechsle K, Arendtsb F. Mechanical performance of composites based on various three-dimensional woven-fibre preforms. *Compos Sci Technol* 1996;3538:381–6.
- [22] Padaki N V., Alagirusamy R, Deopura BL, Fanguero R. Studies on preform properties of multilayer interlocked woven structures using fabric geometrical factors. *J Ind Text*

- 2010;39:327–46. <https://doi.org/10.1177/1528083709349885>.
- [23] Midani M, Seyam A-F, Pankow M. A generalized analytical model for predicting the tensile behavior of 3D orthogonal woven composites using finite deformation approach. *J Text Inst* 2018;5000:1–12. <https://doi.org/10.1080/00405000.2018.1425107>.
- [24] Hu JL. Introduction to three-dimensional fibrous assemblies. *3-D Fibrous Assem* 2008. <https://doi.org/10.1533/B978-1-84569-377-0.50001-1>.
- [25] Behera BK, Dash BP. Mechanical behavior of 3D woven composites. *Mater Des* 2014;67:261–71. <https://doi.org/10.1016/j.matdes.2014.11.020>.
- [26] Chen XG, Zanini I. An experimental investigation into the structure and mechanical properties of 3D woven orthogonal structures. *J Text Inst* 1997;88:449–64. <https://doi.org/10.1080/00405000.1997.11090896>.
- [27] Coman F, Herszberg L, Bannister M, John S. Design and analysis of 3D woven preforms for composite structures. *Sci Eng Compos Mater* 1996;5:83–96. <https://doi.org/10.1515/secm.1996.5.2.83>.
- [28] Chen XG, Lo WY, Tayyar AE. Mouldability of Angle-Interlock Woven Fabrics for Technical Applications. *Text Res J* 2002;72:195–200. <https://doi.org/10.1177/004051750207200302>.
- [29] Wei QH, Wang CH, Wang HS, Li L, Luan Q, Liao R, Dong Bo. Disposing of Silica Fiber' Surface. *Key Eng Mater* 2012;512–515:559–62. <https://doi.org/10.4028/www.scientific.net/KEM.512-515.559>.
- [30] Corbin AC, Kececi A, Boussu F, Ferreira M, Soulat D. Engineering Design and Mechanical Property Characterisation of 3D Warp Interlock Woven Fabrics. *Appl Compos Mater* 2018;25:811–22. <https://doi.org/10.1007/s10443-018-9715-z>.
- [31] Boussu F, Dufour C, Veyet F, Lefebvre M. 3-Weaving processes for composites manufacture. *Adv Compos Manuf Process Des* 2015:55–78. <https://doi.org/10.1016/B978-1-78242-307-2.00003-8>.
- [32] Dittenber DB, Gangarao HVS. Critical review of recent publications on use of natural composites in infrastructure. *Compos Part A Appl Sci Manuf* 2012;43:1419–29. <https://doi.org/10.1016/j.compositesa.2011.11.019>.
- [33] Nilakantan G, Keefe M, Gillespie JW, Bogetti TA, Adkinson R. A Numerical Investigation into the Effects of 3D Architecture on the Impact Response of Flexible Fabrics. *Second WORLD Conf 3D Fabr THEIR Appl* April 6-7, 2009, Greenville, South Carolina, USA 2016.

- [34] Wallenberger FT, Bingham PA. Fiberglass and glass technology. 2010.
- [35] Kulkarni SV, Rice JS, Rosen BW. An investigation of the compressive strength of Kevlar 49 / epoxy composites. *COMPOSITES* 1975;217–25.
- [36] Teijin. Twaron – a versatile high-performance fiber. *WwwTeijinaramidCom* 2012:7.
- [37] <https://www.packagingcomposites-honeywell.com/spectra/product-info/spectra-fiber/>. Honeywell Spectra® 2019.
- [38] <https://www.hexcel.com/Resources/DataSheets/Carbon-Fiber> n.d.
- [39] <http://www.toray-cfe.com/fr/fibres-carbone/fibres-torayca.html> n.d.
- [40] Ansar M, Wang XW, Zhou CW. Modeling strategies of 3D woven composites: A review. *Compos Struct* 2011;93:1947–63. <https://doi.org/10.1016/j.compstruct.2011.03.010>.
- [41] Huang T, Wang YL, Wang G. Review of the mechanical properties of a 3D woven composite and its applications. *Polym Plast Technol Eng* 2017;0:1–17. <https://doi.org/10.1080/03602559.2017.1344857>.
- [42] Boussu F, Cristian I, Nauman S. General definition of 3D warp interlock fabric architecture. *Compos Part B Eng* 2015;81:171–88. <https://doi.org/10.1016/j.compositesb.2015.07.013>.
- [43] Gu H, Zhong ZL. Tensile behavior of 3D woven composites by using different fabric structures. *Mater Des* 2002;23:671–4. [https://doi.org/DOI:10.1016/S0261-3069\(02\)00053-5](https://doi.org/DOI:10.1016/S0261-3069(02)00053-5).
- [44] Gu H. Comparison between laminated and integrated glass fibre reinforced plastic. *Mater Des* 2000;21:461–4.
- [45] Lomova S V., Bogdanovich AE, Ivanov DS, Mungalov D, Karahan M, Verpoest I. A comparative study of tensile properties of non-crimp 3D orthogonal weave and multi-layer plain weave E-glass composites. Part 1: Materials, methods and principal results. *Compos Part A Appl Sci Manuf* 2009;40:1144–57. <https://doi.org/10.1016/j.compositesa.2009.04.032>.
- [46] Bogdanovich AE, Karahan M, Lomov S V., Verpoest I. Quasi-static tensile behavior and damage of carbon/epoxy composite reinforced with 3D non-crimp orthogonal woven fabric. *Mech Mater* 2013;62:14–31. <https://doi.org/10.1016/j.mechmat.2013.03.005>.
- [47] Cristian I, Nauman S, Boussu F, Koncar V. A study of strength transfer from tow to textile composite using different reinforcement architectures. *Appl Compos Mater* 2012;19:427–42. <https://doi.org/10.1007/s10443-011-9215-x>.
- [48] Castaneda N, Wisner B, Cuadra J, Amini S, Kontsos A. Investigation of the Z-binder

- role in progressive damage of 3D woven composites. *Compos Part A Appl Sci Manuf* 2017;98:76–89. <https://doi.org/10.1016/j.compositesa.2016.11.022>.
- [49] Chou S, Chen HC, Chen HE. Effect of weave structure on mechanical fracture behavior of three-dimensional carbon fiber fabric reinforced epoxy resin composites. *Compos Sci Technol* 1992;45:23–35. [https://doi.org/10.1016/0266-3538\(92\)90119-N](https://doi.org/10.1016/0266-3538(92)90119-N).
- [50] Mouritz AP, Bannister MK, Falzon PJ, Leong KH. Review of applications for advanced three-dimensional fibre textile composites. *Compos Part A Appl Sci Manuf* 1999;30:1445–61. [https://doi.org/10.1016/S1359-835X\(99\)00034-2](https://doi.org/10.1016/S1359-835X(99)00034-2).
- [51] Dai S, Cunningham PR, Marshall S, Silva C. Influence of fibre architecture on the tensile, compressive and flexural behaviour of 3D woven composites. *Compos Part A Appl Sci Manuf* 2015;69:195–207. <https://doi.org/10.1016/j.compositesa.2014.11.012>.
- [52] Guenon VA., Chou TW, Gillespie JW. Toughness properties of a three-dimensional carbon-epoxy composite. *J Mater Sci* 1989;24:4168–75. <https://doi.org/10.1007/BF01168991>.
- [53] Rudov-Clark S, Mouritz AP. Tensile fatigue properties of a 3D orthogonal woven composite. *Compos Part A Appl Sci Manuf* 2008;39:1018–24. <https://doi.org/10.1016/j.compositesa.2008.03.001>.
- [54] Hu JL. 3-D fibrous assemblies: Properties, applications and modelling of three-dimensional textile structures. 2008. <https://doi.org/10.1533/9781845694982>.
- [55] Chu TL, Ha-Minh C, Imad A. Analysis of local and global localizations on the failure phenomenon of 3D interlock woven fabrics under ballistic impact. *Compos Struct* 2016;159:267–77. <https://doi.org/10.1016/j.compstruct.2016.09.039>.
- [56] Chen XG, Taylor LW and Tsai LJ. An overview on fabrication of three-dimensional woven textile preforms for composites. *Text Res J* 2011 2011;81:932–44. <https://doi.org/10.1016/B978-1-78242-458-1.00013-3>.
- [57] Bilisik K, Karaduman NS, Bilisik NE. 3D Fabrics for Technical Textile Applications. *IntechOpen*, vol. 2, 2018, p. 64. <https://doi.org/10.5772/32009>.
- [58] Fukuta K and Aoki E. 3D fabrics for structural composites. *Proc. 15th Text. Res. Symp. Philadelphia, PA, 1986*.
- [59] Khokar N. 3D Fabric-forming processes: distinguishing between 2D-weaving, 3D-weaving and an unspecified non-interlacing process. *J Text Inst* 1996;87:97–106. <https://doi.org/10.1080/00405009608659059>.
- [60] Soden JA, Hill BJ. Conventional weaving of shaped preforms for engineering composites. *Compos Part A Appl Sci Manuf* 1998;29:757–62.

- [https://doi.org/10.1016/S1359-835X\(98\)00053-0](https://doi.org/10.1016/S1359-835X(98)00053-0).
- [61] Khokar N. 3D-Weaving: theory and practice. *J Text Inst* 2001;92:193–207. <https://doi.org/10.1080/00405000108659570>.
- [62] Khokar N. Noobing: A nonwoven 3D fabric-forming process explained. *J Text Inst* 2002;93:52–74. <https://doi.org/10.1080/00405000208630552>.
- [63] Chen XG. Technical aspect: 3D Woven architectures. *Proc NWTexNet 2007 Conf Blackburn* 2007.
- [64] Gokarneshan N, Alagirusamy R. Weaving of 3D fabrics: A critical appreciation of the developments. *Text Prog* 2009;41:1–58. <https://doi.org/10.1080/00405160902804239>.
- [65] Bilisik K. Multiaxis three-dimensional weaving for composites: A review. *Text Res J* 2012;82:725–43. <https://doi.org/10.1177/0040517511435013>.
- [66] Umair M, Hamdani S, Asghar MA, Hussain T, Karahan M, Nawab Y, et al. Study of influence of interlocking patterns on the mechanical performance of 3D multilayer woven composites. *J Reinf Plast Compos* 2018;37:429–40. <https://doi.org/10.1177/0731684417751059>.
- [67] Cuong HM, Imad A, Boussu F, Kanit T. Experimental and numerical investigation of a 3D woven fabric subjected to a ballistic impact. *Int J Impact Eng* 2015;88:91–101. <https://doi.org/10.1016/j.ijimpeng.2015.08.011>.
- [68] Ding X, Yi HL. Parametric representation of 3D woven structure. *Proc 6th Asian Text Conf (CD Version)*, Hong Kong, China, No 103, 2001.
- [69] Gu BH. *Modelling of 3D woven fabrics for ballistic protection*. Elsevier Ltd; 2016. <https://doi.org/10.1016/B978-1-78242-461-1.00006-6>.
- [70] Dai S, Cunningham PR, Marshall S, Silva C. Open hole quasi-static and fatigue characterisation of 3D woven composites. *Compos Struct* 2015;131:765–74. <https://doi.org/10.1016/j.compstruct.2015.06.032>.
- [71] Ma P, Jin L, Wu L. Experimental and numerical comparisons of ballistic impact behaviors between 3D angle-interlock woven fabric and its reinforced composite. *J Ind Text* 2019;48:1044–58. <https://doi.org/10.1177/1528083718754903>.
- [72] Pan ZX, Gu BH, Sun BZ, Xiong J. Progressive failure of 3-D textile composites under impact loadings. *Compos Struct* 2017;168:710–24. <https://doi.org/10.1016/j.compstruct.2017.02.067>.
- [73] Yi HL, Ding X. Conventional approach on manufacturing 3D woven preforms used for composites. *J Ind Text* 2004;34:39–50. <https://doi.org/10.1177/1528083704045847>.
- [74] Chen XG, Spola M, Paya JG, Sellabona PM. *Experimental Studies on the Structure and*

- Mechanical Properties of Multi-layer and Angle-interlock Woven Structures. *J Text Inst* 1998;90:91–9. <https://doi.org/10.1080/00405009908658693>.
- [75] Kumar B, Hu JL. Woven fabric structures and properties. *Eng. High-Performance Text.*, 2018, p. 133–51. <https://doi.org/10.1016/B978-0-08-101273-4.00004-4>.
- [76] Bandaru AK, Sachan Y, Ahmad S, Alagirusamy R, Bhatnagar N. On the mechanical response of 2D plain woven and 3D angle-interlock fabrics. *Compos Part B Eng* 2017;118:135–48. <https://doi.org/10.1016/j.compositesb.2017.03.011>.
- [77] Boussu F, Picard S, Soulat D. Interesting mechanical properties of 3D warp interlock fabrics. *Narrow Smart Text.*, 2017, p. 21–31. https://doi.org/10.1007/978-3-319-69050-6_3.
- [78] Hou YQ, Hu HJ, Sun BZ, Gu BH. Strain rate effects on tensile failure of 3-D angle-interlock woven carbon fabric. *Mater Des* 2013;46:857–66. <https://doi.org/10.1016/j.matdes.2012.11.012>.
- [79] Dash AK, Behera BK. Role of weave design on the mechanical properties of 3D woven fabrics as reinforcements for structural composites. *J Text Inst* 2017;109:952–60. <https://doi.org/10.1080/00405000.2017.1393787>.
- [80] Abteew MA, Boussu F, Bruniaux P, Loghin C, Cristian I, Chen Y, et al. Influences of fabric density on mechanical and moulding behaviours of 3D warp interlock para-aramid fabrics for soft body armour application. *Compos Struct* 2018;204:402–18. <https://doi.org/10.1016/j.compstruct.2018.07.101>.
- [81] Corbin AC, Boussu F, Ferreira M, Soulat D. Influence of 3D warp interlock fabrics parameters made with flax rovings on their final mechanical behaviour. *J Ind Text* 2018;152808371880879. <https://doi.org/10.1177/1528083718808790>.
- [82] Lansiaux H, Soulat D, Boussu F, Labanieh AR. Development and multiscale characterization of 3D warp interlock flax fabrics with different woven architectures for composite applications. *Fibers* 2020;8:15. <https://doi.org/10.3390/fib8020015>.
- [83] Dash AK, Behera BK. Role of stuffer layers and fibre volume fractions on the mechanical properties of 3D woven fabrics for structural composites applications. *J Text Inst* 2019;110:614–24. <https://doi.org/10.1080/00405000.2018.1502502>.
- [84] Li MR, Wang P, Boussu F, Soulat D. Effect of Fabric Architecture on Tensile Behaviour of the High-Molecular-Weight Polyethylene 3-Dimensional Interlock Composite Reinforcements. *Polymers (Basel)* 2020;12:1–18. <https://doi.org/10.3390/polym12051045>.
- [85] Nasrun FMZ, Yahya MF, Ghani SA, Ahmad MR. Effect of weft density and yarn crimps

- towards tensile strength of 3D angle interlock woven fabric. AIP Conf Proc 2016;1774. <https://doi.org/10.1063/1.4965051>.
- [86] Zhang DT, Sun Y, Chen L, Pan N. A comparative study on low-velocity impact response of fabric composite laminates. *Mater Des* 2013;50:750–6. <https://doi.org/10.1016/j.matdes.2013.03.044>.
- [87] Bandaru AK, Chavan V V., Ahmad S, Alagirusamy R, Bhatnagar N. Low velocity impact response of 2D and 3D Kevlar/polypropylene composites. *Int J Impact Eng* 2016;93:136–43. <https://doi.org/10.1016/j.ijimpeng.2016.02.016>.
- [88] Cox BN, Dadkhah MS, Morris WL. On the tensile failure of 3D woven composites. *Compos Part A Appl Sci Manuf* 1996;27:447–58. [https://doi.org/10.1016/1359-835X\(95\)00053-5](https://doi.org/10.1016/1359-835X(95)00053-5).
- [89] Behera BK, Dash BP. An experimental investigation into the mechanical behaviour of 3D woven fabrics for structural composites. *Fibers Polym* 2014;15:1950–5. <https://doi.org/10.1007/s12221-014-1950-9>.
- [90] Shim VPW, Lim CT, Foo KJ. Dynamic mechanical properties of fabric armour. *Int J Impact Eng* 2001;25:1–15. [https://doi.org/10.1016/S0734-743X\(00\)00038-5](https://doi.org/10.1016/S0734-743X(00)00038-5).
- [91] Zhu DJ, Mobasher B, Rajan SD. Finite Element Modeling of Ballistic Impact on Kevlar 49 FabricS. *Conf. Proc. Soc. Exp. Mech. Ser.*, vol. 1, 2011, p. 249–58. https://doi.org/10.1007/978-1-4614-0216-9_36.
- [92] Naik D, Sankaran S, Mobasher B, Rajan SD, Pereira JM. Development of reliable modeling methodologies for engine fan blade out containment analysis. Part I: Experimental studies. *Int J Impact Eng* 2009;36:447–59. <https://doi.org/10.1016/j.ijimpeng.2008.08.004>.
- [93] Yang D, Chen XG, Sun DM, Zhang SY, Yi CH, Gong XZ, et al. Ballistic performance of angle-interlock woven fabrics. *J Text Inst* 2017;108:586–96. <https://doi.org/10.1080/00405000.2016.1176622>.
- [94] Cantwell WJ, Morton J. The impact resistance of composite materials - a review. *Composites* 1991;22:347–62. [https://doi.org/10.1016/0010-4361\(91\)90549-V](https://doi.org/10.1016/0010-4361(91)90549-V).
- [95] Jayasundara H. Impact resistance of composite materials. 2012. [https://doi.org/10.1016/0010-4361\(91\)90549-V](https://doi.org/10.1016/0010-4361(91)90549-V).
- [96] Roylance D, Wilde A, Tocci G. Ballistic Impact of Textile Structures. *Text Res J* 1973;43:34–41. <https://doi.org/10.1177/004051757304300105>.
- [97] Behera BK, Dash BP. An experimental investigation into structure and properties of 3D-woven aramid and PBO fabrics. *J Text Inst* 2013;104:1337–44.

- <https://doi.org/10.1080/00405000.2013.805873>.
- [98] Cheeseman BA, Bogetti TA. Ballistic impact into fabric and compliant composite laminates. *Compos Struct* 2003;61:161–73. [https://doi.org/10.1016/S0263-8223\(03\)00029-1](https://doi.org/10.1016/S0263-8223(03)00029-1).
- [99] Yang CC, Ngo T, Tran P. Influences of weaving architectures on the impact resistance of multi-layer fabrics. *Mater Des* 2015;85:282–95. <https://doi.org/10.1016/j.matdes.2015.07.014>.
- [100] Lefebvre M, Boussu F. High energy absorption of warp interlock fabrics : Application to high speed impact of fragments. *Dymat* 2009, 2009, p. 429–35. <https://doi.org/10.1051/dymat/2009061>.
- [101] Ha-Minh C, Boussu F, Kanit T, Crépin D, Imad A. Analysis on failure mechanisms of an interlock woven fabric under ballistic impact. *Eng Fail Anal* 2011;18:2179–87. <https://doi.org/10.1016/j.engfailanal.2011.07.011>.
- [102] Zhang YF, Sun F, Wang YJ, Chen L, Pan N. Study on intra/inter-ply shear deformation of three dimensional woven preforms for composite materials. *Mater Des* 2013;49:151–9. <https://doi.org/10.1016/j.matdes.2013.02.025>.
- [103] Cao J, Akkerman R, Boisse P, Chen J, Cheng HS, de Graaf EF, et al. Characterization of mechanical behavior of woven fabrics: Experimental methods and benchmark results. *Compos Part A Appl Sci Manuf* 2008;39:1037–53. <https://doi.org/10.1016/j.compositesa.2008.02.016>.
- [104] Carvelli V, Pazmino J, Lomov S V., Verpoest I. Deformability of a non-crimp 3D orthogonal weave E-glass composite reinforcement. *Compos Sci Technol* 2012;73:9–18. <https://doi.org/10.1016/j.compscitech.2012.09.004>.
- [105] Hivet G, Duong AV. A contribution to the analysis of the intrinsic shear behavior of fabrics. *J Compos Mater* 2011;45:695–716. <https://doi.org/10.1177/0021998310382315>.
- [106] Orliac J. Analyse et simulation du comportement anisotrope lors de la mise en forme de renforts tissés interlock. 2012. [https://doi.org/10.5712/rbmfc7\(1\)628](https://doi.org/10.5712/rbmfc7(1)628).
- [107] Boisse P, Hamila N, Guzman-Maldonado E, Madeo A, Hivet G, dell’Isola F. The bias-extension test for the analysis of in-plane shear properties of textile composite reinforcements and prepregs: a review. *Int J Mater Form* 2017;10:473–92. <https://doi.org/10.1007/s12289-016-1294-7>.
- [108] Bogdanovich A E. Advancements in manufacturing and applications of 3-D woven preforms and composites. 16TH Int. Conf. Compos. Mater., 2006, p. 1–10.
- [109] Charmetant A, Orliac JG, Vidal-Sallé E, Boisse P. Hyperelastic model for large

- deformation analyses of 3D interlock composite preforms. *Compos Sci Technol* 2012;72:1352–60. <https://doi.org/10.1016/j.compscitech.2012.05.006>.
- [110] Guan LX, Li JL, Jiao YN. The influence of yarn fineness and number of yarn layers on in-plane shear properties of 3-D woven fabric. *Adv Compos Lett* 2020;29:2633366X1989792. <https://doi.org/10.1177/2633366x19897921>.
- [111] Ullah H, Harland AR, Silberschmidt V V. Experimental and numerical analysis of damage in woven gfrp composites under large-deflection bending. *Appl Compos Mater* 2012;19:769–83. <https://doi.org/10.1007/s10443-011-9242-7>.
- [112] Tien DT, Kim J S., Huh Y. Stab-resistant property of the fabrics woven with the aramid/cotton core-spun yarns. *Fibers Polym* 2010;11:500–6. <https://doi.org/10.1007/s12221-010-0500-3>.
- [113] Chadwick EKJ, Nicol AC, Lane J V, Gray TGF. Biomechanics of knife stab attacks. *Forensic Sci Int* 1999;105:35–44. [https://doi.org/10.1016/S0379-0738\(99\)00117-6](https://doi.org/10.1016/S0379-0738(99)00117-6).
- [114] Larsen B, Netto K, Skovli D, Vincs K, Vu S, Aisbett B. Body armor, performance, and physiology during repeated high-intensity work tasks. *Mil Med* 2012;177:1308–15. <https://doi.org/10.7205/MILMED-D-11-00435>.
- [115] Miao XH, Kong XY, Jiang GM. The experimental research on the stab resistance of warp-knitted spacer fabric. *J Ind Text* 2013;43:281–301. <https://doi.org/10.1177/1528083712464256>.
- [116] Miao XH, Jiang GM, Kong XY. Experimental investigation on the stab resistance of warp knitted fabrics. *Fibres Text East Eur* 2014;5:65–70.
- [117] El Messiry M, Eltahan E. Stab resistance of triaxial woven fabrics for soft body armor. *J Ind Text* 2016;45:1062–82. <https://doi.org/10.1177/1528083714551441>.
- [118] Nayak R, Kanalingam S, Wang LJ, Padhye R. Stab resistance and thermophysiological comfort properties of boron carbide coated aramid and ballistic nylon fabrics. *J Text Inst* 2018;0:1–10. <https://doi.org/10.1080/00405000.2018.1548800>.
- [119] Wang P, Sun BZ, Gu BH. Comparison of stab behaviors of uncoated and coated woven fabrics from experimental and finite element analyses. *Text Res J* 2012;82:1337–54. <https://doi.org/10.1177/0040517511418560>.
- [120] Annaidh AN, Cassidy M, Curtis M, Destrade M, Gilchrist MD. Toward a predictive assessment of stab-penetration forces. *Am J Forensic Med Pathol* 2015;36:162–6. <https://doi.org/10.1097/PAF.0000000000000075>.
- [121] Li W, Xiong DS, Zhao XD, Sun LL, Liu J. Dynamic stab resistance of ultra-high molecular weight polyethylene fabric impregnated with shear thickening fluid. *Mater*

- Des 2016;102:162–7. <https://doi.org/10.1016/j.matdes.2016.04.006>.
- [122] Xu Y, Chen XG, Wang Y, Yuan ZS. Stabbing resistance of body armour panels impregnated with shear thickening fluid. *Compos Struct* 2017;163:465–73. <https://doi.org/10.1016/j.compstruct.2016.12.056>.
- [123] Horsfall I, Watson C, Champion S, Prosser P, Ringrose T. The effect of knife handle shape on stabbing performance. *Appl. Ergon.*, vol. 36, 2005, p. 505–11. <https://doi.org/10.1016/j.apergo.2004.12.001>.
- [124] Pazmino J, Carvelli V, Lomov S V. Formability of a non-crimp 3D orthogonal weave E-glass composite reinforcement. *Compos Part A Appl Sci Manuf* 2014;61:76–83. <https://doi.org/10.1016/j.compositesa.2014.02.004>.
- [125] Dufour C, Wang P, Boussu F, Soulat D. Experimental Investigation About Stamping Behaviour of 3D Warp Interlock Composite Preforms. *Appl Compos Mater* 2014;21:725–38. <https://doi.org/10.1007/s10443-013-9369-9>.
- [126] Dufour C, Boussu F. Local strain measurements of yarns inside of 3D warp interlock fabric during forming process. *Int J Mater Form* 2018;11:775–788. <https://doi.org/https://doi.org/10.1007/s12289-017-1385-0>.
- [127] Behera BK, Mishra R. 3-Dimensional weaving. *Indian J Fibre Text Res* 2008;33:274–87.
- [128] Standard test method for linear density of yarn (yarn number) by the skein method, n.d.
- [129] ISO 2062: 199. Textiles — Yarns from packages — Determination of single-end breaking force and elongation at break n.d.
- [130] Boussu F, Dufour C, Veyet F, Lefebvre M. Weaving processes for composites manufacture. *Adv. Compos. Manuf. Process Des.*, Woodhead Publishing; 2015, p. 55–78. <https://doi.org/10.1016/B978-1-78242-307-2.00003-8>.
- [131] Lee L, Rudov-Clark S, Mouritz AP, Bannister MK, Herszberg I. Effect of weaving damage on the tensile properties of three-dimensional woven composites. *Compos Struct* 2002;57:405–13. [https://doi.org/10.1016/S0263-8223\(02\)00108-3](https://doi.org/10.1016/S0263-8223(02)00108-3).
- [132] Syed U, Jhatial RA. Influence of warp yarn tension on cotton woven fabric structures. *Mehran Univ Res J Eng Technol* 2013;32:125–32.
- [133] Afroz F, Siddika A. Effect of warp yarn tension on crimp % in woven fabric. *Eur Sci J* 2014;10:202–7. <https://doi.org/https://doi.org/10.19044/esj.2014.v10n24p%25p>.
- [134] Neogi SK. Role of yarn tension in weaving. Woodhead publishing india in textiles; 2016. <https://doi.org/10.1201/b19896>.
- [135] Ghosh S, Chary P, Roy S. Development of warp yarn tension during shedding: a

- theoretical approach. *J Inst Eng Ser E* 2015;96:107–24. <https://doi.org/10.1007/s40034-014-0044-y>.
- [136] Abtew MA, Boussu F, Bruniaux P, Loghin C, Cristian I, Chen Y, et al. Yarn degradation during weaving process and its effect on the mechanical behaviours of 3D warp interlock p-aramid fabric for industrial applications. *J Ind Text* 2020. <https://doi.org/10.1177/1528083720937288>.
- [137] Lefebvre M, Francois B, Daniel C. Influence of high-performance yarns degradation inside three-dimensional warp interlock fabric. *J Ind Text* 2013;42:475–88. <https://doi.org/10.1177/1528083712444298>.
- [138] Kharitonov A P., Maksimkin A V., Mostovaya K S., Kaloshkin S D., Gorshenkov M V., D'yachkova T P., et al. Reinforcement of bulk ultrahigh molecular weight polyethylene by fluorinated carbon nanotubes insertion followed by hot pressing and orientation stretching. *Compos Sci Technol* 2015;120:26–31. <https://doi.org/10.1016/j.compscitech.2015.10.009>.
- [139] Li BY, Li MJ, Fan C, Ren MM, Wu P, Luo LB, et al. The wear-resistance of composite depending on the interfacial interaction between thermoplastic polyurethane and fluorinated UHMWPE particles with or without oxygen. *Compos Sci Technol* 2015;106:68–75. <https://doi.org/10.1016/j.compscitech.2014.11.005>.
- [140] Holloway JL, Lowman AM, VanLandingham MR, Palmese GR. Chemical grafting for improved interfacial shear strength in UHMWPE/PVA-hydrogel fiber-based composites used as soft fibrous tissue replacements. *Compos Sci Technol* 2013;85:118–25. <https://doi.org/10.1016/j.compscitech.2013.06.007>.
- [141] Sa R, Wei ZH, Yan Y, Wang L, Wang WC, Zhang LQ, et al. Catechol and epoxy functionalized ultrahigh molecular weight polyethylene (UHMWPE) fibers with improved surface activity and interfacial adhesion. *Compos Sci Technol* 2015;113:54–62. <https://doi.org/10.1016/j.compscitech.2015.03.017>.
- [142] Nauman S. Geometrical modelling and characterization of 3D warp interlock composites and their on-line structural health monitoring using flexible. 2011.
- [143] Hou YQ, Sun BZ, Gu BH. An analytical model for the ballistic impact of three dimensional angle-interlock woven fabric penetrated by a rigid cylindro-spherical projectile. *Text Res J* 2011;81:1287–303. <https://doi.org/10.1177/0040517511399966>.
- [144] Pan N, Yoon MY. Behavior of yarn pullout from woven fabrics: theoretical and experimental. *Text Res J* 1993;63:629–37. <https://doi.org/10.1177/004051759306301103>.

- [145] Taylor HM. 9—Tensile and tearing strength of cotton cloths. *J Text Inst Trans* 1959;50:T161–88. <https://doi.org/10.1080/19447025908662490>.
- [146] Peirce FT. 5—The geometry of cloth structure. vol. 28. 1937. <https://doi.org/10.1080/19447023708658809>.
- [147] Kovar R. Length of the yarn in plain-weave crimp wave. *J Text Inst* 2011;102:582–97. <https://doi.org/10.1080/00405000.2010.498175>.
- [148] Jung C, Ganghoffer J-F, Durand B. A Generalized Continuum Model for Textile n.d.:1–10.
- [149] Barella A. Law of Critical Yarn Diameter and Twist: Influence on Yarn Characteristics. *Text Res J* 1951;21:166–8. <https://doi.org/10.1177/004051755102100308>.
- [150] Govarthanam KK, Anand SC, Rajendran S. Development of advanced personal protective equipment fabrics for protection against slashes and pathogenic bacteria part 1: Development and evaluation of slash-resistant garments. *J Ind Text* 2010;40:139–55. <https://doi.org/10.1177/1528083710366722>.
- [151] Henderson JP, Morgan SE, Patel F, Tiplady ME. Patterns of non-firearm homicide. *J Clin Forensic Med* 2005;12:128–32. <https://doi.org/10.1016/j.jcfm.2004.10.011>.
- [152] Sheng SZ, Hoa S V. Modeling of 3D angle interlock woven fabric composites. *J Thermoplast Compos Mater* 2003;16:45–58. <https://doi.org/10.1106/089270503023206>.
- [153] Erlandsson Å, Meloy J R. The Swedish School Attack in Trollhättan. *J Forensic Sci* 2018;63:1917–27. <https://doi.org/10.1111/1556-4029.13800>.
- [154] Payne T, O'Rourke S, Malbon C. *Body Armour Standard (2017) Guidance*. 2017.
- [155] Sun B, Zhang R, Zhang Q, Gideon R, Gu B. Drop-weight impact damage of three-dimensional angle-interlock woven composites. *J Compos Mater* 2013;47:2193–209. <https://doi.org/10.1177/0021998312454904>.
- [156] Reiners P. Investigation about the stab resistance of textile structures, methods for their testing and improvements. University of Upper Alsace. Ph.D thesis, 2016.
- [157] Tien DT, Kim JS, Huh Y. Evaluation of anti-stabbing performance of fabric layers woven with various hybrid yarns under different fabric conditions. *Fibers Polym* 2011;12:808–15. <https://doi.org/10.1007/s12221-011-0808-7>.
- [158] Li TT, Wang R, Lou CW, Lin JH. Static and dynamic puncture behaviors of compound fabrics with recycled high-performance Kevlar fibers. *Compos Part B Eng* 2014;59:60–6. <https://doi.org/10.1016/j.compositesb.2013.10.063>.
- [159] Wang Y, Chen XG, Young R, Kinloch I, Wells G. A numerical study of ply orientation on ballistic impact resistance of multi-ply fabric panels. *Compos Part B Eng*

- 2015;68:259–65. <https://doi.org/10.1016/j.compositesb.2014.08.049>.
- [160] Wang L, Zhang S, Gao WM, Wang X. FEM analysis of knife penetration through woven fabrics. *CMES - Comput Model Eng Sci* 2007;20:11–20. <https://doi.org/10.3970/cmes.2007.020.011>.
- [161] Horsfall I. Stab resistant body armour. Cranfield university. Ph.D thesis, 1999.
- [162] Yang Z, Peng HD, Wang WZ, Liu TX. Crystallization behavior of poly(ϵ -caprolactone)/layered double hydroxide nanocomposites. *J Appl Polym Sci* 2010;116:2658–67. <https://doi.org/10.1002/app>.
- [163] Johnson A. Establishing design characteristics for the development of stab resistant Laser Sintered body armour. Loughborough University. Ph.D thesis, 2014.
- [164] Hejazi SM, Kadivar N, Sajjadi A. Analytical assessment of woven fabrics under vertical stabbing – The role of protective clothing. *Forensic Sci Int* 2016;259:224–33. <https://doi.org/10.1016/j.forsciint.2015.12.036>.
- [165] Shen H, Wang P, Legrand X, Liu LS. Characterisation and optimisation of wrinkling during the forming of tufted three-dimensional composite preforms. *Compos Part A Appl Sci Manuf* 2019;127:105651. <https://doi.org/10.1016/j.compositesa.2019.105651>.
- [166] Aspert N, Santa-Cruz D, Ebrahimi T. MESH: Measuring errors between surfaces using the Hausdorff distance. *Proc. - 2002 IEEE Int. Conf. Multimed. Expo, ICME 2002*, vol. 1, 2002, p. 705–8. <https://doi.org/10.1109/ICME.2002.1035879>.
- [167] El Messiry M. Investigation of puncture behaviour of flexible silk fabric composites for soft body armour. *Fibres Text East Eur* 2014;22:71–6.
- [168] Usman Javaid M, Militký J, Wiener J, Jabbar A, Salačová J, Umair M. Effect of surface modification and knife penetration angle on the quasi-static knife penetration resistance of para-aramid fabrics. *J Text Inst* 2019;110:590–9. <https://doi.org/10.1080/00405000.2018.1496988>.
- [169] Gürgen S, Yıldız T. Stab resistance of smart polymer coated textiles reinforced with particle additives. *Compos Struct* 2020;235. <https://doi.org/10.1016/j.compstruct.2019.111812>.
- [170] D. Tabor. *The harness of metal*, Clarendon Press, Oxford; 1951, p. 95–114.
- [171] Hosur MV, Mayo JB, Wetzel E, Jeelani S. Studies on the fabrication and stab resistance characterization of novel thermoplastic-kevlar composites. *Solid State Phenom* 2008;136:83–92. <https://doi.org/10.4028/www.scientific.net/SSP.136.83>.
- [172] Bhatnagar A. *Lightweight ballistic composites: Military and law-enforcement applications*. 2006. <https://doi.org/10.1533/9781845691554>.

- [173] Singletary J, Bogdanovich A. 3-D orthogonal woven soft body armor. *J Ind Text* 2000;29:287–305. <https://doi.org/10.1106/UQ6J-EMCW-U3Q5-VU31>.
- [174] Boussu F, Bruniaux P. Customization of a lightweight bullet-proof vest for the female form. Woodhead Publishing Limited; 2012. <https://doi.org/10.1533/9780857095572.2.167>.
- [175] Rozant O, Bourban PE, Månson JAE. Drapability of dry textile fabrics for stampable thermoplastic preforms. *Compos Part A Appl Sci Manuf* 2000;31:1167–77. [https://doi.org/10.1016/S1359-835X\(00\)00100-7](https://doi.org/10.1016/S1359-835X(00)00100-7).
- [176] Cheon J, Lee M, Kim M. Study on the stab resistance mechanism and performance of the carbon , glass and aramid fi ber reinforced polymer and hybrid composites. *Compos Struct* 2020;234. <https://doi.org/10.1016/j.compstruct.2019.111690>.
- [177] Roedel C, Chen XG. Innovation and analysis of police riot helmets with continuous textile reinforcement for improved protection. *IMACS Multiconference "Computational Eng. Syst. Appl.*, 2007, p. 187–94. <https://doi.org/10.1109/cesa.2006.4281648>.
- [178] Abtew MA, Boussu F, Bruniaux P, Loghin C, Cristian I, Chen Y, et al. Forming characteristics and surface damages of stitched multi-layered para-aramid fabrics with various stitching parameters for soft body armour design. *Compos Part A Appl Sci Manuf* 2018;109:517–37. <https://doi.org/10.1016/j.compositesa.2018.02.037>.
- [179] Souter BJ. Effects of fibre architecture on formability of textile preforms. University of Nottingham, 2001.
- [180] Boisse P, Gasser A, Hagege B, Billoet J-L. Analysis of the mechanical behavior of woven fibrous material using virtual tests at the unit cell level. *J Mater Sci* 2005;40:5955–62. <https://doi.org/10.1007/s10853-005-5069-7>.
- [181] Zouari B, Daniel JL, Boisse P. A woven reinforcement forming simulation method. Influence of the shear stiffness. *Comput Struct* 2006;84:351–63. <https://doi.org/10.1016/j.compstruc.2005.09.031>.
- [182] Khan MA. Analyse numérique et expérimentale de la mise en forme des renforts de composite textiles basée sur un comportement hypoélastique. 2009.
- [183] Boisse P, Hamila N, Vidal-Sallé E, Dumont F. Simulation of wrinkling during textile composite reinforcement forming. Influence of tensile, in-plane shear and bending stiffnesses. *Compos Sci Technol* 2011;71:683–92. <https://doi.org/10.1016/j.compscitech.2011.01.011>.
- [184] Hunter JD. Matplotlib: A 2D graphics environment. *Comput Sci Eng* 2007;9:90–5. <https://doi.org/10.1109/MCSE.2007.55>.

- [185] MacHado M, Murenu L, Fischlschweiger M, Major Z. Analysis of the thermomechanical shear behaviour of woven-reinforced thermoplastic-matrix composites during forming. *Compos Part A Appl Sci Manuf* 2016;86:39–48. <https://doi.org/10.1016/j.compositesa.2016.03.032>.
- [186] Prodromou AG, Chen J. On the relationship between shear angle and wrinkling of textile composite preforms. *Compos Part A Appl Sci Manuf* 1997;28:491–503. [https://doi.org/10.1016/S1359-835X\(96\)00150-9](https://doi.org/10.1016/S1359-835X(96)00150-9).
- [187] Boisse P, Colmars J, Hamila N, Naouar N, Steer Q. Bending and wrinkling of composite fiber preforms and prepregs. A review and new developments in the draping simulations. *Compos Part B Eng* 2018;141:234–49. <https://doi.org/10.1016/j.compositesb.2017.12.061>.
- [188] Mayo JB, Wetzel ED, Hosur M V., Jeelani S. Stab and puncture characterization of thermoplastic-impregnated aramid fabrics. *Int J Impact Eng* 2009;36:1095–105. <https://doi.org/10.1016/j.ijimpeng.2009.03.006>.